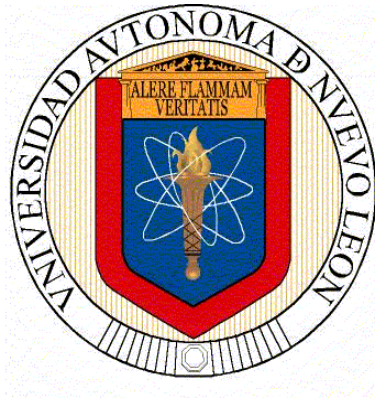


**UNIVERSIDAD AUTÓNOMA DE NUEVO LEÓN  
FACULTAD DE CIENCIAS QUÍMICAS**



**TESIS**

**"EFFECT OF ETHYL ESTER-MgO MIXTURES ON EMISSIONS OF GASES  
AND PROPERTIES OF BIODIESEL PRODUCED WITH INCORPORATION OF  
DEEP EUTECTIC SOLVENTS: ANALYSIS OF ENVIRONMENTAL IMPACT"**

**PRESENTA**

**BRAYAN STEVEN MORENO CABALLERO**

**COMO REQUISITO PARA OBTENER EL GRADO DE  
DOCTORADO EN CIENCIAS  
CON ORIENTACIÓN EN PROCESOS SUSTENTABLES**

**DICIEMBRE 2023**

THÈSE

Pour obtenir le grade de

**DOCTEUR DE L'UNIVERSITÉ GRENOBLE ALPES  
et de l'UNIVERSIDAD AUTÓNOMA DE NUEVO LEÓN**

École doctorale : I-MEP2 - Ingénierie-Matériaux, Mécanique, Environnement,  
Énergétique, Procédés, Production.  
Spécialité : MEP - Mécanique des fluides, énergétique, procédés.  
Unité de recherche : Laboratoire Rhéologie Et Procédés.

**EFFET DES MÉLANGES ETHYL ESTER-MgO SUR LES ÉMISSIONS DE GAZ ET LES PROPRIÉTÉS  
DU BIODIESEL PRODUIT AVEC INCORPORATION DE SOLVANTS EUTECTIQUES PROFONDES :  
ANALYSE DE L'IMPACT ENVIRONNEMENTAL**

**EFFECT OF ETHYL ESTER-MgO MIXTURES ON EMISSIONS OF GASES AND  
PROPERTIES OF BIODIESEL PRODUCED WITH INCORPORATION OF DEEP EUTECTIC  
SOLVENTS: ANALYSIS OF ENVIRONMENTAL IMPACT**

Présentée par :

**MORENO CABALLERO, Brayen Steven**

Direction de thèse :

**Jean-Marc LEVEQUE**

MAITRE DE CONFERENCES HDR, Université Grenoble Alpes

**José Julián Cano Gómez**

FULL PROFESSOR, Universidad Autónoma de Nuevo León

Rapporteurs :

**Ulla LASSI**

DIRECTRICE DE RECHERCHE, University of Oulu

**Sabine VALANGE**

MAITRESSE DE CONFERENCES, Université de Poitiers

Thèse soutenue publiquement le « **1 décembre 2023** », devant le jury composé de :

**Jean-Marc LEVEQUE**

MAITRE DE CONFERENCES HDR, Université Grenoble Alpes

Directeur de thèse

**José Julián CANO GÓMEZ**

FULL PROFESSOR, Universidad Autónoma de Nuevo León

Directeur de thèse

**Ulla LASSI**

DIRECTRICE DE RECHERCHE, University of Oulu

Reportrice

**Sabine VALANGE**

MAITRESSE DE CONFERENCES, Université de Poitiers

Reportrice

**Stéphane BAUP**

FULL PROFESSOR, Université Grenoble Alpes

Examinateur

**Gustavo Arturo IGLESIAS SILVA**

FULL PROFESSOR, Instituto Tecnológico de Celaya

Examinateur

**Carlos Enrique ESCÁRCEGA GONZÁLEZ**

FULL PROFESSOR,, Universidad Autónoma de Nuevo León

Examinateur

**François DELATTRE**

FULL PROFESSOR, University of Littoral Côte d'Opale.

Examinateur



**Autonomous University of Nuevo León**

**Grenoble Alpes University**

**Thesis to obtain the degree of Doctor in Sciences with Orientation in Sustainable Processes and Doctor in fluid mechanics, energy and process**



Thesis Title:

**"EFFECT OF ETHYL ESTER-MgO MIXTURES ON EMISSIONS OF GASES AND PROPERTIES OF BIODIESEL PRODUCED WITH INCORPORATION OF DEEP EUTECTIC SOLVENTS: ANALYSIS OF ENVIRONMENTAL IMPACT "**

**Number:**

2-105814-PST-20/288

M.C. BRAYAN STEVEN MORENO CABALLERO  
**Author**

LGAC: Technology and Engineering of Sustainable Processes

Dr. JOSÉ JULIÁN CANO GÓMEZ  
Dr. JEAN-MARC LEVEQUE  
**Thesis Directors**

Laboratory of Physicochemical Analysis - Faculty of Chemical Sciences  
Laboratory of Rheology and Processes – Grenoble Alpes University

San Nicolás de los Garza, Nuevo León, México. December 2023

-Realizar esta tesis ha sido, quizás, el trabajo más desafiante que he emprendido hasta ahora. Ha requerido esfuerzo constante, pensar en cómo superarme día tras día, noches sin dormir y, en muchas ocasiones, enfrentar la frustración y la tentación de rendirme. Por eso, deseo dedicar este logro a la persona que durante 29 años ha llevado a cabo una labor aún más exigente, sin tener más recompensa que mi amor incondicional. Esta tesis está dedicada a mi madre,  
Nancy Caballero.

-Doing this thesis has been, perhaps, the most challenging work I have undertaken so far. It has required constant effort, thinking about how to improve myself day after day, sleepless nights and, on many occasions, facing frustration and the temptation to give up. For this reason, I wish to dedicate this achievement to the person who for 29 years has carried out an even more demanding task, with no other reward than my unconditional love. This thesis is dedicated to my mother,  
Nancy Caballero.

## CONTENTS

RÉSUMÉ .....	2
ABSTRACT .....	3
1. INTRODUCTION.....	4
2. BACKGROUND .....	15
2.1. Biodiesel production from sewage sludge.....	15
2.2. Use of DES in biodiesel production .....	17
2.3. Implementation of additives in biodiesel .....	18
2.4. Biodiesel emissions analysis using CFD.....	19
2.5. Life cycle analysis in biodiesel production from wastewater sludge.....	20
3. SCIENTIFIC CONTRIBUTION .....	22
4. HYPOTHESIS .....	22
5. OBJECTIVES .....	23
5.1. GENERAL OBJECTIVE.....	23
5.2. SPECIFICS OBJECTIVES.....	23
6. METHODOLOGY .....	24
6.1 Laboratory materials and equipment .....	24
6.2 Experimental Procedure: .....	26
6.2.1 Stage 1: Catalyst preparation.....	26
6.2.2 Stage 3: Biodiesel Production and Characterization .....	26
6.2.4 Stage 4: Additive implementation and additive-biodiesel mixtures characterization.....	30
6.2.5 Stage 5: Combustion simulation.....	31
6.2.6 Stage 6: Environmental Impact Assessment.....	37
7. RESULTS.....	41
7.1. Stage 1: DESs synthesis .....	41
7.2. Stage 2: Biodiesel Production and Characterization .....	43
7.3. Stage 4: Biodiesel-Ethyl levulinate-MgO mixtures characterization .....	52
7.4. Stage 5. CFD Simulation validation.....	68
7.4. Stage 6. Environmental impact assessment .....	78
8. INTENSIFICATION OF THE BIODIESEL PRODUCTION BY USING ULTRASOUND.....	87
8.1. INTRODUCTION .....	87

8.2. METHODOLOGY .....	93
8.2.1 DES synthesis and characterization .....	93
8.2.2. Ultrasound-assisted biodiesel production .....	96
8.2. RESULTS .....	98
8.2.1. DES synthesis and characterization .....	98
8.2.2. Ultrasound-assisted biodiesel production .....	105
REFERENCES .....	120
APPENDIX A.....	132

## FIGURES LIST

<b>Figure 1.</b> Diagram of investigation stages.....	20
<b>Figure 2.</b> CFD geometry for combustion analysis.....	28
<b>Figure 3.</b> Boundary diagram for: (a) Scenario A; (b) Scenarios B and C.....	30
<b>Figure 4.</b> Effect of ChCl: PTSA molar ratio (mol DES/mol FFA) on biodiesel yield at methanol ratio 10 (mol methanol/mol FFA), temperature 60°C and time 3h.....	36
<b>Figure 5.</b> Effect of ChCl: OA molar ratio (mol DES/mol FFA) on biodiesel yield at methanol ratio 15 (mol methanol/mol FFA), temperature 60°C and time 3h. ....	37
<b>Figure 6.</b> Effect of ChCl: CA molar ratio (mol DES/mol FFA) on biodiesel yield at methanol ratio 15 (mol methanol/mol FFA), temperature 60°C and time 3h. ....	37
<b>Figure 7.</b> Esterification mechanism by using DES (TOAB:PTSA) as catalyst proposed by Liu et al. ....	45
<b>Figure 8.</b> Liquid-Liquid equilibrium for ternary system: a) BuHE + HeAc + DES , b) BuHE + BuOH + DES .....	46
<b>Figure 9.</b> DES mass mechanism adapted from Zhou et al. [69].....	47
<b>Figure 10.</b> Effect of time for ChCl: PTSA on biodiesel yield at 0.1 (mol DES/mol FFA), methanol ratio 10 (mol methanol/mol FFA), and temperature 60°C. ....	48
<b>Figure 11.</b> Effect of time for ChCl: OA on biodiesel yield at 0.2 (molDES/mol FFA), methanol ratio 15 (mol methanol/mol FFA), and temperature 60°C.....	48
<b>Figure 12.</b> Properties of Biodiesel-Ethyl Levulinate mixtures at different mass fraction and temperature. ....	54
<b>Figure 13.</b> Comparison of experimental kinematic viscosity $\nu$ (exp) at 313.15 K, <span style="color: red;">■</span> and density $\rho$ (exp) at 288.15 K, <span style="color: blue;">●</span> , of biodiesel mixtures as a function of mass fraction $w_2$ : (a) biodiesel (1) + ethyl levulinate (2) + MgO; (b) biodiesel (1) + ethyl acetoacetate (2) + MgO; (c) biodiesel (1) + ethyl pyruvate (2) + MgO, with the EN14214 standard limits for the kinematic viscosity, <span style="color: red;">— —</span> , and density, <span style="color: blue;">- . - .</span> . ....	58
<b>Figure 14.</b> Excess molar volumes, $V^E$ , for biodiesel mixtures as a function of the mole fraction $x_2$ : (a) biodiesel (1) + ethyl levulinate (2) + MgO; (b) biodiesel (1) + ethyl acetoacetate (2) + MgO; (c) biodiesel (1) + ethyl pyruvate (2) + MgO: <span style="color: black;">■</span> , 288.15 K; <span style="color: black;">○</span> , 293.15 K; <span style="color: black;">▲</span> , 298.15 K; <span style="color: black;">▽</span> , 303.15 K; <span style="color: black;">◆</span> , 308.15 K; <span style="color: black;">◁</span> , 313.15 K; <span style="color: black;">▶</span> , 318.15 K; <span style="color: black;">◻</span> , 323.15 K; <span style="color: black;">●</span> , 328.15 K; <span style="color: black;">◻</span> , 333.15 K; <span style="color: black;">★</span> , 338.15 K. . ....	61

<b>Figure 15.</b> Viscosity deviations, $\Delta\eta$ , for biodiesel mixtures as a function of the mole fraction $x_2$ : (a) biodiesel (1) + ethyl levulinate (2) + MgO; (b) biodiesel (1) + ethyl acetoacetate (2) + MgO; (c) biodiesel (1) + ethyl pyruvate (2) + MgO: ■, 288.15 K; ○, 293.15 K; ▲, 298.15 K; ▽, 303.15 K; ◆, 308.15 K; ◁, 313.15 K; ►, 318.15 K; ◊, 323.15 K; ●, 328.15 K; ◑, 333.15 K; ★, 338.15 K.....	63
<b>Figure 16.</b> Refractive index deviations, $\Delta n_D$ , for biodiesel mixtures as a function of the mole fraction $x_2$ : (a) biodiesel (1) + ethyl levulinate (2) + MgO; (b) biodiesel (1) + ethyl acetoacetate (2) + MgO; (c) biodiesel (1) + ethyl pyruvate (2) + MgO: ■, 288.15 K; ○, 293.15 K; ▲, 298.15 K; ▽, 303.15 K; ◆, 308.15 K; ◁, 313.15 K; ►, 318.15 K; ◊, 323.15 K; ●, 328.15 K; ◑, 333.15 K; ★, 338.15 K.....	64
<b>Figure 17.</b> Combustor 2D geometry mesh.....	65
<b>Figure 18.</b> Temperature contour for Diesel combustion (a) this work (b) Dixit et al. ....	68
<b>Figure 19.</b> CO <sub>2</sub> mass fraction contour for Diesel combustion (a) this work (b) Dixit et al.....	69
<b>Figure 20.</b> Biodiesel mass fraction profile for sample 0.9 biodiesel + 0.1 Levulinate.....	72
<b>Figure 21.</b> Biodiesel mass fraction profile for 0.9 biodiesel + 0.1 Levulinate mixture with adjusted air:fuel ratio.....	73
<b>Figure 22.</b> Five midpoint environmental impact indicators for scenario A (Base scenario) .....	81
<b>Figure 23.</b> Five midpoint environmental impact indicators for scenario B (DES ChCl:PTSA) .....	82
<b>Figure 24.</b> Five midpoint environmental impact indicators for scenario C (DES ChCl:OA) .....	83
<b>Figure 25.</b> IR spectra superposition for Menthol:DA.....	99
<b>Figure 26.</b> IR spectra superposition for ChCl:CA.....	99
<b>Figure 27.</b> UV absorbance spectrums for Hammett method.....	102
<b>Figure 28.</b> UV absorbance comparison between HBD and HBA pairs.....	104
<b>Figure 29.</b> Effect of ultrasound intensity in biodiesel yield by using ChCl:PTSA as catalyst.....	106
<b>Figure 30.</b> Effect of pulse in biodiesel yield by using ChCl:PTSA as catalyst.....	107
<b>Figure 31.</b> Effect of time in biodiesel yield by using ChCl:PTSA as catalyst....	108
<b>Figure 32.</b> Effect of DES quantity in biodiesel yield by using ChCl:PTSA as catalyst.....	109
<b>Figure 33.</b> Biodiesel yield by using magnetic stirring and ultrasonic irradiation for five different DES.....	111

## TABLES LIST

<b>Table 1.</b> Reagents to be used in research.....	21
<b>Table 2.</b> Laboratory equipment.....	21
<b>Table 3.</b> Reaction conditions to biodiesel production. ....	23
<b>Table 4.</b> Analytical methods for the physicochemical properties of biodiesel and the limits established by standard EN14214. ....	25
<b>Table 5.</b> Density and refractive index comparison with literature reports for obtained DES. ....	34
<b>Table 6.</b> Fatty acid profile for biodiesel produced by using different catalysts...	41
<b>Table 7.</b> Beef tallow and residual fat biodiesel fatty acid methyl esters composition .....	42
<b>Table 8.</b> Biodiesel properties comparison with EN14214 standard.....	43
<b>Table 9.</b> Comparison between the experimental ethyl esters viscosity, $\eta$ (mPa·s), Density, $\rho$ (g·cm <sup>-3</sup> ), and Refractive Index, $n_D$ , at Temperature T and Literature values at Pressure, p = 0.1 Mpa. ....	44
<b>Table 10.</b> Flash point, Cetane Index, and Calorific Value of Biodiesel Mixtures	47
<b>Table 11.</b> Simulated values for combustion temperature (T Max) and CO <sub>2</sub> mass fraction for Biodiesel pure biodiesel and biodiesel binary mixtures.....	70
<b>Table 12.</b> Simulated temperatures and emissions for Biodiesel + Ethyl evulinate + MgO mixture. ....	74
<b>Table 13.</b> Reaction conditions for the three scenarios analyzed in the LCA.....	76
<b>Table 14.</b> Environmental inventory. ....	77
<b>Table 15.</b> DES components and molar ratios.....	94
<b>Table 16.</b> Hammet acidity values for seven DES.....	102

## NOMENCLATURE

GHG: Greenhouse gas	CFD: Computational fluid dynamics
PP: Pour point	WTG: Waste trap grease
CP: Cloud point	SO: Soya oil
DES: Deep eutectic solvent	LSD: Low sulfur diesel
HBD: Hydrogen bond donor	FFA: Free fatty acid
HBA: Hydrogen bond acceptor	%FFA: Free fatty acid percentage
ChCl: Choline chloride	FU: Functional unit
ChAc: Choline acetate	CC: Climate change indicator
MTPB: Methyl triphenyl phosphonium bromide	TA: Terrestrial acidification indicator
TOAB: Tetra octyl ammonium bromide	OD: Ozone depletion indicator
PTSA: P-Toluene sulfonic acid	FE: Freshwater eutrophication indicator
OA: Oxalic acid	FD: Fossil depletion indicator
CA: Citric acid	AAPD: Average absolute percentage deviation
LCA: Life cycle assessment	HLB: Hydrophilic-Lipophilic Balance
EL: Ethyl levulinate	VE: Excess molar volume
EA: Ethyl acetoacetate	FAME: Fatty acid methyl ester
EP: Ethyl pyruvate	ED: Eddy dissipation
BTEAC: Benzyltriethylammonium chloride	

## RÉSUMÉ

**Brayan Steven Moreno Caballero** Date de soutenance de thèse : 01/12/2023  
Université Autonome de Nuevo León - Université Grenoble Alpes  
Faculté des sciences chimiques - École doctorale IMEP-2

**Titre de la recherche** : EFFET DES MÉLANGES ETHYL ESTER-MgO SUR LES ÉMISSIONS DE GAZ ET LES PROPRIÉTÉS DU BIODIESEL PRODUIT AVEC L'INCORPORATION DE SOLVANTS EUTECTIQUES PROFONDS : ANALYSE DE L'IMPACT SUR L'ENVIRONNEMENT.

**Nombre de pages** :144

**Candidat au doctorat en sciences avec orientation vers les processus durables et doctorat en mécanique des fluides, énergie et procédés**

**Objectif de l'étude** : L'objectif principal de ce travail est de proposer une méthodologie plus propre pour produire du biodiesel à partir de boues d'épuration en utilisant des solvants eutectiques profonds et d'évaluer son impact sur l'environnement par le biais d'une analyse du cycle de vie. En outre, il s'agit d'évaluer l'effet des additifs d'ester éthylique-MgO sur les propriétés du biodiesel et ses émissions.

**Contribution et conclusions** : Dans cette recherche, une méthodologie standardisée a été développée pour produire du biodiesel à partir de boues d'épuration en utilisant un solvant eutectique profond (DES) comme catalyseur. Le rendement le plus élevé obtenu était de 97% en utilisant le DES Chlorure de choline (ChCl) : Acide *p*-Toluène Sulfonique (PTSA) à 0,1 (mol<sub>DES</sub>/mol<sub>FFA</sub>), méthanol à 10 (mol<sub>méthanol</sub>/mol<sub>FFA</sub>) ratios respectifs, 60°C et 4h de temps de réaction. L'analyse du cycle de vie souligne que la production de biodiesel à l'aide de DES comme catalyseurs a un impact environnemental global plus faible que la méthodologie conventionnelle utilisant H<sub>2</sub>SO<sub>4</sub>. Cela s'explique notamment par des temps de réaction plus courts, des étapes de séparation/purification moins nombreuses entraînant une réduction de la consommation d'électricité et l'élimination totale de l'hexane tout au long du processus. La densité, la viscosité et l'indice de réfraction des mélanges de biodiesel avec du lévulinate d'éthyle, de l'acétoacétate d'éthyle et du pyruvate d'éthyle avec une quantité constante de 5ppm<sub>m</sub> de MgO ont été déterminés expérimentalement sur toute la gamme de compositions et de (288,15 à 333,15) K. Les mélanges biodiesel-esters d'éthyle-MgO ont montré des diminutions de viscosité et des augmentations de densité par rapport à l'ajout d'esters d'éthyle. Cela est dû aux faibles viscosités et aux densités élevées des esters éthyliques par rapport au biodiesel. Les mélanges de biodiesel avec des fractions pondérales d'esters éthyliques inférieures à 0,2 étaient conformes à la norme de qualité EN14214 pour le biodiesel. La combustion du biodiesel pur et des mélanges biodiesel + ester éthylique a été simulée dans le logiciel Ansys fluent. Les valeurs simulées de la température de combustion et de la fraction massique de NO<sub>x</sub> ont diminué jusqu'à 1 % et 17 % respectivement avec l'ajout d'une fraction massique de 0,1 lévulinate d'éthyle et de 0,0020 kg/s de particules de MgO en raison de l'effet de dissipation thermique des particules. D'autre part, la fraction de masse de CO<sub>2</sub> a augmenté de 0,78 % en raison de l'augmentation de la viscosité des mélanges causée par les particules de MgO. Enfin, l'irradiation par ultrasons a été incorporée à la réaction du biodiesel en utilisant le ChCl:PTSA DES comme catalyseur à 0,2 (mol<sub>DES</sub>/mol<sub>FFA</sub>) et le méthanol à 10 (mol<sub>méthanol</sub>/mol<sub>FFA</sub>). Cela a permis d'obtenir un rendement plus élevé de 96,3 % avec un temps court de 1 heure et une température plus basse de 40°C ; ces réductions ont été obtenues principalement grâce à l'effet émulsifiant favorisé par les ultrasons.

## ABSTRACT

**Brayan Steven Moreno Caballero**

**Thesis defense date:** December 2023

Autonomous University of Nuevo León - Grenoble Alpes University

Faculty of Chemical Sciences - Doctoral School IMEP-2

**Research title:** EFFECT OF ETHYL ESTER-MgO MIXTURES ON EMISSIONS OF GASES AND PROPERTIES OF BIODIESEL PRODUCED WITH INCORPORATION OF DEEP EUTECTIC SOLVENTS: ANALYSIS OF ENVIRONMENTAL IMPACT.

**Number of pages:** 144

**Candidate for Doctor in sciences with orientation in sustainable processes and Doctor in fluid mechanics, energy and process**

**Purpose of study:** The main objective of this work is to propose a cleaner methodology to produce biodiesel from wastewater sludge using deep eutectic solvents and to evaluate its environmental impact through life cycle analysis. Additionally, evaluate the effect of ethyl ester-MgO additives on the properties of biodiesel and its emissions.

**Contribution and conclusions:** In this research, a standardized methodology was developed to produce biodiesel from sewage sludge using deep eutectic solvent (DES) as catalyst. The highest obtained yield was 97% using the DES Choline chloride (ChCl): P-Toluene Sulfonic Acid (PTSA) at 0.1 ( $\text{mol}_{\text{DES}}/\text{mol}_{\text{FFA}}$ ), methanol at 10 ( $\text{mol}_{\text{methanol}}/\text{mol}_{\text{FFA}}$ ) respective ratios, 60°C and 4h reaction time. The life cycle assessment emphasizes that biodiesel production using DES as catalysts displays a lower global environmental impact than conventional methodology using  $\text{H}_2\text{SO}_4$ . This, notably because of shorter reaction times, lesser separation/purification stages leading to a reduced electricity consumption and total elimination of hexane throughout the entire process. Density, viscosity, and refraction index of biodiesel blends with ethyl levulinate, ethyl acetoacetate and ethyl pyruvate with a constant amount of 5ppm<sub>m</sub> MgO were experimentally determined over the entire range of compositions and from (288.15 to 333.15) K. Biodiesel-Ethyl ester-MgO mixtures showed viscosity decreases, and density increases with respect to ethyl esters addition. This due to the ethyl esters low viscosities and high densities compared to biodiesel. Biodiesel blends with ethyl ester weight fractions less than 0.2 complied with EN14214 quality standard for biodiesel. These blends could be considered as new potential ecofriendly biodiesel-based blends. The combustion of pure biodiesel and biodiesel + ethyl ester mixtures were simulated in Ansys fluent software. The simulated values of combustion temperature and NO<sub>x</sub> mass fraction decreased up to 1% and 17% respectively with the addition of 0.1 ethyl levulinate mass fraction and 0.0020 kg/s MgO particles because the heat sink effect of the particles. On the other hand, the CO<sub>2</sub> mass fraction increased a 0.78% due to MgO caused increase in the viscosity of the mixtures. Finally, ultrasound irradiation was incorporated to the biodiesel reaction using ChCl:PTSA DES as catalyst at 0.2 ( $\text{mol}_{\text{DES}}/\text{mol}_{\text{FFA}}$ ) and methanol at 10 ( $\text{mol}_{\text{methanol}}/\text{mol}_{\text{FFA}}$ ). It resulted in higher yield of 96.3% with a short time time of 1 hour and lower temperature of 40°C; these reductions were achieved mainly because of the emulsifying effect promoted by the ultrasound.

## 1. INTRODUCTION

In recent times, economic growth and social development have generated an accelerated population increase, it is estimated that the world population will increase from 7400 to 9000 million habitants over the next 20 years [1]. This will generate an increase in energy demand, which nowadays is covered in 95% by fossil fuels [2]. The use of these fuels contributes to global warming and depletion of the ozone layer, due to their non-renewable origin and greenhouse gas (GHG) emissions they produce.

The transport industry is one of the biggest contributors to GHG emissions increase, with 23% of total global emissions. These emissions are mainly composed of carbon dioxide from the use of fossil fuels in vehicle engines [3]. Biofuels represents an alternative to reduce transport sector environmental impact; this due to its renewable origin that makes that GHG emissions are not counted towards the greenhouse gas emissions from the fuel [4] .

The main biofuels are bio hydrogen, bio alcohols, biogas, and biodiesel. Among those, biodiesel have the advantage that its application as a fuel would not imply major changes in the existing technologies of engines and supply centers, it also comes from renewable sources, is biodegradable, its use reduces up to 51% of the CO<sub>2</sub> full fuel-cycle emissions [4], and has a calorific value around 39.76 kJ /kg comparable to Diesel. These conditions favor their use in compression internal combustion engines [5]. However, biodiesel has higher values of density, viscosity,

pour point (PP), cloud point (CP) and surface tension than Diesel, these decreasing the performance of combustion and injection systems of engines.

Density directly influences the volume of fuel fed to the engine, then high density values increase the amount of fuel that is injected into the combustion chamber, causing incomplete combustion problems, and increasing pollutant emissions [6].

High viscosity produces low atomization of biodiesel in the combustion chamber, increasing the energy needed to pump the fuel into the engine, which can cause damage to the pumping system and filters [6].

The atomization of the fuel relies on the surface tension because it determines the degree of dispersion and the formation of droplets, two factors that affect the efficiency of combustion. A low surface tension improves engine efficiency and decreases the emission of pollutants by ensuring full fuel combustion, the product of good atomization [7].

Another important factor about biodiesel is its raw materials source. Nowadays, biodiesel is mainly obtained from vegetable oils (coconut, palm, soybean oils, among others) and animal fats (beef, chicken, pork, and fish fats). However, the disadvantage of these raw materials lies in the economic cost, environmental sustainability, and food security [8]. For this reason, the use of alternative raw materials such as fats obtained from waste from industries such as trails, restaurants and wastewater treatment plants represent a viable option, because they are

available in large quantities, and have almost zero costs (regarding its acquisition as raw material) and do not affect food security.

Wastewater sludge is a waste produced by treatment plants; currently, its disposal and storage represents about 50% of operating costs and so far, none economic viable and environmentally sustainable method has been found [9]. Sludges contain about 60% of different origins of fat [10], and as a waste, it does not have any commercial value, is produced in large quantities and is costly to dispose. Mu et al. [9] highlighted that an average wastewater plant in the United States can generate approximately 3.5 tons of sludge daily. When scaled up nationally, this could yield about 9.54 kt of biodiesel annually, constituting nearly 1% of the USA's yearly biodiesel output. This substantial sewage sludge biodiesel production is projected to lead to a reduction of approximately 27.6 million kg of GHG emissions each year.

In Mexican context, Tacias Pascacio et al. [11] studied residual fat production of the city Tuxtla Gutiérrez in Chiapas state. They found that the city produces 174 tons per year of residual greases that can be converted in biodiesel. . Also, they extended the estimation to the national level and suggested that Mexico could produce 34.9 kt/year of biodiesel from residual fats, with the avoidance of emissions of 92 kt of CO<sub>2</sub>/year.

Residual fats obtained from sewage sludge are projected as an alternative raw material for biodiesel production, because it would contribute to cleaner production and reduction in sludge disposal costs for water treatment plants.

Therefore, this research will study the biodiesel production from fats extracted from wastewater sludge with the aim to study an alternative biodiesel synthesis that could promote a cleaner production.

The production of biodiesel from sewage sludge is achieved with a series of steps that begin with the extraction of fats; commonly using organic solvents such as hexane, generating impacts on the sustainability of the process. Residual fats are mainly composed of free fatty acids and triglycerides, so they must be subjected to two types of processes to obtain biodiesel. The first process is esterification, where free fatty acids are converted to fatty acid methyl esters (biodiesel), as result of this reaction two phases are obtained, the lower phase is a mixture of water and catalyst and the upper phase is a mixture of biodiesel and triglycerides. The biodiesel + triglycerides mixture is taken to a transesterification process to convert triglycerides that were not esterified into biodiesel. Commonly, esterification and transesterification use homogeneous catalysts such as sulfuric acid and potassium hydroxide, respectively [12].

The homogeneous catalysts used in transesterification and esterification have the disadvantage of difficulty separation at the end of the reaction, so they cannot be recovered. Also, the basic homogeneous catalyst promotes the formation of soaps, decreasing the yield [13]. To avoid these problems, the use of heterogeneous catalysts such as calcium oxide CaO represents a better alternative, because it can achieve yields above 90%, can be easily separated at the end of the process, is reusable and comes from renewable sources such as eggshell [14]. However, calcium oxide is susceptible to deactivation due to exposure to the environment and

the presence of free fatty acids, so it requires reactivation by calcination with each use and requires a previous esterification step [15].

Recently, a novel class of catalysts known as ionic liquids (ILs) has gained prominence in biodiesel production. IL consist on ionic mixtures that, for the most part, remains in a liquid state at room temperature. Commonly, IL cations contains nitrogen or phosphorus, such us alkylammonium or alkylphosphonium, respectively. Meanwhile, common anions include halides,  $\text{BF}_4^-$ ,  $\text{NO}_3^-$ ,  $\text{CH}_3\text{CO}_2^-$ , among others [15]. The primary advantage of employing ILs as catalysts lies in their adaptability, wherein specific anion-cation combinations can be tailored to meet specific requirements. For instance, non-miscible compounds can be utilized with reaction products to facilitate easier product isolation. Additionally, compounds that confer basic or acidic characteristics to the IL can be employed. These adjustable properties are particularly advantageous in biodiesel production, given its reliance on esterification and transesterification reactions, where factors like acid character and the miscibility of the reaction medium hold significant importance. [16].

Wu et al. [17] performed biodiesel production from cottonseed oil by using five acidic IL as catalyst. They correlated the reaction yield with the IL acidity finding that the best yield (92%) was obtained by the IL with the higher acidity strength, 1-(4-sulfonic acid) butylpyridinium hydrogen sulfate at methanol:oil:IL molar ratio of 12:1:0.057 at 170°C and 5 h reaction time. On the other hand Han et al. produced biodiesel from waste oils with 94% yield by using acidic IL of 1,4-butane sulfone, the reaction conditions where methanol:oil:IL of 12:1:0.06 at 170°C during 4 h. They reported that high reaction temperatures promoted a better catalytic performance. In

addition to their high yields, ILs come with a significant drawback - their elevated cost in comparison to conventional catalysts. Furthermore, their intricate preparation methods often necessitate the use of volatile solvents, adding to the complexity and environmental considerations in their production [16].

In the last times another alternative have raised to overcome the IL disadvantages, those are the deep eutectic solvents (DES). DES are eutectic mixtures of two pure compounds that forms stable networks by hydrogen bounding associations [18]. Usually, DES are composed of a Hydrogen Bond Acceptor (HBA) such as common halide salts (choline chloride (ChCl), choline acetate (ChAc), methyl triphenyl phosphonium bromide (MTPB), among others) and a Hydrogen Bond Donor (HBD) such as amines, alcohols, carboxylic acids, among others. These compounds represent an option as substitutes for Volatile Organic Solvents (VOCs) in several industrial applications, this due to their natural origin, low cost, simple preparation, and high solvation capacity [19].

One of the biggest advantages of neoteric molecules such as DESs (and Ionic Liquids) is that they can play several roles in a chemical reaction. For biodiesel production, DESs endorse three different roles: (1) solvent to biodiesel purification, (2) cosolvent in reaction media or (3) catalyst.

Some DESs such as ChCl: glycerol, ChCl: ethylene glycol, and MTPB: glycerol, have shown a high efficiency in purification stage, reducing biodiesel's glycerol content at around 0.02 wt%. This is mainly because DESs have high miscibility in glycerol but are immiscible with biodiesel [20].

Some DESs have been also used as co-solvents for biodiesel production to increase the active sites availability of conventional catalyst like CaO and KOH. When ChCl: glycerol is used as cosolvent of CaO, it removes inactive layers formed on the catalyst surface during the reaction [21]. Also, when ChCl: glycerol is combined with NaOH, the presence of DES helps to increase the overall reaction yield by lowering side reactions like saponification [22].

DESs can also be used as catalyst by including an acid as proton donator, like tetra octyl ammonium bromide (TOAB): P-Toluenesulfonic acid (PTSA). TOAB: PTSA DES was used as catalyst for biodiesel production reaching 99.2% of yield, this because the DES enhanced the methanol and oil miscibility, accelerating the interphase (methanol:oil) reaction rate due to its effect as cation surface active agent [18]. The main advantage of this process is that the use of DES leads to high yields under shorter reaction times (between 0.5 and 4 h) compared to the use of conventional catalyst like sulfuric acid (between 6 and 8h) mainly because DES improves the reactive species contact in the reaction media [20].

Based on the above, in this research three different DESs: ChCl: P-Toluenesulfonic acid (ChCl: PTSA), ChCl: oxalic acid (ChCl: OA), and ChCl: citric acid (ChCl: CA) will be evaluated as catalyst for biodiesel production from sewage sludge. This, to find whether these can promote simultaneous transesterification and esterification reactions, decreasing the reaction time and obtaining a biodiesel

cleaner production with respect to the conventional two-step process (esterification-transesterification).

On the other hand, the quality of biodiesel is directly related to its physicochemical properties, which are established by international standards EN 14214 and ASTM 6751, guaranteeing the applicability of biofuel [23]. As mentioned above, biodiesel properties limit its use as a fuel in compression internal combustion engines. However, to improve these properties, the use of compounds such as alcohols, esters, metal oxides, among others as additives of biodiesel has been implemented [24].

Alcohols such as methanol and ethanol are the most widely used additives as they produce improvements in transport properties, however, due to some of their characteristics such as low calorific value, low solubility in all the range of concentrations, low lubricity, and low cetane number negatively affect combustion properties [6]. Additionally, the use of alcohols as additives can increase the cost of biodiesel production, thereby decreasing its competitiveness with diesel.

Short-chain esters such as ethyl levulinate and ethyl acetoacetate represent an alternative to alcohols, as they show high solubility with biodiesel due to their similar composition. Additionally, being products for industrial use, they are available in large quantities, are less costly than some alcohols and are obtained from renewable sources. The implementation of esters as biodiesel additives produces improvements in transport properties such as decreases in viscosity and freezing point, also improves combustion properties by increasing the number of cetane.

However, due to their high oxygen content, the introduction of ethyl esters increases emissions of carbon dioxide and nitrous oxides. This, because they increase the oxygen content of the fuel [24]–[26].

The use of metal oxides particles such as magnesium oxide and titanium oxide as biodiesel additives has shown favourable results to reduce the emissions of polluting gases such as: CO, CO<sub>2</sub>, NO<sub>x</sub>, and particulate matter. This, because the metal oxide nanoparticles supplies additional energy to the fuel, promoting changes in its thermophysical properties like thermal conductivity and heat transfer rate, additionally it promotes a fast oxidation reaction due to large surface to volume ratio between particles and fuel. A lower combustion temperature and better oxidation minimizes the fuel consumption for the same brake power and with this reducing the emissions [27]. Additionally, it has been reported that the use of magnesium and manganese oxides as additives of diesel and biodiesel increases flash point and decreases freezing point because the oxides affect the colligative properties of the mixtures [28] However, these decreases are not as effective as those obtained by using liquid phase additives such as alcohols and esters. Therefore, in this work will be proposed to explore the use of mixtures of magnesium oxide with ethyl esters (ethyl levulinate, ethyl acetoacetate and ethyl pyruvate) to evaluate whether these mixtures produce an additional or combined effect of improvement on the physicochemical properties and gas emissions of the so-called biodiesel.

Mostly research about fuel emissions is made through experimentation on Diesel engines, although needed resources and equipment to perform these studies are rather substantial. Available alternative to perform this kind of analysis can be found through computational fluid dynamics (CFD) analysis, what is an integration of fluids dynamics with numerical analysis and computational science, allowing the study of fluids behaviour through the discretization of the representative geometry of any system and the numerical solution of the mathematical equations that describe the process [29]. CFD software like ANSYS Fluent, can analyze combustion process by calculating parameters like highest combustion temperature and combustion products' mass fraction (CO<sub>2</sub> and NO<sub>x</sub>). This is obtained by solving equations of continuity, momentum, energy, turbulence, and transport by using the system geometry and the fluids thermos-physical properties.

ANSYS Fluent has been already used to simulate Diesel-biodiesel mixtures combustion. Notably, it allowed to calculate combustion temperature as well as gas emissions to determine best possible mixtures' use in a Diesel engine [30], [31]. Some reported studies ([32],[33]) have obtained similar results between simulated and experimental values, showing that CFD combustion simulations can be used to estimate biodiesel combustion characteristics with low variation (around 6.9%) with respect to real Diesel engines. In this work ANSYS Fluent software will be subsequently used to analyze the combustion temperature and gas emissions (CO<sub>2</sub> and NO<sub>x</sub>) of biodiesel + ethyl ester + MgO mixtures, analyzing the problem from a physical approach by using its experimentally obtained thermos-physical properties.

When proposing new methodologies to produce biofuels, it is important to analyze the economic viability and the environmental impact that they may display, to support the benefits and applicability of these fuels, as well as to compare it with existing conventional methodologies and fuels. To carry out this type of analysis there are tools such as life cycle analysis (LCA), which allows to evaluate the environmental impacts and the resources consumption of any process, through environmental impact indicators that allow quantifying the effects produced by the generation of products. For that reason, LCA method will be used to calculate five environmental impact indicators to produce 1 MJ (megajoule) of biodiesel using the method proposed in this work.

The aim of this research is: *i)* to develop a process to produce biodiesel from wastewater sludge using DESs as catalysts. *ii)* To analyze the effect of MgO-ester additives on the physicochemical properties of the biodiesel obtained. *iii)* To simulate the combustion of mixtures comprising biodiesel-ethyl ester-MgO, employing the observed physical properties, and *iv)* to estimate the environmental impacts associated with the DESs catalyzed biodiesel production process.

## 2. BACKGROUND

Biodiesel production processes commonly use vegetable oils as a raw material. 84% of biodiesel is produced from rapeseed oil, 13% sunflower oil, 1% palm oil and 2% from other oils [34]. Although vegetable oils are of natural origin, they represent up to 85% of production costs, decreasing the economic competitiveness of biodiesel compared with traditional fuels without forgetting its affectation to alimentary security. Certainly, utilizing waste materials for biodiesel synthesis has emerged as a sustainable, cost-effective, and socially equitable alternative [35]. The following section provides a selection of pertinent references corresponding to each topic under study in this research.

### 2.1. Biodiesel production from sewage sludge

In 2007, where they extracted lipids content from sewage sludge using hexane, methanol, and acetone molecular organic solvents. The extracted lipids were then converted into biodiesel by using sulphuric acid as catalyst to afford a 6.23% yield based on dried sludge content. In 2009, Mondala et al. [36] produced biodiesel from wastewater sludge through a one-step process, with 5 %v/v  $\text{H}_2\text{SO}_4$  as catalyst and hexane as co-solvent, affording a yield of 14.5% based on extracted lipid after 24 hours of reaction. Years later in 2011 Siddiquee et al. [37] substituted homogeneous  $\text{H}_2\text{SO}_4$  catalyst by a heterogeneous acidic catalyst  $\text{H}_3\text{PO}_4 \cdot 12\text{WO}_3 \cdot x\text{H}_2\text{O}$  (PW12), reported a 34 wt% yield based on extracted lipid

after 3 hours reaction time by using 15%  $PW_{12}$ , however the process is energetically greedy and technically complex as it required temperatures of 135°C and 135 psi pressure. The authors mentioned that studies about reaction optimization and catalyst reuse could improve the process. In 2015, Bi et al. [38] produced biodiesel from sewage sludge through a two-steps method, using firstly homogeneous catalysis with 5 %w/w  $H_2SO_4$  for esterification and secondly 1 %w/w KOH for transesterification. They obtained a 70% yield based on extracted lipid. but the biodiesel purification process required vacuum distillation in order to separate afforded biodiesel from reaction medium containing the unfriendly homogeneous catalysts. Last but not least, Moreno-Caballero et al. (2020) [39] reported an as high as 90% yield based on extracted lipid after 9h from wastewater sludge, using a two-step process by esterification with 3 %v/v  $H_2SO_4$  and transesterification with 0.1 % w/w CaO obtained from eggshell. All of these cited examples highlight rapid progresses in understanding and processing of sewage sludge to enable biodiesel production. However, major problems still rely on the nature, efficiency and recyclability of catalysts and processing operating parameters such as temperature, pressure and time. Greener, cheaper, more environmentally-friendly alternatives to those catalysts are therefore highly demanded and DES may appear as a valuable and plausible one.

## 2.2. Use of DES in biodiesel production

The study of DESs begun with the investigation of Long et al. [40] in 2010, when they proposed a  $\text{ChCl}:\text{ZnCl}_2$  ionic liquid (nowadays known as DES, emphasizing the tiny border between both families) from soybean oil. They obtained 54.52% yield after 72 hours using 10%w DES and attributed this low yield to the weak acidity of the DES. In 2011 Isahak et al. [41] obtained biodiesel from palm oil using with  $\text{ChCl}:\text{ZnCl}_5$  DES, reported a 70.4% yield after only 4h. Additionally, they improved the initial yield to 92% by adding 20 w% of  $\text{H}_2\text{SO}_4$ , showing also potential benefits of combining DES with conventional catalysts. Similarly, in 2013, Huang et al. [21] implemented  $\text{ChCl}:\text{glycerol}$  as a cosolvent and  $\text{CaO}$  as a catalyst in the transesterification of pure rapeseed oil, with a reaction time of 3 hours. Not only they obtained a yield of 92%, but also separation of the products was much easier and the reuse of the catalyst enabled for up to 5 cycles.

Hayyan et al. (2014) used DESs to produce biodiesel from residual raw materials (crude palm oil) using a two-step process. They performed an esterification with 0.75 %w/w DES ( $\text{ChCl}:\text{PTSA}$ ) as catalyst, and then for transesterification used  $\text{KOH}$  as catalyst to reach a total yield of 92%. On the other hand, Manurung et al. (2017) [42] developed a one-step transesterification process starting from palm oil residues by using 4 %w/w DES ( $\text{ChCl}:\text{Glycerol}$ ) as a cosolvent and  $\text{NaOH}$  as a catalyst reaching a maximum yield of 83% together with an easy separation process to isolate biodiesel. More recently, Liu et al. (2020) [18] reported 99.2% yield from waste vegetal oil by using a  $\text{PTSA}$  based DES, at  $70.5^\circ\text{C}$  temperature, 24.6 wt% DES and 12.5 methanol molar ratio. Additionally, they studied the kinetic, finding

that it follows a pseudo-first order, this mainly because methanol was in excess in the reaction but the kinetics showed a first order behavior.

### **2.3. Implementation of additives in biodiesel**

Oxygenated additives such as short-chain ethyl esters have been implemented as additives of biodiesel and diesel-biodiesel mixtures obtaining improvements in transport properties like density and viscosity. Cao et al. [43] prepared biodiesel blends with ethyl acetoacetate (EA) at concentrations from 0 to 20 vol% EA and measured the viscosity (at 313.15K), Cloud point (CP), Pour point (PP), and Flash point (FP). They reported substantial decreases in viscosity, CP, PP and FP values for all the studied mixtures. Joshi et al. (2011) [25] measured viscosity (at 313.15K) CP, PP, and FP values for biodiesel blends incorporating ethyl levulinate (EL) at concentrations from 2.5 to 20 vol% of EL. They also reported reductions of 4-5°C in CP, 3-4°C in PP, at concentrations of 20 vol% (EL) as well as decreases in viscosity (23%) and flash point (43%) values.

Similarly, Lei et al. (2015) [44] studied ternary mixtures of ethyl levulinate-Diesel-biodiesel at concentrations from 0 to 4 vol% EL. They reported decrease of viscosity but a slight increase in density with the increase of ethyl levulinate in the mixtures. Additionally, they found that NO<sub>x</sub> and CO<sub>2</sub> emissions for all blends showed higher values (18.5% for NO<sub>x</sub> and 44.1% for CO<sub>2</sub>) than Diesel emissions. Wang et al. (2017) [45] prepared ethyl levulinate-Diesel-biodiesel ternary mixtures with 5 to 10 vol% EL. Such as previously described article, they also observed a decrease of

viscosity (20.8% decrease at 10 vol% EL), and increase in density (3.9% increase at 10 vol% EL) together with an increase in CO<sub>2</sub> and NO<sub>x</sub> emissions due to the presence of several oxygen atoms in ethyl levulinate.

Magnesium oxide has been also implemented as a biodiesel additive to reduce emissions of polluting gases. Keskin et al (2008) [46], prepared mixtures of biodiesel with magnesium and molybdenum oxides (MoO) at concentrations of 4, 8, and 12  $\mu\text{mol}\cdot\text{L}^{-1}$  and measured the flash point, viscosity (at 313.15K) and the CO<sub>2</sub> and NO<sub>x</sub> emissions in a Diesel engine. They notably reported decreases in the NO<sub>x</sub> (23.19% at 8  $\mu\text{mol}\cdot\text{L}^{-1}$  MoO) and CO<sub>2</sub> (8.82% at 12  $\mu\text{mol}\cdot\text{L}^{-1}$  MgO) emissions. Ranjan et al. (2018) [47] evaluated mixtures of biodiesel with the same additive from 20 to 50 ppm, and noted decreases in CO<sub>2</sub> (1.2% average) and NO<sub>x</sub> (2.67% average) emissions such as for cetane number as well, but also that the use of MgO caused increases in viscosity. Moreno-Caballero et al. (2020) [39] studied densities and viscosities of mixtures of biodiesel with MgO from  $1.6 \times 10^{-6}$  to  $5 \times 10^{-6}$  in mass fraction and from 288.15 to 338.15 K, and reported a maximum reduction of 4% in viscosity and increases in density of less than 1%.

#### **2.4. Biodiesel emissions analysis using CFD.**

Fluid flow systems can be analyzed by computational fluid dynamics (CFD); it allows to have estimations close to the reality. Diesel and biodiesel blends combustion have been analyzed using CFD software. Govindam et al. (2014) [30] have studied Diesel-biodiesel combustion through simulation using the software

ANSYS Fluent, and obtained simulated data for high peak temperature and in-cylinder pressure. The pressure was experimentally validated, and they found a difference below 2% compared with simulated data. Similarly, Dixit et al. (2019) [32] realized a CFD combustion analysis of biodiesel blended with Diesel modelling a cylindrical combustor (250mm x 1800mm) using ANSYS Fluent. The simulation generated contour plots of the combustion temperature at various blend ratios from 0 to 100%, temperature varied from 2100 K to 1100 K, respectively. They concluded that appropriate blend ratio for biodiesel-Diesel blends was with up to 20 vol% of biodiesel, because showed a low temperature of combustion (1750 K), maximum efficiency and lower emissions. However, the simulation was not experimentally validated. Balasubramanian et al. (2021) [31] used Dixit's combustor model to analyze biodiesel-Diesel blends and compared it with real engine emissions. They reported average error between simulated and experimental results around  $\pm 6.9\%$  for CO<sub>2</sub> and 6.7% for NO<sub>x</sub> emissions showing that combustor model can provide emissions predictions near to reality.

## **2.5. Life cycle analysis in biodiesel production from wastewater sludge**

Life cycle analyses (LCA) have been carried out to assess the environmental impacts generated by the production of biodiesel from residual fats. Dufour et al. (2012) [48] evaluated the environmental impact of biodiesel production processes using different raw materials such as: used cooking oil, beef fat, chicken fat and wastewater sludge, and it was observed that for all evaluated environmental

indicators the processes using residual raw materials had lower values than diesel. Mu et al. (2016) [9] performed a LCA of the two-step (esterification and transesterification) biodiesel production process using wastewater sludge as raw material. They concluded that with the implementation of such a kind of greener process in United States wastewater treatment plants would reduce GHG emissions about 27.6 million kg of CO<sub>2</sub>, evidencing the high environmental and economic potential of the process. Hums et al. (2016) [49] realized the LCA of the biodiesel production process by using waste trap grease (WTG) from restaurants as raw material with a bubble column reactor system and sulfuric acid as catalyst for the biodiesel production process. Additionally, the authors compared the environmental impact of the WTG process with biodiesel production using soya oil (SO) and with low sulfur diesel (LSD) production process. They found that the environmental impacts of WTG process were comparable to the one using SO and lower than that of LSD one and concluded that WTG biodiesel could lead to reduces GHG emissions impacts between 20–75% by comparison with LSD process.

### **3. SCIENTIFIC CONTRIBUTION**

The scientific contributions of this project are:

- Proposal of a methodology to produce biodiesel from sewage sludge using deep eutectic solvents.
- Understanding the effect of the implementation of two-phase additives (ethyl esters-MgO) in biodiesel on physicochemical properties and exhaust gas emissions.
- Estimate by life cycle assessment (LCA) methodology the environmental impact generated by the production of biodiesel from wastewater sludge using deep eutectic solvents.

### **4. HYPOTHESIS**

The use of deep eutectic solvents as catalyst will reduce the reaction time and increase the yield of biodiesel production from sewage sludge, thereby decreasing its environmental impact. Likewise, the addition of ethyl esters and MgO as biodiesel additives will enhance its physicochemical properties, contributing to the reduction of its greenhouse gas emissions.

## **5. OBJECTIVES**

### **5.1. GENERAL OBJECTIVE**

Develop a biodiesel production process from sewage sludge using DES as catalyst and determine the effect of the use of ethyl ester-MgO mixtures as additives on the physicochemical properties and simulated exhaust emissions.

### **5.2. SPECIFICS OBJECTIVES**

- Synthesize and characterize acid deep eutectic solvents (DES) by using carboxylic acids as Hydrogen Bond Donors.
- Implement the use of DES as catalysts in the production of biodiesel from wastewater sludge.
- To determine experimentally the physicochemical properties of biodiesel + additive mixtures (ethyl ester-MgO) such as: density, viscosity, refractive index, cetane index, flash point, and calorific power.
- Estimate by numerical simulations the exhaust gas emissions produced by biodiesel + additive mixtures (ethyl ester-MgO).
- To analyze the environmental impact associated with the biodiesel production process from wastewater sludge using eutectic solvents as catalysts by using life cycle assessment.

## 6. METHODOLOGY

This section presents the materials and the methodology proposed for the fulfilment of the general objective and of the specific objectives established in this research project. Figure 1 outlines the followed methodology for the project with a five stages roadmap.

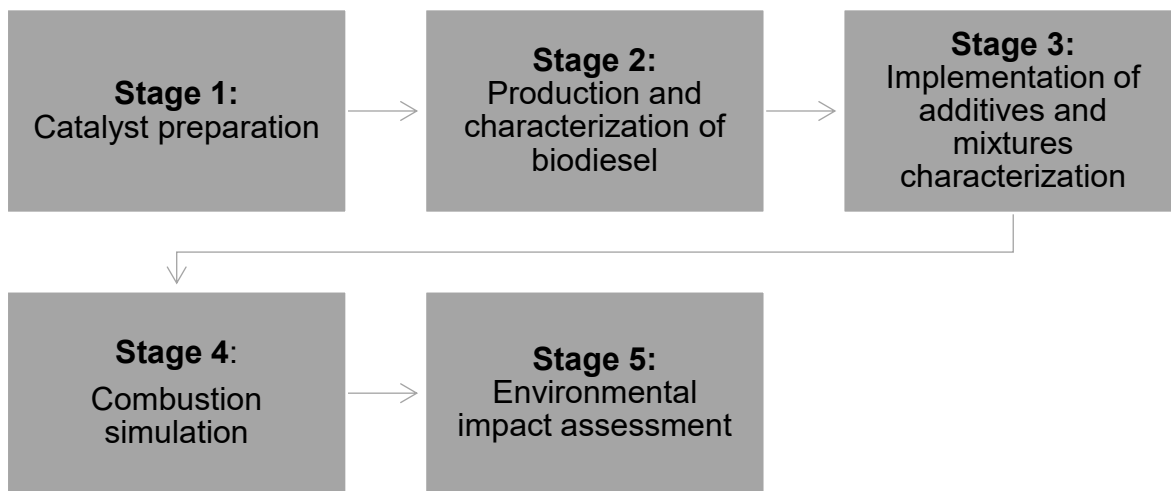


**Figure 1.** Diagram of investigation stages.

### 6.1 Laboratory materials and equipment

In this research, wastewater sludge was used to produce biodiesel; it was obtained from the northeast water and drainage plant of Monterrey, México. The reagents implemented with their purity and identification number are shown in Table 1.

**Table 1.** Reagents used in this research.

<b>Reagent</b>	<b>Purity (Mass fraction)</b>	<b>Brand</b>	<b>No CAS</b>
Methanol	0.990	Merck	67-56-1
Choline Chloride	0.980	Sigma-Aldrich	67-48-1
Oxalic acid	0.975	Sigma-Aldrich	144-62-7
P-toluenesulfonic acid	0.985	Sigma-Aldrich	6192-52-5
Citric acid	0.995	Sigma-Aldrich	77-92-9
Magnesium nitrate hexahydrate	0.981	Sigma-Aldrich	13446-18-9
Ethyl levulinate	0.997	Sigma-Aldrich	539-88-8
Ethyl pyruvate	0.995	Sigma-Aldrich	617-35-6
Ethyl acetoacetate	0.996	Sigma-Aldrich	141-97-9

The equipment used and respective locations are given in Table 2.

**Table 2.** Laboratory equipment.

<b>Equipment</b>	<b>Location</b>
Chromatograph with flame ionization detector (HP 5890A)	Faculty of Chemical Sciences-Food Laboratory
X-ray diffractometer	Faculty of Chemical Sciences
Tensiómetro Sigma 701 de anillo Vibrant Tube Densimeter DMA 5000 Anton Paar Cannon-Fenske Viscometer Muffle thermo scientific thermolyne FB1410M-33	Laboratory of Physiochemistry-Faculty of Chemical Sciences Graduate Division

## **6.2 Experimental Procedure:**

The different experimental and analytical procedures engaged in the five stages of this project are hereafter introduced and described.

### **6.2.1 Stage 1: Catalyst preparation**

Three different DESs to be used as catalysts were synthesized according to published procedures [50] [51] and then. The deep eutectic solvents compounds were dried before use in a furnace at 105°C, during 12 hours. Typically, DES were synthesized by mixing two components: (1) a halide salt (choline chloride) as a base compound and (2) a hydrogen bond donor (PTSA, OA and CA). To form the solvent, both components were mixed gently at 80 °C with constant stirring of 300 rpm for one hour, until a liquid homogeneous mixture was obtained. Moisture was controlled with the implementation of a filter filled with molecular sieve on the top of the reaction flask [21]. Their respective density and refractive index were measured and compared with literature reports to for further confirmation.

### **6.2.2 Stage 3: Biodiesel Production and Characterization**

Biodiesel production form sewage sludge was performed in three stages: (1) grease extraction, (2) biodiesel synthesis, and (3) biodiesel characterization.

For the extraction stage, sewage sludge was filtered using sieves (500 µm) to remove undesired solids they may contain. Then, the filtrated solution was subjected to a process so-called “acid bath”, where the sludge was mixed at a 1:1 volume ratio

with a 6%v/v aqueous solution of sulphuric acid during 1 hour at 60°C to promote the separation of the lipids contained in the sludge. The free fatty acid percentage (%FFA) of the obtained lipids was measured through titration method (AOAC 942.15) by using phenolphthalein as indicator, this to establish the reaction parameters (methanol molar ratio and DES quantity) based on the FFA content of the residual grease.

Biodiesel was produced from the extracted grease through a one-step process. Methanol and grease were added in a constant molar ratio of 10 (mol methanol/mol FFA) to a batch system at a constant temperature of 60 °C. DES was added at different DES: FFA molar ratios between 0.1 and 0.4 (mol DES/mol FFA) to maximize the production of biodiesel. Explored experimental conditions are given in Table 3.

**Table 3.** Reaction conditions for biodiesel production.

DES	Temperature (°C)	Reaction time (h)	Methanol to FFA molar ratio	DES to FFA molar ratio
ChCl: PTSA	60	3	10	0.05
				0.1
				0.2
				0.3
ChCl: OA	60	3	10	0.1
				0.2
				0.3
				0.4
ChCl: CA	60	3	10	0.1
				0.2
				0.3
				0.4

The biodiesel yield was assessed by measuring the reduction of the %FFA content between starting material and resulting product after isolation/purification. To determine the kinetic profile, the reaction time of the experiments displaying best yields was also prolonged up to 8 hours with taken samples every 30 minutes subsequently titrated to measure the %FFA.

The physicochemical properties of pure produced biodiesel were determined using different analytical methods shown in Table 4. Additional properties such as refractive index, density, viscosity, flash point and cetane number were experimentally determined for biodiesel + additive mixtures, and their quality evaluated by comparison with the EN14214 standard.

The density was measured with a DMA 5000 vibrating tube density meter (Anton Paar). A glass tube was filled with the fluid to be analyzed and was subjected to a harmonic electromagnetic force. The oscillation period of the tube, which is related to the density of the fluid, was measured by a built-in oscilloscope,. The density meter was calibrated periodically using dry air and ultra-pure water (density value =  $0.99817 \text{ g}\cdot\text{cm}^{-3}$  at 293.15 K, and resistivity  $\leq 1 \mu\text{S}\cdot\text{cm}^{-1}$ ) as reference fluids [52]. The estimated relative standard uncertainty for density is  $5\times 10^{-4}$ . This value was calculated by error propagation.

To measure the kinematic viscosity, Cannon-Fenske glass capillary viscometers number 75 and 100 were used. The viscometer is a container surrounded with insulating water, controlling the temperature by means of an Isotemp 3016D (Fisher Scientific) recirculating bath. The measurement was made

by accounting the time it takes the fluid to cross two standard marks in the viscometer, the time directly relying on the kinematic viscosity by calibration equations provided by the manufacturer [52]. The estimated relative standard uncertainty for viscosity values is 0.03.

**Table 4.** Analytical methods for the physicochemical properties of biodiesel and the limits established by standard EN14214.

Property	Analysis method	Limits EN 14214
Acid value (mg KOH·g <sup>-1</sup> )	EN 14104	Max. 0.5
Sediment content (% in volume fraction)	EN ISO 12937	Max. 0.05
Flash point (K)	EN ISO 3679	> 393.15
Methanol content (% in mass fraction)	EN 14110	Max. 0.2
Sulfur content (mg/kg)	EN ISO 20884	Max. 10
Iodine value	EN 14111	Max. 120
Density, 15 °C (g·cm <sup>-3</sup> )	EN ISO 12185	0.86-0.90
Kinematic viscosity, 40°C (mm <sup>2</sup> ·s <sup>-1</sup> )	EN ISO 3104	3.5-5.0
Calorific value (MJ·kg <sup>-1</sup> )	ASTM D-240	Not reported
Cetane index	ASTM D-4737	Min. 51
Distillation (K, 98% in volume fraction recovered)	ASTM D-86	Not reported

Refractive index was measured with an Abbemat 300 refractometer; the sample was located on a prism radiated by a LED from different angles. The refractometer measured the critical angle of total reflection and, from this value, the refractive index (IR) of the sample was determined. The estimated relative standard uncertainty for refractive index is  $2 \times 10^{-4}$ .

The flash point was determined within a Pensky-Martens meter of closed cup (K16203, Koehler); the measurement consists of increasing the temperature of the studied fluid while in contact with an ignition source to reach the spontaneous ignition temperature [53]. The estimated standard uncertainty in the flash point is 1 K.

Calorific value was measured using a bomb calorimeter (Parr, 6200) according to the ASTM D-240 norm. The sample cup was filled with 1 g of fuel and placed inside the steel pump where the fuel sample ignited in the presence of oxygen at 3 MPa. The exothermic combustion reaction increases the temperature inside the bomb and transfers energy to the pump jacket. The calorific value was calculated in terms of the rise in temperature and the mass of the fuel sample. The estimated standard uncertainty in the calorific value is 0.2 MJ/kg.

The cetane index was calculated with ASTM D-4737 method, using the sample density (EN ISO 12185) and the distillation curve (ASTM D-86) temperatures recorded at 10, 50, and 90% of the volume recovered. Distillation curve was measured with a petroleum product distillation tester (TBT-6536A). The estimated standard uncertainty in the cetane index is 0.4.

#### **6.2.4 Stage 4: Additive implementation and additive-biodiesel mixtures characterization**

In this research, a biphasic additive was used. Whereas the liquid phase was a short-chain ethyl ester, the solid phase was magnesium oxide powders dispersed into the liquid phase.

Magnesium oxide was obtained using a hydrothermal synthesis. Magnesium nitrate  $\text{Mg}(\text{NO}_3)_2 \cdot 6\text{H}_2\text{O}$  was used as precursor and sodium hydroxide solution of 0.1M as solvent. The reaction was ran for 2 hours at 180 °C in an autoclave to afford  $\text{Mg}(\text{OH})_2$ , which was then calcined in a muffle to obtain MgO [54].

Biodiesel was mixed with MgO and three different ethyl esters (ethyl levulinate, ethyl acetoacetate and ethyl pyruvate) with a constant concentration of 5 ppm mass ( $\text{ppm}_m$ ) of MgO, but with biodiesel-ethyl ester mass fraction varied from 0 to 1. To obtain the biodiesel-Ethyl levulinate-MgO mixtures, small amounts of MgO were weighed on a microbalance (model XPR10, Mettler Toledo) with a resolution of 0.001 mg, linearity deviation of 0.003 mg and repeatability of 0.0004 mg. To ensure a vigorous and efficient mixing, each ternary mixture was submitted to ultrasonic irradiation in an ultrasonic bath (model Bransonic MH, Fisher scientific, 40 kHz) for 30 minutes. Mixtures were stored in transparent glass containers to check oxide powder agglomeration and before all the measures the mixtures were again putted in ultrasonic bath for 15 minutes to homogenize it. So-called mixtures were then characterized in accordance with the procedures set out in step 3.

### **6.2.5 Stage 5: Combustion simulation**

For the combustion analysis, a cylindrical combustor (Figure 2) was simulated in Ansys Fluent following the methodology reported by Dixit et al. [32], whose used a 2D axisymmetric geometry to perform combustion analysis of Diesel-Biodiesel mixtures. The system's 2D geometry is showed in Figure 2, the whole domain was

discretized using fine mesh generation. Then, fuel and air fluxes were applied using boundary conditions, the fuel entered into the combustor through a small nozzle placed at the center of the cylinder at 50 m/s while ambient air at 0.5 m/s coaxially.

In order to simulate biodiesel combustion within the combustion chamber, it is essential to account for the mixing and transport of chemical species. Ansys facilitates this by solving conservation equations that address convection, diffusion, and reactions for each species present in the fluid. This combustion is a turbulent flame, which is the most common kind of flame for internal combustion engines and industrial burners. Where fuel and the oxidizer enter into the combustion chamber in turbulent flows to improve its mixing process [55].

In turbulent flames simulation, Ansys considers two model options: Non-premixed model (NPM) and Species Transport Model (STM). The choice between the two models depends on the desired level of accuracy and the available computational capacity. STM allows a clear understanding about chemical reactions by predicting the local mass fraction of each specie opposite to NPM that solve the system transport equations for one or two conserved scalars (the mixture fractions) [56]. Given that the primary goal of this simulation is to analyze the combustion emissions of biodiesel mixtures, the STM model was selected for its capacity to deliver a more precise calculation of combustion products, fuel consumption, and the transport of these species within the combustion chamber.

The STM model predicts the local mass fractions in the simulated system through solving convection-diffusion equation of each specie like showed in Equation 1.

$$\frac{\partial}{\partial t}(\rho Y_i) + \nabla \cdot (\rho \vec{v} Y_i) = -\nabla \cdot \vec{J}_i + R_i \quad (1)$$

Where  $Y_i$  is the local mass fraction on specie  $i$ ,  $\rho$  is the density, and  $\vec{v}$  is the velocity. The terms in the left, represents the rate of change of the species and the convective transport, respectively. The right side the terms represent the diffusion flux of the species ( $-\nabla \cdot \vec{J}_i$ ) and the production rate of species ( $R_i$ ) [56].

The production rate of species is calculated using a combustion chemistry model known as the Eddy Dissipation Model (EDM). This model accurately predicts the combustion chemistry, accounting the effects of temperature and species concentration fluctuations induced by the turbulent flow. EDM utilizes the rate of dissipation of eddies (fluid swirls) containing reactants and products to determine the reaction rates [57], the EDM model calculates the reaction rate of reaction  $r$  ( $R_{i,r}$ ) as the minimum value of the Equation 2 and Equation 3.

$$R_{i,r} = v'_{i,r} M_{w,i} A \rho \frac{\varepsilon}{\kappa} \frac{Y_R}{v'_{R,r} M_{w,R}} \quad (2)$$

$$R_{i,r} = v'_{i,r} M_{w,i} A B \rho \frac{\varepsilon}{\kappa} \frac{\sum_P Y_P}{\sum_j v'_{j,r} M_{w,j}} \quad (3)$$

Where  $Y_R$  is the mass fraction of any product specie,  $Y_p$  is the mass fraction of any reactant,  $\nu'_{R,r}$  stoichiometric coefficient of product  $j$  in reaction  $r$ ,  $M_{w,R}$  molecular weight for reactant  $R$ ,  $\varepsilon$  is the turbulent dissipation,  $\kappa$  is the turbulent energy,  $\rho$  is the fluid density,  $A$  is an empirical constant, and  $B$  is an empirical constant. For combustion in turbulent flames  $A$  is 4.0 and  $B$  is 0.5.

The energy changes in the system are calculated by using the energy equation as:

$$\frac{d}{dt}(\rho H) + \nabla \cdot (\rho \vec{v} H) = \nabla \cdot \left( \frac{k_t}{c_p} \nabla H \right) + S_h \quad (4)$$

Where  $\rho$  is the mixture density,  $\vec{v}$  is the mixture velocity,  $H$  the enthalpy,  $k_t$  the thermal conductivity,  $c_p$  is the specific heat capacity. The terms in the right side of the equation represents the enthalpy variation and the enthalpy due to convective transport respectively. On the left side, the first term represents the conductive-diffusive term and  $S_h$  includes reaction heat or other external heat sources.

To include the effect of solid particles in the fluid the Discrete Phase Model was used. This model calculates the trajectory of the particles in the fluid by making a force balance on the particle, using an Eulerian-Lagrangian frame, for x direction in Cartesian coordinates is expressed as:

$$\frac{dv_p}{dt} = F_D(v - v_p) + \frac{g_x(\rho_p - \rho)}{\rho_p} + F_x \quad (5)$$

$$F_D = \frac{18\mu C_D Re}{24d_p^2} \quad (6)$$

Where  $v$  is flow phase velocity,  $v_p$  is the particle velocity,  $g$  is gravity,  $\rho$  is fluid density,  $\rho_p$  is particle density,  $C_D$  is the drag coefficient,  $Re$  is the Relative Reynolds number, and  $d_p$  is the particle diameter. In the right side of the equation the  $F_D$  term is the drag force related with the relative velocity, the second term is related with the gravity force component and  $F_x$  represents another external forces that could be applied to the particle motion.

For this simulation, only the physical effects of the particle will be considered this mainly to the lack of information in the literature about the chemical effect of the metal particles on the fuel combustion. Based on this only the heat transfer model of the DPM was used, this model calculates the inert heating or cooling of the particles in a fluid by using a heat balance (Equation 7) to relate the particle temperature ( $T_p$ ) to the convective heat transfer.

$$m_p c_p \frac{dT_p}{dt} = h A_p (T_\infty - T_p) \quad (7)$$

Where  $m_p$  is the mass of the particle,  $c_p$  is the heat capacity of the particle,  $h$  is the convective heat transfer coefficient,  $A_p$  is the surface area of the particle,  $T_\infty$  is the local temperature of the fluid phase and  $T_p$  is the temperature of the particle.

Initially, we simulated the combustion of Diesel, obtaining data profiles (combustion temperature and exhaust gases mass fraction), and compared the results with those reported by Dixit et al. [32] to validate the simulation. After that the

biodiesel-Ethyl ester mixtures that complied with the EN14214 in the experimental stage were simulated.

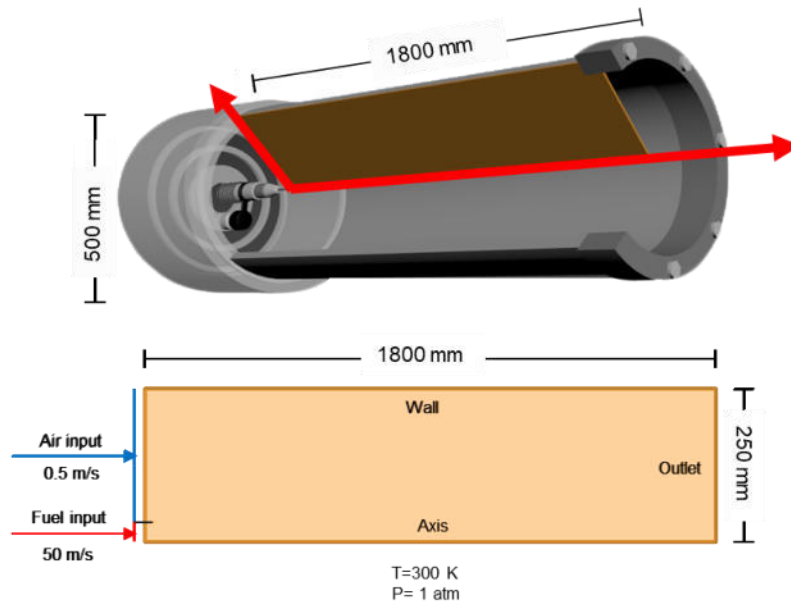


**Figure 2.** CFD geometry for combustion analysis [32].

In the simulation, mixtures of biodiesel, ethyl esters, and MgO were incorporated using the materials interface of ANSYS Fluent. Where properties such as density, viscosity, and specific heat capacity were input into the software based on a combination of experimental data from the additive implementation step (stage 4) and literature sources. To account for the presence of MgO nanoparticles, we employed the Discrete Phase Model (DPM) to analyze inert heat transfer. The chemical effect was not considered, given the absence of a comprehensive reaction mechanism for MgO additives. Consequently, available data for a chemical simulation in current studies on nanoparticle combustion was limited. The average

MgO particle size (16.1  $\mu\text{m}$ ) was input into the simulation based on data obtained in a previous study [39].

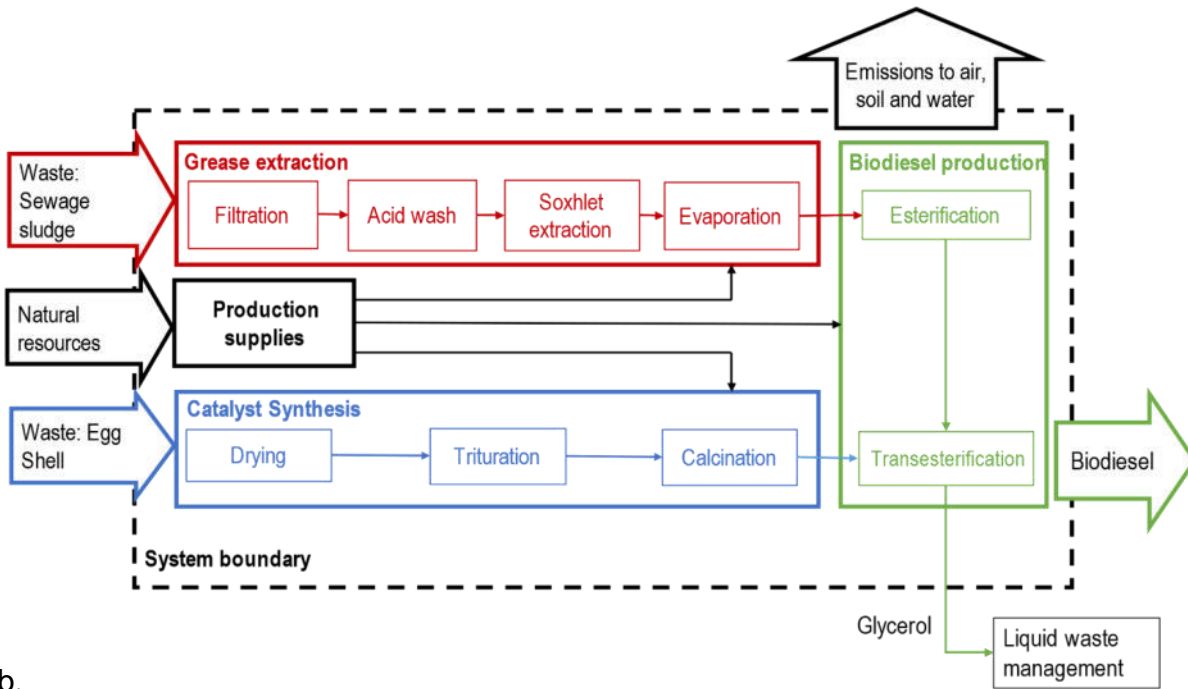
### **6.2.6 Stage 6: Environmental Impact Assessment**

An environmental impact assessment of biodiesel production from wastewater sludge using deep eutectic solvents was conducted using ISO 14044 method. The method establishes four LCA stages: goal and scope definition, inventory analysis, impact assessment and interpretation of results. Each LCA stage will be detailed below.

The goal of the LCA was to evaluate the environmental impact generated by the production of biodiesel on a laboratory scale, using wastewater sludge as raw material with the implementation of deep eutectic solvents as catalyst. 1 MJ of biodiesel was used as a functional unit (FU).

Three scenarios were evaluated to analyse if the use of DES in biodiesel production reduces the environmental impact when compared with a process using conventional catalysts. The base scenario (scenario A) was two-step process (esterification and transesterification) based on methodology reported by Moreno-Caballero et al. [39] using sulphuric acid and calcium oxide as successive catalysts. The other two scenarios were based on the one-step biodiesel production methodology proposed in this research by using two different DES as catalyst: ChCl: PTSA for scenario B and ChCl: OA for scenario C. Flux diagram and system boundaries for the three scenarios are showed in Figure 3.

a.



b.

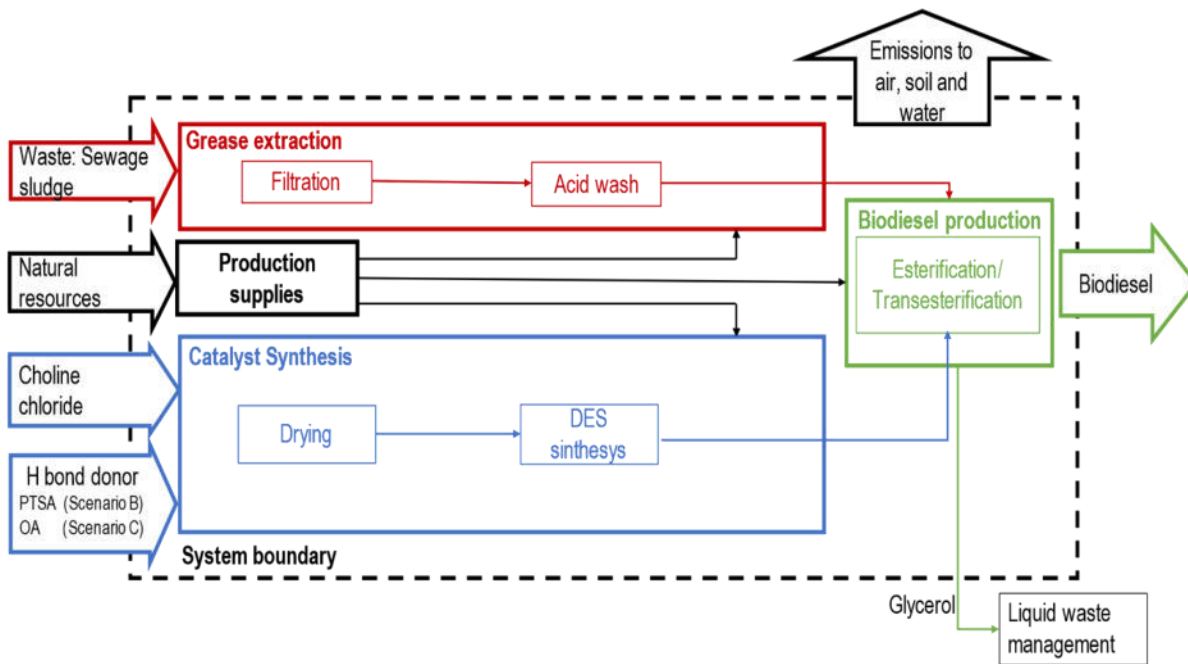


**Figure 3.** Boundary diagram for: (a) Scenario A; (b) Scenarios B and C.

The environmental inventory was compiled using experimental data across three scenarios. For each scenario, we calculated energy and mass inputs and

outputs based on Functional Unit (FU). Mass quantification relied on experimentally obtained mass yields for the process stages of each scenario, while energy requirements were determined using specific equations. These equations covered sensible heat (Equation 8) for stages involving material heating, latent heat (Equation 9) for phase changes, and maintaining heat (Equation 10) for processes requiring temperature stability over a defined period.

$$Q = m \cdot C_p \cdot \Delta T_1 \quad (8)$$

$$Q = m \cdot \lambda_{vap} \quad (9)$$

$$Q = U \cdot A \cdot \Delta T_2 \cdot t \quad (10)$$

Where  $m$  is total mass,  $C_p$  is the heat capacity,  $\Delta T_1$  is the temperature difference between ambient and system,  $\lambda_{vap}$  is the latent heat of vaporization,  $U$  is the heat transfer coefficient,  $A$  is the heat transference area,  $t$  is the time, and  $\Delta T_2$  is the temperature difference between heating source and heated system. Indeed, it's worth mentioning that all scenarios showed minimal gas emissions, primarily because methanol and hexane gases were effectively condensed, preventing any notable releases. Moreover, in the case of hexanol, it was recycled. As for the solid residues produced during the grease extraction stages, they were properly managed in line with the hazardous waste management program established at the Autonomous University of Nuevo León [58]. Due to this effective handling, gas and solid emissions from the process were not included into the Life Cycle Assessment (LCA) calculations.

The LCA was carried out by using an attributional approach, utilizing the SimaPro version 8.3 software to construct the assessment model. The LCA inventory results were analyzed using the ReCiPe 2008 method [18], which condenses the environmental inventory results into a set of indicator scores that represent the comparative magnitude of the environmental impact categories.

Five environmental impact midpoint indicators scores were evaluated: climate change (CC), terrestrial acidification (TA), ozone depletion (OD), freshwater eutrophication (FE), and fossil depletion (FD). Data for materials production and electrical generation were taken from the EcolInvent v3.1 database.

## 7. RESULTS

In this section, results obtained from each stage of the methodology are presented.

### 7.1. Stage 1: DESs synthesis

Three DESs (ChCl: PTSA, ChCl: OA and ChCl: CA) have been successfully prepared according to the previously described methodology. All DES were obtained from solid phase choline chloride and solid Hydrogen Bond Donors PTSA, OA and CA at molar ratios of 2 ( $\text{mol}_{\text{PTSA}}/\text{mol}_{\text{ChCl}}$ ), 1 ( $\text{mol}_{\text{OA}}/\text{mol}_{\text{ChCl}}$ ) and 0.4 ( $\text{mol}_{\text{CA}}/\text{mol}_{\text{ChCl}}$ ), respectively. At the end of the synthesis, all the DESs were transparent showing a homogeneous phase. Whereas ChCl: PTSA and ChCl: OA were completely fluid at room temperature, ChCl: CA showed an almost solid character at room temperature, but turned to liquid estate for temperatures over 40°C, this being due to the high melting point of the citric acid (156°C) [59]. The homogeneous and fluid character of the three DES evidences the melting point depletion characteristic of the eutectic mixtures and confirms the DES formation. The melting point decrease occurs due to interactions between HBD molecules and choline chloride anions. Those interactions increase the anions effective size, decreasing their interaction with cation and leading to the melting point depression [60].

Densities and refractive index of ChCl: PTSA and ChCl: OA were measured and compare with literature data to verify DESs formation. However, for ChCl: CA the density and refractive index measurements were not possible due to the DES's

high viscosity (almost solid consistence) rendering difficult to obtain reliable data with available equipment. However, some researchers have also reported this behaviour when CA is used as HBD for DES formation [59], [61].

For other DES, density was measured using Anton Paar Vibrant Tube Densimeter DMA 5000 from 288.15 to 338.15 K at atmospheric pressure. On the other hand, refractive index was measured with an Anton Paar digital refractometer Abbemat 350 at the same conditions. Table 5 shows the average absolute percentage deviation (AAPD) between our densities and refractive indices values and those reported in literature [51]-[62]. The AAPD was calculated as,

$$AAPD = \frac{100}{N} \left( \sum_{i=1}^N \frac{|J_i^{exp} - J_i^{lit}|}{J_i^{exp}} \right) \quad (11)$$

where  $J_i^{exp}$  and  $J_i^{lit}$  are the experimental measurements and reported values in the literature, respectively, and  $N$  is the total amount of data. All DESs density showed similar values those reported in literature, within average absolute percentage deviations (AAPDs) of 0.38 and 1.69% for ChCl: PTSA and ChCl: OA, respectively. As well as density, the refractive index values showed low deviations compared with literature with AAPDs of 0.30% for ChCl: PTSA and 0.56% for ChCl:OA. The low deviations on the two evaluated properties allowed to confirm that we successfully synthesized deep eutectic solvents.

**Table 5.** Density and refractive index comparison with literature reports for obtained DES.

DES	Literature	Temperature range (K)	AAPD (%)
	<i>Density (g·cm<sup>-3</sup>)</i>		
ChCl: PTSA (1:2)	Cui et al. [51]	288.15 – 338.15	0.49
	Zhu et al. [63]	298.15	0.24
		318.15 – 333.15	0.40
	Rodriguez et al. [64]		
ChCl: OA (1:1)	Florindo et al. [65]	293.15 – 338.15	1.42
	Saha et al. [66]	298.15 – 338.15	1.95
ChCl: CA (1:0.4)	Non available		
	<i>Refractive Index</i>		
ChCl: PTSA (1:2)	Cui et al. [51]	288.15 – 338.15	0.30
ChCl: OA (1:1)	Florindo et al. [65]	293.15 – 338.15	0.18
	Abbott et al. [50]	298.15	0.27
	Jablonosky et al. [62]	298.15	1.22
ChCl: CA (1:0.4)	Non available		

## 7.2. Stage 2: Biodiesel Production and Characterization

The free fatty acid percentage (%FFA) of the grease extracted from the raw sewage sludge was measured by titration method (AOAC 942.15) and was found to be 81.1%. Once the initial %FFA value was determined, the experiments in Table 3 were performed according to the proposed methodology. As biodiesel is the product of the esterification of the FFAs contained in the grease, the yield of each experiment was evaluated by measuring the decrease in the %FFA as shown in Eq. 12.

$$Yield = \left( 1 - \frac{\%FFA_{after-reaction}}{\%FFA_{grease}} \right) \times 100 \quad (12)$$

Where  $\%FFA_{grease}$  is initial %FFA of the grease (81.14%) and  $\%FFA_{after-reaction}$  is the %FFA at the end of the reaction.

The biodiesel yield obtained in experiments with ChCl: PTSA are shown in Figure 4. The yield increases with increasing in the DES ratios from 0.05 to 0.1 where it reaches a 97.01% value and for DES ratios greater than 0.1 the yield value keeps constant. This could because reaction have leads to equilibrium at that point. On the other hand, ChCl: OXA (Figure 5) and ChCl: CA (Figure 6), showed a parabolic behavior. This probably because an excess of DES in the reaction can increase the viscosity of the reaction medium, hindering the mass transfer between the grease and methanol and reducing the yield [18]. It can be noted, that the parabolic behavior is more pronounced for ChCh: citric acid that this DES have a considerable higher viscosity value than the other two DES, evidencing the viscosity effect on the reaction yield.

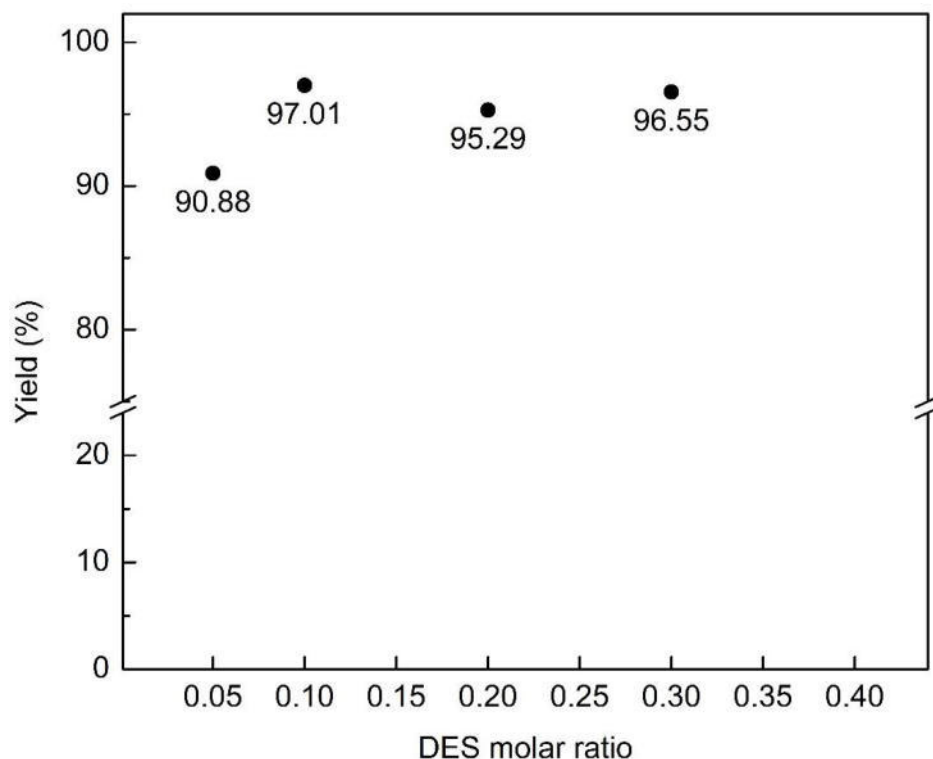


**Figure 4.** Effect of ChCl: PTSA molar ratio (mol DES/mol FFA) on biodiesel yield at methanol ratio 10 (mol methanol/mol FFA), temperature 60°C and time 3h.

Experiments at conditions showed in Table 3 for ChCl: OA and ChCl: CA were also performed by using 10 (mol methanol/mol FFA). However, at that methanol ratio, the yields of the reactions barely reached values over 43% and 0% for ChCl:OA and ChCl: CA respectively. This decrease of yield according to the used DES matches our previous hypothesis that their high viscosity was increasing the reaction media viscosity and substantially decreasing the mass transfer. To tackle this, the methanol ratio was increased from 10 (mol methanol/mol FFA) to 15 (mol methanol/mol FFA). Both following Figure, Figure 5 and Figure 6, displays results obtained with ChCl: OA and ChCl:CA DES respectively.

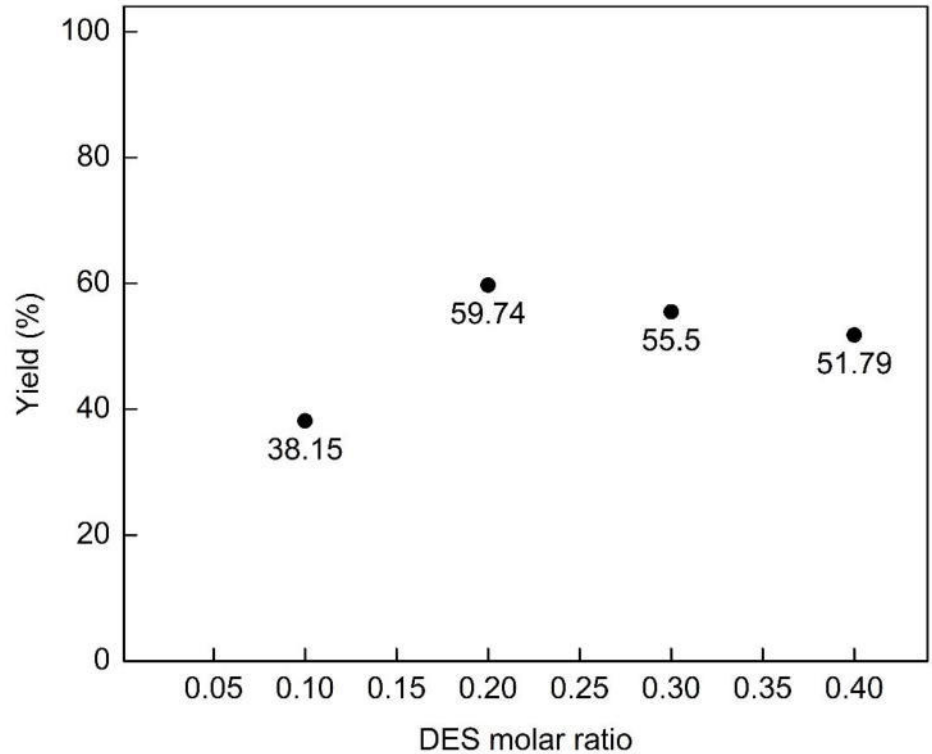


**Figure 5.** Effect of ChCl: OA molar ratio (mol DES/mol FFA) on biodiesel yield at methanol ratio 15 (mol methanol/mol FFA), temperature 60°C and time 3h.

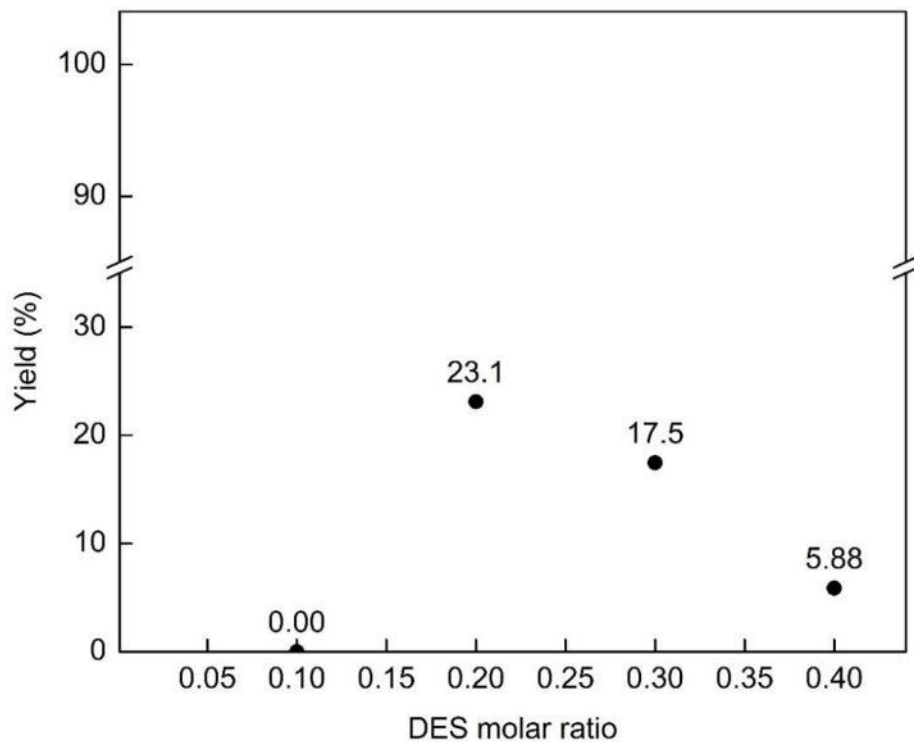


**Figure 6.** Effect of ChCl: CA molar ratio (mol DES/mol FFA) on biodiesel yield at methanol ratio 15 (mol methanol/mol FFA), temperature 60°C and time 3h

The yield increase for DES molar ratios from 0.1 to 0.2 to reach 59.74% (Figure 5) and for DES molar ratios greater than 0.2 the yield reduces to 51.79% for ChCl:OA one. Whereas similar trend is shown with ChCl:CA DES but definitely with less conversion yield, probably emphasizing also the less acidity of citric acid as compared to oxalic acid or paratoluene sulfonic acid.

The results of the experimentation indicates that the most effective DES for biodiesel production is ChCl: PTSA with a yield of 97.01% at 0.1 (mol DES/mol FFA) and 10 (mol methanol/mol FFA). Subsequently, ChCl: OA with yield of 59.74% at 0.2 (mol DES/mol FFA) and 15 (mol methanol/mol FFA), and then ChCl: CA with yield of 23.10% at 0.2 (mol DES/mol FFA) and 15 (mol methanol/mol FFA).

The trend obtained for biodiesel yields can be explained through two distinct effects of DESs in the reaction. Firstly, the catalytic effect, which is related with the acidity exhibited by the HBD of the DES couple. It promotes esterification/transesterification reactions through a three steps mechanism: (1) the carbonyl group changes into a carbocation by DES protonation, (2) the carbocation undergoes a nucleophilic attack from methanol, forming an intermediate (3) the decomposition of the intermediate into an ester and release of the  $H^+$  for the next cycle [18].

The second effect is a physical effect, which is mainly related with the mass transfer increase that DES bring out to the reaction media. The lipophilic nature of DES promotes the contact between grease and methanol, decreasing the interphase tension [18]. This can be explained by liquid-liquid equilibrium between two ternary

systems: DES + Alcohol + Ester (Biodiesel) and DES + Alcohol + carboxylic acid (fats).

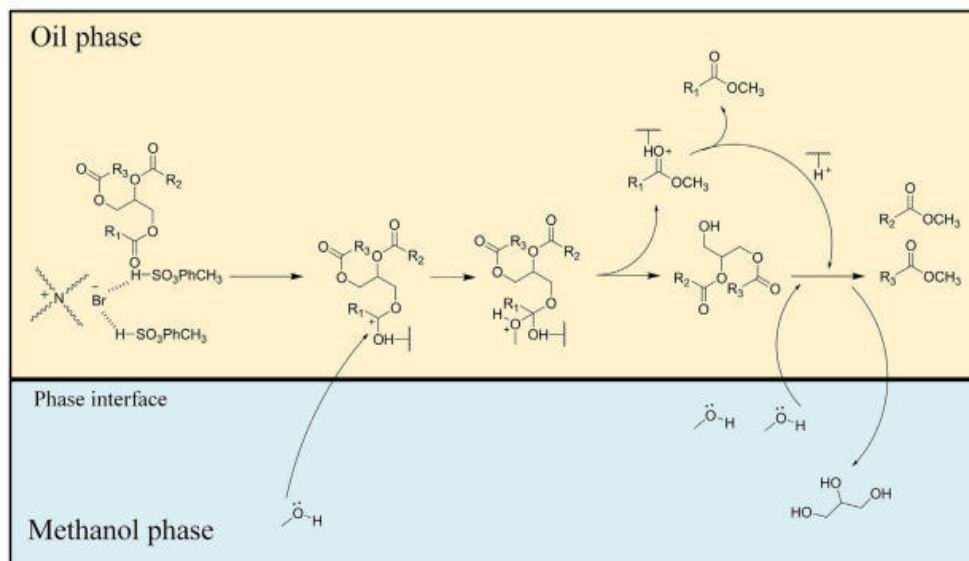


**Figure 7.** Esterification mechanism by using DES (TOAB:PTSA) as catalyst proposed by Liu et al. [18]

In Figure 8a, the liquid-liquid equilibrium diagram for the system DES + Butyl hexanoate (BuHE) + Hexanoic acid (HeAc) is presented. It exhibits a negative slope in the tie lines, indicating the stronger affinity of the HeAc for BuHE compared to the DES. Additionally, a large immiscible gap is observed, suggesting that varying HeAc dosage has a minor impact in the phase splitting. Furthermore, Figure 8b (BuHE + BuOH + DES system) displays tie lines with a positive slope, signifying that BuOH exhibits greater solubility in the DES than in BuHE. Moreover, the smaller immiscible gap in Figure 8b implies that BuOH dosage can significantly influence phase separation. Upon analyzing both systems, it evidences that the poor miscibility

between DES and BuHE accounts for the pronounced repulsion observed between them [67].

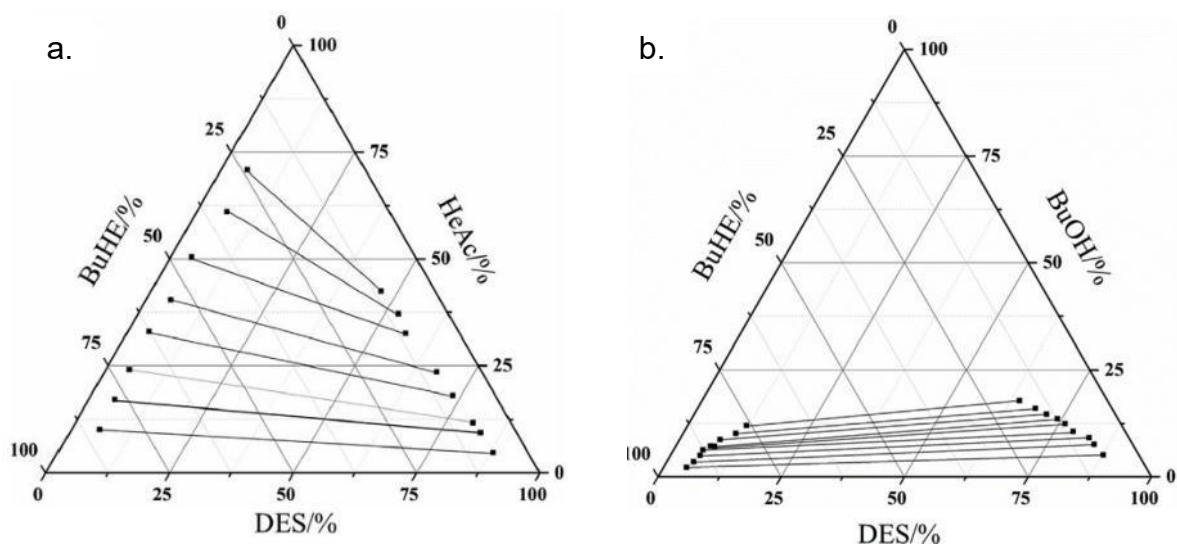


**Figure 8.** Liquid-Liquid equilibrium for ternary system: a) BuHE + HeAc + DES , b) BuHE + BuOH + DES [67]

The Liquid-Liquid diagrams evidences the DES capacity to form a homogeneous phase with alcohol (BuOH) and carboxylic acids (HeAc), facilitating the contact between the reactants and the catalyst, thereby enhancing the esterification reaction rate. Additionally, the ester (BuHE) is separated from homogeneous phase due to its poor miscibility with DES, this mechanism have been proposed by Zhou et al. [67] as shown in Figure 9.

To correlate the reaction yields with some DES properties related with mass transfer we have measured the viscosity at 60°C and found that ChCl: PTSA is the less viscous with 79.93 mPa·s followed by oxalic acid with 309.32 mPa·s. Additionally, we have performed and a HLB (Hydrophilic-Lipophilic Balance) by using the Davies method [68] to analyze hydrophilic (polar) and lipophilic (non-polar)

character of the DESs. The obtained values were 7.91, 8.40, and 8.49 for ChCl: PTSA, ChCl: OA, and ChCl: CA, respectively. This indicates a hydrophilic/lipophilic nature for the three DESs however the ChCl: PTSA showed the lower value indicating better affinity with lipophilic species, allowing it to better interact with the grease phase in the reaction media. Moreover, to further confirm the acidic catalytic effect of the DES, the acidity of their precursors HBDs have been reported in the literature, being the PTSA the most acid with a pKa of -2.8 followed by OA (pKa: 1.25) and CA (pKa: 4.14) [59] .

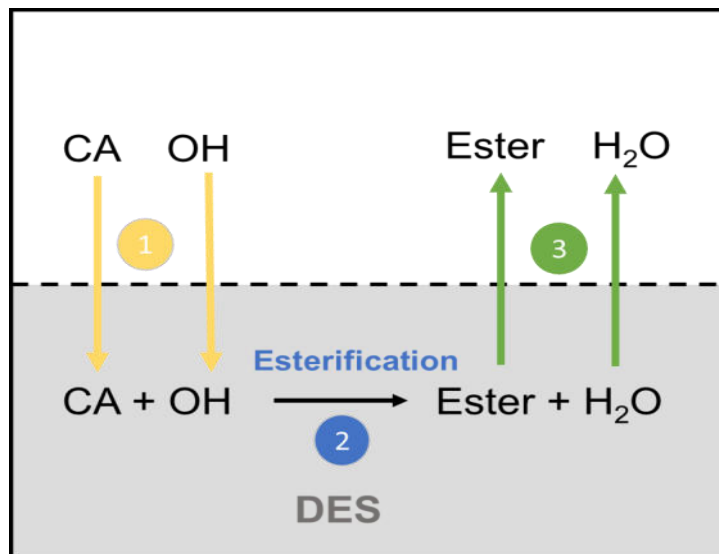


**Figure 9.** DES mass mechanism adapted from Zhou et al. [67] (CA: Carboxylic acid, OH: Alcohol)

Based on the above, the highest yield (97%) obtained using ChCl: PTSA is due to the DES physical effects because of its lowest viscosity and higher lipophilic character and its catalytic effect due to its higher acidity when compared with ChCl:OA and ChCl:CA.

Finally, the impact of reaction time on the conversion yield has been also studied for ChCl: PTSA and ChCl: OA, with respective results shown in Figures 10-11. In Figure 10 the reaction yield for ChCl: PTSA increases with time up to 4 hours reaching 98.8% and then reaches a plateau with no more significant change in yield values.. The same behavior can be observed in Figure 11 for ChCl: OA where the yield increases the first 6 hours to reach a 56% value followed by a plateau.

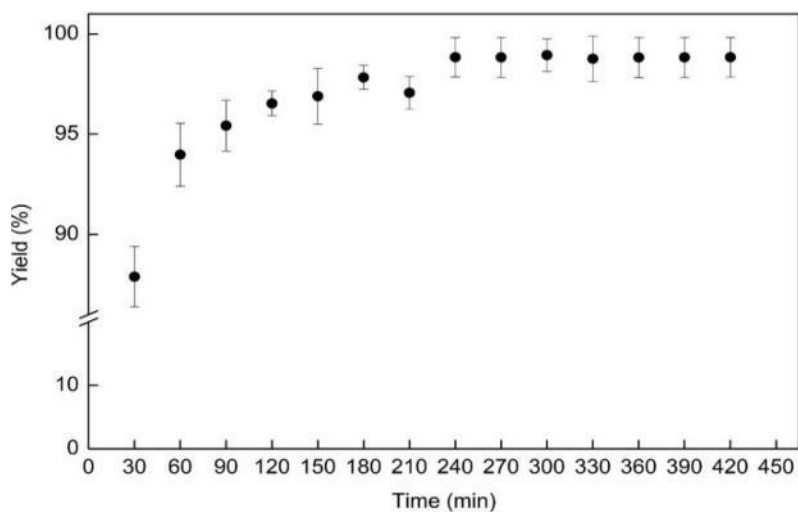


**Figure 10.** Effect of time for ChCl: PTSA on biodiesel yield at 0.1 (mol DES/mol FFA), methanol ratio 10 (mol methanol/mol FFA), and temperature 60°C.

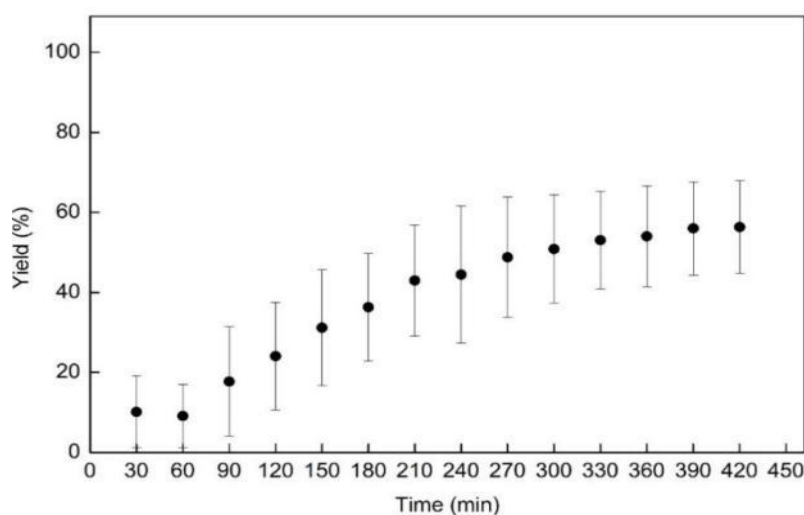


**Figure 11.** Effect of time for ChCl: OA on biodiesel yield at 0.2 (mol DES/mol FFA), methanol ratio 15 (mol methanol/mol FFA), and temperature 60°C.

The samples obtained from the experiments with ChCl: PTSA and ChCl: OA were characterized by using gas chromatography (AOAC 969.33) to obtain the fatty acid profile (Table 6). The predominant methyl esters were palmitate, oleate, linoleate and stearate what is match with the typical composition of biodiesel [69].

**Table 6.** Fatty acid profile for biodiesel produced by using different catalysts.

<b>Fatty acid methyl ester</b>	<b>Biodiesel ChCl:PTSA (w)</b>	<b>Biodiesel ChCl:OA (w)</b>	<b>Biodiesel H<sub>2</sub>SO<sub>4</sub>-CaO (w)</b>
Methyl butyrate	0.0014	0.0000	0.0033
Methyl hexanoate	0.0000	0.0019	0.0043
Methyl tridecanoate	0.0000	0.0000	0.0584
Methyl undecanoate	0.0029	0.0037	0.0000
Methyl myristate	0.0319	0.0344	0.0000
Methyl palmitate	0.4030	0.4129	0.4279
Methyl oleate	0.4135	0.2270	0.2689
Methyl linoleate	0.1029	0.2054	0.0000
Methyl stearate	0.0000	0.0000	0.1749
Methyl arachidate	0.0103	0.0715	0.0000
Methyl-gamma-Linolenate	0.0281	0.0229	0.0000
Methyl tricosanoate	0.0060	0.0150	0.0399

w: mass fraction

### 7.3. Stage 4: Biodiesel-Ethyl levulinate-MgO mixtures characterization

Characterization of biodiesel + ethyl esters + MgO mixtures are showed next. Due to delays on sewage sludge collection related with the COVID-19 emergency, these mixtures have been prepared with biodiesel from a similar raw material (beef tallow) as some studies showed that sewage sludge biodiesel had similar properties than the one from beef tallow as showed in Table 7 [39]. The composition of beef tallow biodiesel (Table 7) was obtained by gas chromatography (AOAC 969.33). It can be observed that oleate, palmitate and linoleate are the predominant methyl

esters, like biodiesel from sewage sludge (Table 6). Beef tallow biodiesel was produced based on methodology presented by Vargas-Ibañez et al. [70].

Physicochemical properties of biodiesel were determined according to the quality standard EN14214. Property values and its comparison with the standard limits are shown in Table 8. Biodiesel complies with the permitted limits in all the properties except in viscosity which shows a slightly higher value than the limit. However, this problem was overcome with the use of ethyl esters as we will see later on in that thesis.

The experimental measurements were validated by comparing the viscosity, density, and refractive index values of pure ethyl esters with literature reports (Table 9). Ethyl pyruvate was not included in the validation because its properties are not reported in literature under the temperature and pressure conditions covered in this research. The measured viscosity, density, and refractive index values agree with literature values with AAPDs of 3.140, 0.056, and 0.027% respectively.

**Table 7.** Beef tallow and residual fat biodiesel fatty acid methyl esters composition [39]

Fatty acid methyl ester	Biodiesel from Residual fats (w)	Biodiesel from beef tallow (w)
C9:0 Methyl Caprilate	0.12	0
C13:0 Methyl Laureate	0.25	0
C15:0 Methyl Myristate	3.05	2.86
C15:1 Methyl Myristoleate	0.55	0.52
C16:0 Methyl Pentadecanate	0.41	0.39
C16:1 Methyl Pentadecenoate	0.12	0.11
<b>C17:0 Methyl Palmitate</b>	<b>30.24</b>	<b>24.72</b>
C17:1 Methyl Palmitoleate	2.65	3.09
C18:0 Methyl Margarate	0.84	1.03
C18:1 Methyl Margaroleate	0.64	0.76
C18:0 Methyl Estearate	1.55	1.89
<b>C20:1 Methyl Oleate</b>	<b>55.56</b>	<b>58.48</b>
<b>C19:2 Methyl Linoleate</b>	<b>0.68</b>	<b>4.92</b>
C19:3 Methyl Linolenate	0.42	0.14
C21:0 Methyl Arquidate	0.16	0.11
C21:1 Methyl Gadoleate	0.71	0.58
C23:2 Methyl Eicosadienate	0.22	0.15
C23:1 Methyl Eruciate	0.12	0.25
C23:0 Methyl Docosadienoate	1.71	0

w: mass fraction

**Table 8.** Biodiesel properties comparison with EN14214 standard.

Parameters	EN Test method	Limits EN 14214	Beef tallow biodiesel
Acid value (mg KOH·g <sup>-1</sup> )	EN 14104	Max. 0.5	0.27
Sediment content (% in volume fraction)	EN ISO 12937	Max. 0.05	0.02
Flash point (K)	EN ISO 3679	> 393.15	405.15
Methanol content (% in mass fraction)	EN 14110	Max. 0.2	No detected
Sulfur content (mg/kg)	EN ISO 20884	Max. 10	<0.005
Iodine value	EN 14111	Max. 120	61
Density, 15 °C (g·cm <sup>-3</sup> )	EN ISO 12185	0.86-0.90	0.8881
Kinematic viscosity, 40°C (mm <sup>2</sup> ·s <sup>-1</sup> )	EN ISO 3104	3.5-5.0	5.46
Calorific value (MJ·kg <sup>-1</sup> )	ASTM D-240	Not reported	41.2
Cetane index	ASTM D-4737	Min. 51	62
Distillation (K, 98% in volume fraction recovered)	ASTM D-86	Not reported	
Initial boiling point (K)			588.15
Final boiling point (K)			625.15
Average molecular weight (g·mol <sup>-1</sup> ) <sup>a</sup>	Not reported		286.96

<sup>a</sup>Equation 14.

Biodiesel was mixed with magnesium oxide and ethyl esters. Magnesium oxide was maintained constant at 5 ppm<sub>m</sub> for all the mixtures but ethyl levulinate, ethyl acetoacetate and ethyl pyruvate were added with varying mass fraction from 0 to 1. Density, Viscosity, and refraction index were measured for all the mixtures in a temperature range from 288.15 to 338.15 K at atmospheric pressure. Our previous study on the MgO concentration effects over pure biodiesel properties has revealed that at concentration near to 5 ppm<sub>m</sub>, density, viscosity, and refractive index values are near to biodiesel pure values [39]. For that reason, we will analyze the three systems: ethyl levulinate-biodiesel; ethyl acetoacetate; ethyl pyruvate as pseudo-binary systems.

Density, viscosity, and refractive index values for biodiesel + ethyl levulinate+ MgO are shown in Figure 12 as a representative of the three systems, the measured values for the three systems are reported in Tables A1-A3 in the appendix section. It was found that densities of the mixtures showed a linear decreasing trend as the temperature increased (Figure 12a.) this in reason of a rise in the kinetic energy of the molecules, disrupting intermolecular forces and creating new ones between different and equal molecules, increasing the volume of the mixture and therefore reducing the density. As for viscosity (Figure 12b), values showed a decreasing tendency with increasing temperature, because of a decrease in the cohesion forces and the ungrouping between the molecules caused by kinetic energy increase. Finally, refraction index shows linear trend reducing with the increase of both ethyl levulinate mass fraction and temperature (Figure 12c).

**Table 9.** Comparison between the experimental ethyl esters viscosity,  $\eta$  (mPa·s), Density,  $\rho$  (g·cm<sup>-3</sup>), and Refractive Index,  $n_D$ , at Temperature T and Literature values at Pressure,  $p = 0.1$  Mpa.

T/K	$\rho / \text{mPa}\cdot\text{s}$			$\rho / \text{g}\cdot\text{cm}^{-3}$			$n_D$		
	This work	Literature	AAPD%	This work	Literature	AAPD%	This work	Literature	AAPD%
<i>Ethyl levulinate</i>									
288.15	2.4362	2.3151 [71] 2.4068 [73]	4.969 3.961	1.01740	1.01728 [72]	0.0118	1.4246	-	-
293.15	2.2278	2.0966 [71] 2.1483 [73]	5.891 2.470	1.01253	1.01239 [72]	0.0138	1.4224	1.4229 [74] 1.4220 [71]	0.035 0.028
298.15	1.9627	1.9049 [71] 1.9308 [73]	2.943 1.357	1.00765	1.00749 [72]	0.0159	1.4201	1.4205 [75]	0.023
303.15	1.7688	1.7363 [71] 1.7462 [73]	1.836 0.567	1.00277	1.00260 [72]	0.0170	1.4180	1.4183 [75] 1.4179 [71]	0.019 0.009
308.15	1.6183	1.5874 [71] 1.5883 [73]	1.910 0.055	0.99789	0.99771 [72]	0.0180	1.4159	1.4163 [75]	0.026
313.15	1.5003	1.4554 [71] 1.4522 [73]	2.993 0.217	0.99301	0.99281 [72]	0.0201	1.4138	1.4142 [75] 1.4138 [71]	0.024 0.003
318.15	1.383	1.3380 [71] 1.3343 [73]	3.252 0.280	0.98812	0.98791 [72]	0.0213	1.4117	1.4120 [75]	0.017
323.15	1.2794	1.2333 [71] 1.2313 [73]	3.602 0.160	0.98323	0.98300 [72]	0.0234	1.4097	1.4099 [75] 1.4097 [71]	0.015 0.001
328.15	1.1813	1.1396 [71] 1.1410 [73]	3.527 0.123	0.97833	0.98007 [72]	0.0179	1.4076	-	-
333.15	1.1058	1.0556 [71] 1.0614 [73]	4.542 0.550	0.97342	0.97316 [72]	0.0267	1.4055	1.4056 [71]	0.008
338.15	1.0254	0.9799 [71] 0.9908 [73]	4.435 1.105	0.96851	0.96823 [72]	0.0289	1.4034	-	-
<i>Ethyl Acetoacetate</i>									
288.15	1.8738	1.9020 [76] -	1.505 -	1.03282	1.03392 [76] 1.03392 [77]	0.107 0.107	1.42100	1.42091 [77] 1.42091 [76]	0.006 0.006
293.15	1.6900	1.8200 [78] -	7.694 -	1.02766	1.02830 [78] -	0.062 -	1.41879	- -	- -
298.15	1.5279	1.5810 [76] 1.4800 [79] 1.6500 [78]	3.473 3.137 7.989	1.02243	1.02345 [76] 1.02090 [79]	0.100 0.150	1.41656	1.41660 [79] 1.41658 [78]	0.003 0.001
303.15	1.3941	1.3390 [79] 1.5100 [78]	3.954 8.312	1.01721	1.01490 [79] -	0.227 -	1.41434	1.41450 [79] -	0.011 -
308.15	1.2704	1.3440 [76] 1.2390 [79] 1.3900 [78]	5.796 2.469 9.417	1.01198	1.01300 [76] 1.01020 [79] -	0.101 0.176 -	1.41214	1.41200 [79] 1.41246 [78] -	0.010 0.023 -
313.15	1.1668	1.2900 [78] -	10.562 -	1.00674	1.00740 [78] -	0.066 -	1.40994	- -	- -
318.15	1.0825	1.1440 [76] -	5.682 -	1.00150	1.00254 [76] 1.00254 [77]	0.104 0.104	1.40774	1.40803 [78] 1.40803 [76]	0.021 0.021
323.15	1.0036	- -	- -	0.99625	- -	- -	1.40554	- -	- -
328.15	0.9341	0.9810 [76] -	5.021 -	0.99099	0.99226 [77] -	0.128 -	1.40331	1.40386 [78] -	0.039 -
333.15	0.8712	- -	- -	0.98572	- -	- -	1.40106	- -	- -
338.15	0.8153	0.8470 [76]	3.892	0.98044	0.98158 [77]	0.116	1.39882	1.39949 [78]	0.048

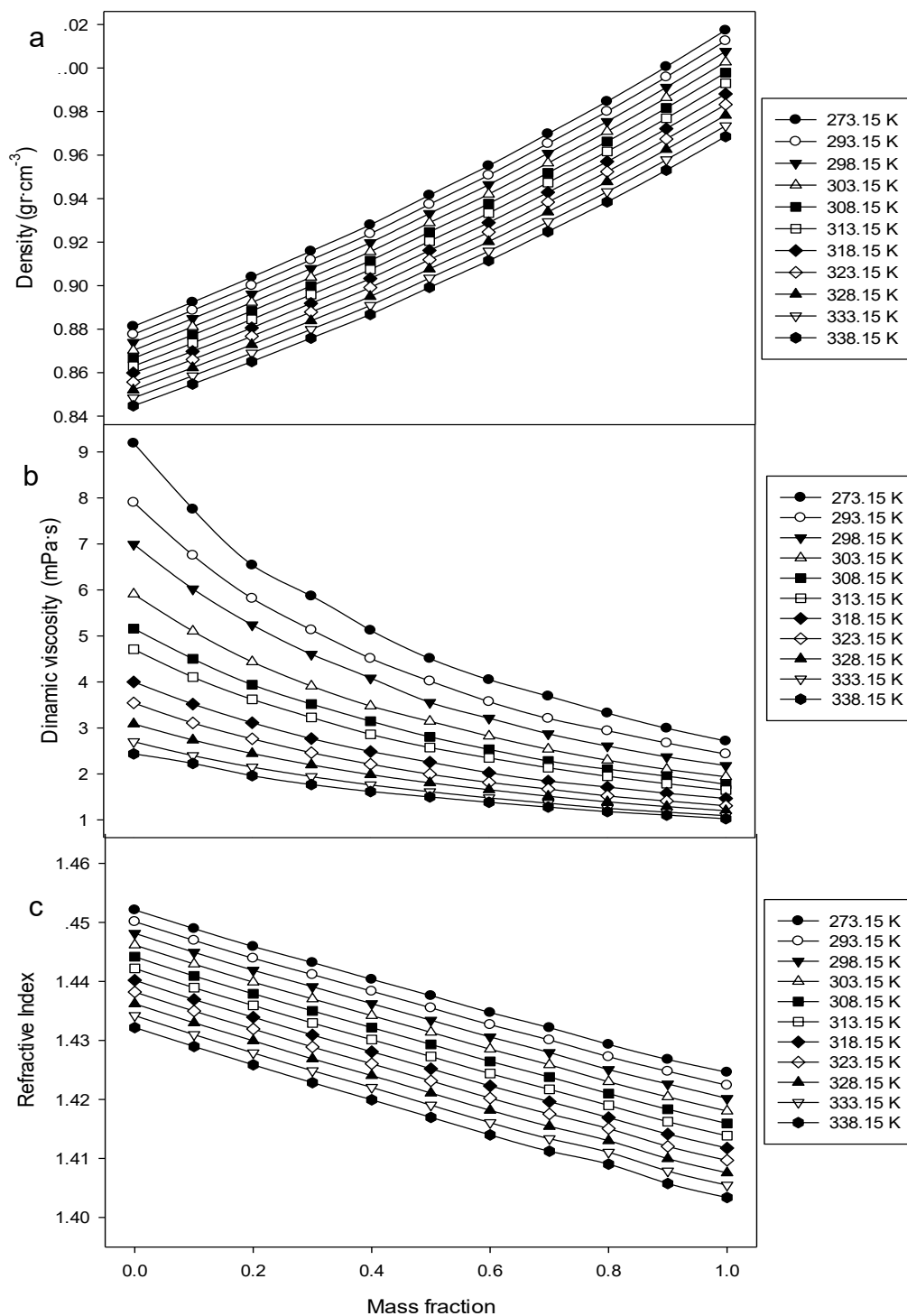


**Figure 12.** Properties of Biodiesel-Ethyl Levulinate mixtures at different mass fraction and temperature

Density and viscosity values of all mixtures were compared with European standard EN 14214, this in the aim to select adequate mixtures that could be used as a new biodiesel-based alternative fuel. EN 14214 standard establishes density limit between 0.86 and 0.90 g/cm<sup>3</sup> at 15°C and viscosity limit between 3.5 and 5 mm<sup>2</sup>s<sup>-1</sup> at 40°C. Figure 13 shows values comparison with EN 14214 standard. Viscosity and density values complies with the standard limits at ethyl levulinate mass fractions from 0.1 to 0.2. For ethyl acetoacetate and ethyl pyruvate, viscosity and density values comply the standard limits at ester mass fractions of 0.1. Therefore, those mixtures could be considered a new biodiesel-based fuel alternative.

Flash point, cetane index, and calorific value were measured for the biodiesel mixtures that complies with EN14214 standard. The results are shown in Table 10.

**Table 10.** Flash point, Cetane Index, and Calorific Value of Biodiesel Mixtures.

Sample	Flash Point (EN ISO 3679)	Cetane index (ASTM D-4737)	Calorific value (ASTM D-240)
	K		MJ/kg
Biodiesel (1)	405	62.4	41.2
Biodiesel (1) + MgO (5 ppm <sub>m</sub> )	407	62.4	41.5
Biodiesel (0.9) + Ethyl Levulinate (0.1)	379	57.1	39.8
Biodiesel (0.8) + Ethyl Levulinate (0.2)	347	59.1	37.9
Biodiesel (0.9) + Ethyl Acetoacetate (0.1)	356	45.8	36.6
Biodiesel (0.9) + Pyruvate (0.1)	366	59.3	35.0
Biodiesel (0.9) + Ethyl Levulinate (0.1) + MgO (5ppm <sub>m</sub> )	381	57.0	40.1
Biodiesel (0.8) + Ethyl Levulinate (0.2) + MgO (5 ppm <sub>m</sub> )	349	59.2	38.3
Biodiesel (0.9) + Ethyl Acetoacetate (0.1) + MgO (5 ppm <sub>m</sub> )	358	45.9	36.8
Biodiesel (0.9) + Ethyl Pyruvate (0.1) + MgO (5 ppm <sub>m</sub> )	368	59.2	35.3

It can be observed that addition of 5 ppm<sub>m</sub> of MgO promoted the increase of the pure biodiesel flash point from 405 to 407K. Probably because of attractive interactions between MgO particles and biodiesel molecules, that promotes a less presence of biodiesel molecules at the mixture's free surface [80]-[81]. On the other

hand, the addition of ethyl esters led to the decrease of pure biodiesel flash point due to the high volatility and low flash point of the ethyl esters. Furthermore, addition of MgO and ethyl esters together resulted in a lower flash point than pure biodiesel. It can be observed in Table 10 that flash point showed a linear cumulative effect of the pure components present in the mixture.

The calorific value of biodiesel increased with the addition of MgO (5 ppm<sub>m</sub>) from 41.2 to 41.5 MJ/kg, certainly due to the high energy density of MgO nanoparticles [82]. Also, it can be seen in Table 10 that the addition of the ethyl esters diminished the calorific power, this may be attributed to the addition of the shorter carbon chains of the ethyl esters to the mixtures. Additionally, it can be observed that the decrease of the calorific value is concomitant with the decrease of the carbon chain (ethyl levulinate (C<sub>7</sub>) > ethyl acetoacetate (C<sub>6</sub>) > ethyl pyruvate (C<sub>5</sub>)), emphasizing the major impact of the presence of ethyl esters on calorific values of biodiesel mixtures.

Cetane index did not change with the addition of MgO as shown in Table 10 but decreased with the addition of the ethyl esters, probably because of the low cetane number of the ethyl esters.

Excess molar volumes (VE) were calculated from experimental data using Equation 13.

$$V^E / (cm^3 \cdot mol^{-1}) = x_1 M_1 \left( \frac{1}{\rho} - \frac{1}{\rho_1} \right) + x_2 M_2 \left( \frac{1}{\rho} - \frac{1}{\rho_2} \right) \quad (13)$$

Where  $\rho$  is the mixture density;  $\rho_1$  y  $\rho_2$  are the densities of pure components biodiesel (1) and ethyl levulinate (2), respectively;  $M_1$  y  $M_2$  are molecular mass of components 1 and 2. Biodiesel molar mass have been calculated using Equation 14.

$$\overline{M_{Biodiesel}}/(g \cdot mol^{-1}) = \sum_{i=1}^{i-FAME} x_i \cdot M_i \quad (14)$$

Where  $M_{Biodiesel}$  is the average molar mass of biodiesel,  $M_i$  and  $x_i$  are the molar mass and the molar fraction of the FAME in the mixture, and i-FAME is the FAME that compounds biodiesel. The molar fractions of mixtures were calculated using Equations 15 and 16.

$$x_1 = \frac{\frac{m_1}{M_1}}{\sum_{i=1}^2 \frac{m_i}{M_i}} \quad (15)$$

$$x_2 = 1 - x_1 \quad (16)$$

Where  $m_i$  and  $M_i$  are the mass and molecular mass of pure component i. Additionally, the hydrophilic (polar) and lipophilic (non-polar) character of biodiesel and ethyl esters were evaluated through a HLB (Hydrophilic-Lipophilic Balance) by using the Davies method [68]. Biodiesel showed a lipophilic character with HLB value of 1.60 while ethyl levulinate, ethyl acetoacetate, and ethyl pyruvate showed a hydrophilic-lipophilic character with HLB values of 7.50, 7.98, and 8.45, respectively.

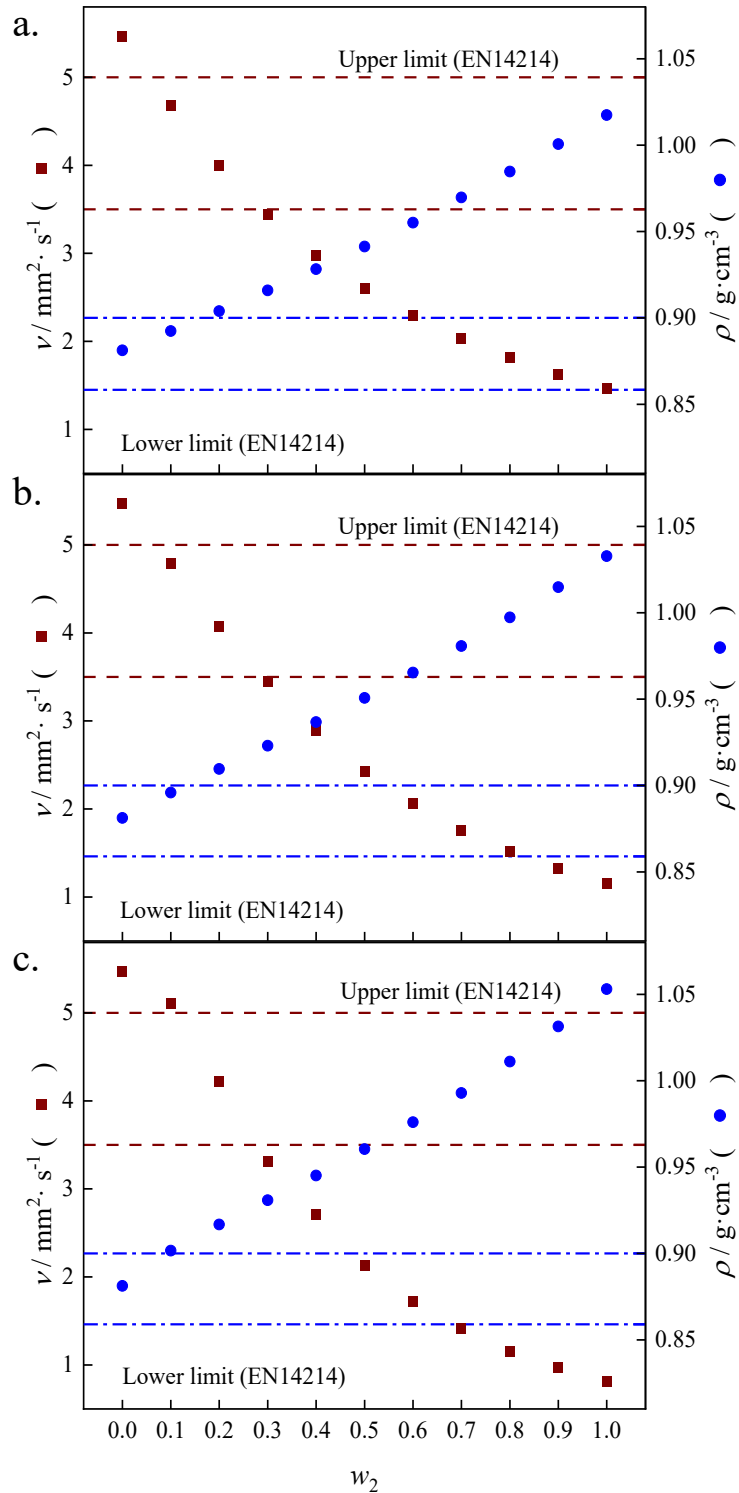


**Figure 13.** Comparison of experimental kinematic viscosity  $\nu$  (exp) at 313.15 K,  $\blacksquare$  and density  $\rho$  (exp) at 288.15 K,  $\bullet$ , of biodiesel mixtures as a function of mass fraction  $w_2$ : (a) biodiesel (1) + ethyl levulinate (2) + MgO; (b) biodiesel (1) + ethyl acetoacetate (2) + MgO; (c) biodiesel (1) + ethyl pyruvate (2) + MgO, with the EN14214 standard limits for the kinematic viscosity,  $-\ -$ , and density,  $- \cdot - \cdot$ .

VE of biodiesel-ethyl levulinate mixtures (MgO 5 ppm) showed positive deviations in all concentration and temperature ranges (Figure 14a), it also increased with temperature increase for all the mixtures. Positive deviations in excess molar volume indicates an increase of the mixture volume derived from a rise in the kinetic energy of the molecules, this reduces intermolecular associations between ethyl levulinate and methyl ester molecules [83]. Although, ethyl ester-biodiesel mixtures have not yet been widely studied, similar studies with systems like biodiesel-alcohol mixtures are available. As for example, Iglesias-Silva and Vargas-Ibañez [6] attributed VE positive values due to a volume expansion of the mixture produced by a higher molecular interaction between different types of molecules compared to the interactions between molecules of the same type. On the other hand, Barabás [84] and Djojoputro [83] reported that positive VE may be attributed to different factors like repulsion forces due to electronic charges between ethyl levulinate and biodiesel molecules and steric hindrance in methyl ester molecules.

On the other hand, VE of biodiesel-ethyl acetoacetate and biodiesel-ethyl pyruvate (both with MgO 5 ppm<sub>m</sub>) mixtures showed a sign change from negative to positive (Figures 14b and 14c) at molar fractions between 0.65 and 0.7. Negative values of VE are the result of dipole-induced dipole interactions between FAME and ethyl ester molecules, leading to the mixture contraction. This molecular behavior matches results obtained from the HLB of the pure components. Likewise, negative values of VE arise from differences in the structure and size of the ethyl acetoacetate (or ethyl pyruvate) and FAME molecules. This leads to the packing of the smaller molecules (ethyl esters) into the free volume of the FAME molecules, reducing the

molar volume of the mixture [85]-[86]. At high ester concentrations (between 0.65-0.7 molar fractions), the VE changed from negative to positive. This occurs because the increase of ethyl ester concentration in the mixture decreases the free volume into the FAME molecules, causing a dispersion of the molecules in the medium and therefore an increase in the volume of the mixture.

It can be noted that biodiesel + ethyl levulinate (MgO 5 ppm<sub>m</sub>) mixtures shows positive VE deviations in all compositions and at all the temperatures. This behavior could be due to the greater carbon chain length (C7) of ethyl levulinate compared to ethyl acetoacetate (C6), and ethyl pyruvate (C5). This could hinder the packing of ethyl levulinate molecules into the free volume of the biodiesel molecules and prevent the ungrouping of the ethyl levulinate molecules in the medium.

Viscosity deviation ( $\Delta\eta$ ) was calculated using Equation 17.

$$\Delta\eta/(mPa \cdot s) = \eta - \sum_{i=1}^2 x_i \eta_i \quad (17)$$

Where  $\eta$  and  $\eta_i$  are the dynamic viscosities of mixtures and pure components, respectively,  $x_i$  is the molar fraction; and  $i$  indicates the component. Figure 15 show viscosity deviation values for the three systems at all the considered temperature and concentration ranges. It can be seen in Figure 15a that  $\Delta\eta$  tends to negative values over the whole concentration range for biodiesel-ethyl levulinate mixtures. This indicates the presence of dispersion forces between the mixture components due to their different molecular shapes and sizes. [6], [70], [87].

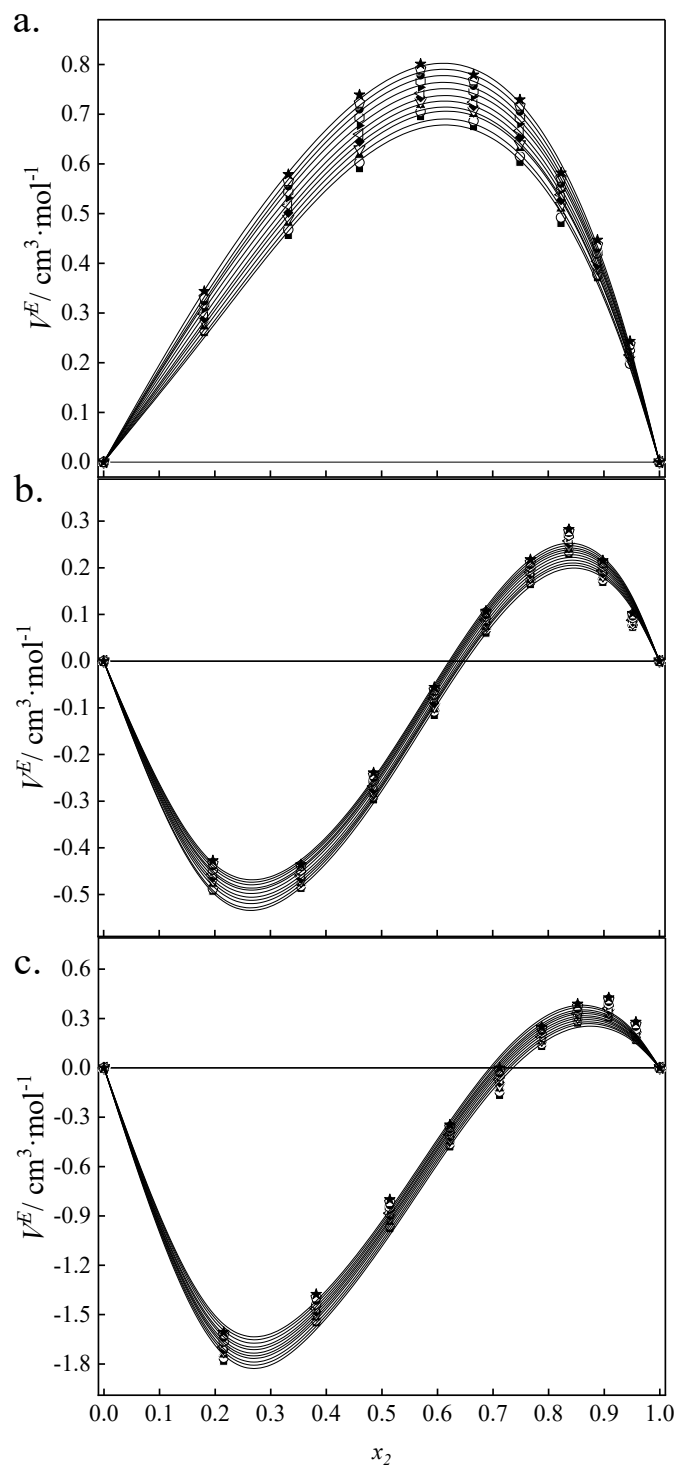


**Figure 14.** Excess molar volumes,  $V^E$ , for biodiesel mixtures as a function of the mole fraction  $x_2$ : (a) biodiesel (1) + ethyl levulinate (2) + MgO; (b) biodiesel (1) + ethyl acetoacetate (2) + MgO; (c) biodiesel (1) + ethyl pyruvate (2) + MgO:  $\blacksquare$ , 288.15 K;  $\circ$ , 293.15 K;  $\blacktriangle$ , 298.15 K;  $\nabla$ , 303.15 K;  $\blacklozenge$ , 308.15 K;  $\blacktriangleleft$ , 313.15 K;  $\blacktriangleright$ , 318.15 K;  $\blacklozenge$ , 323.15 K;  $\bullet$ , 328.15 K;  $\blacklozenge$ , 333.15 K;  $\star$ , 338.15 K.

On the other hand, biodiesel-ethyl acetoacetate (Figure 15b) and biodiesel-ethyl pyruvate (Figure 15c) mixtures presents a  $\Delta\eta$  sign change from positive to negative at ethyl ester molar fractions of 0.65 and 0.75, respectively. The initial negative deviations are attributed to dipolar interactions between unlike molecules (biodiesel–ethyl ester). This kind of interactions are promoted when does exist a great difference between the hydrophilic and lipophilic parts of the molecules that constitute the mixture [88]. Additionally, it can be noted that  $\Delta\eta$  negatives values increase with the increase in the chain length of ethyl ester (ethyl acetoacetate > ethyl pyruvate), indicating that dispersion interactions increase is proportional to the molecular size of ethyl esters [89].

Refractive index deviation ( $\Delta n_D$ ) was calculated using Equation 18.

$$\Delta n_D / (mPa \cdot s) = n_D - \sum_{i=1}^2 x_i n_{D_i} \quad (18)$$

Where  $n_D$  and  $n_{D_i}$  are the refractive index of mixtures and pure components, respectively,  $x_i$  is the molar fraction; and  $i$  indicates the component. Figure 16 shows refractive index deviation for the three systems at all the considered temperature and concentration range. It shows that deviation tents to zero, this allowing to approximate mixture refractive index as a weighted mole fraction average of the refractive index of the pure components [70].

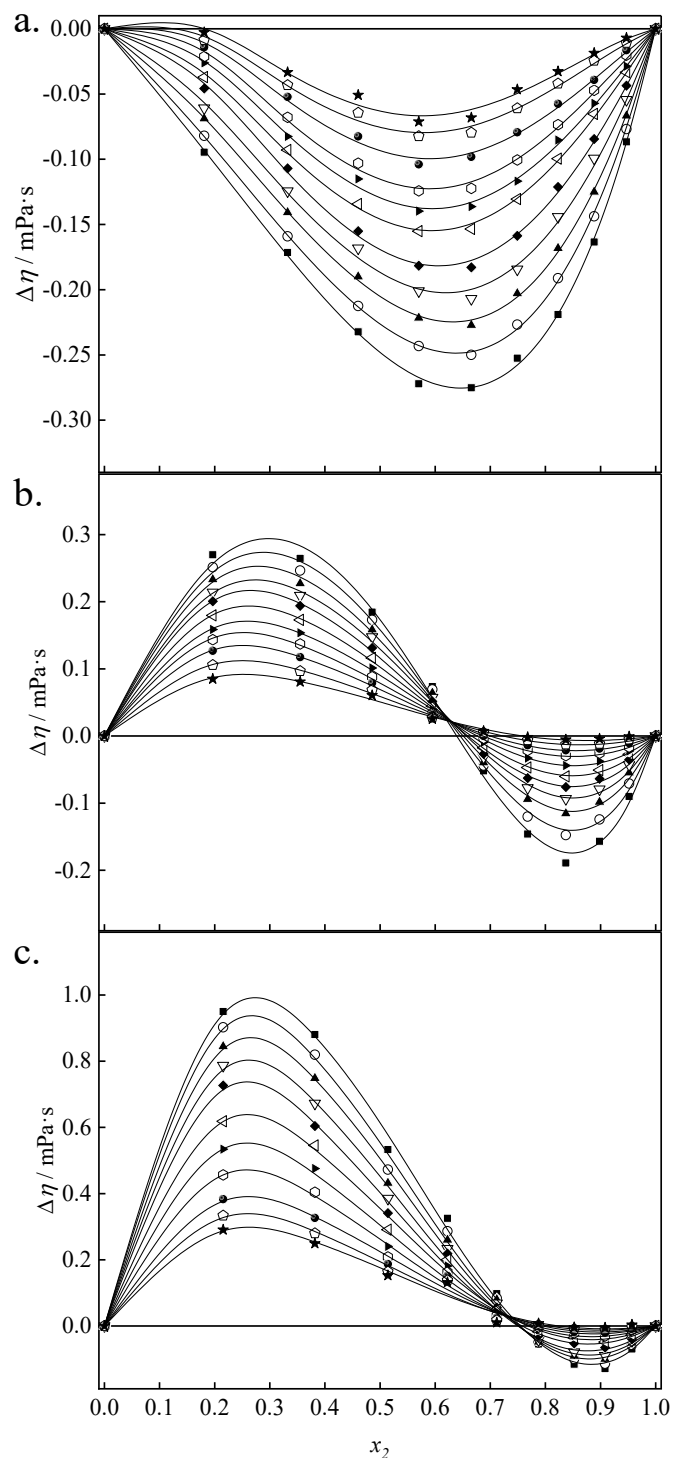


**Figure 15.** Viscosity deviations,  $\Delta\eta$ , for biodiesel mixtures as a function of the mole fraction  $x_2$ : (a) biodiesel (1) + ethyl levulinate (2) + MgO; (b) biodiesel (1) + ethyl acetoacetate (2) + MgO; (c) biodiesel (1) + ethyl pyruvate (2) + MgO: ■, 288.15 K; ○, 293.15 K; ▲, 298.15 K; ▽, 303.15 K; ◆, 308.15 K; ◁, 313.15 K; ►, 318.15 K; ◻, 323.15 K; ●, 328.15 K; ◊, 333.15 K; ★, 338.15 K

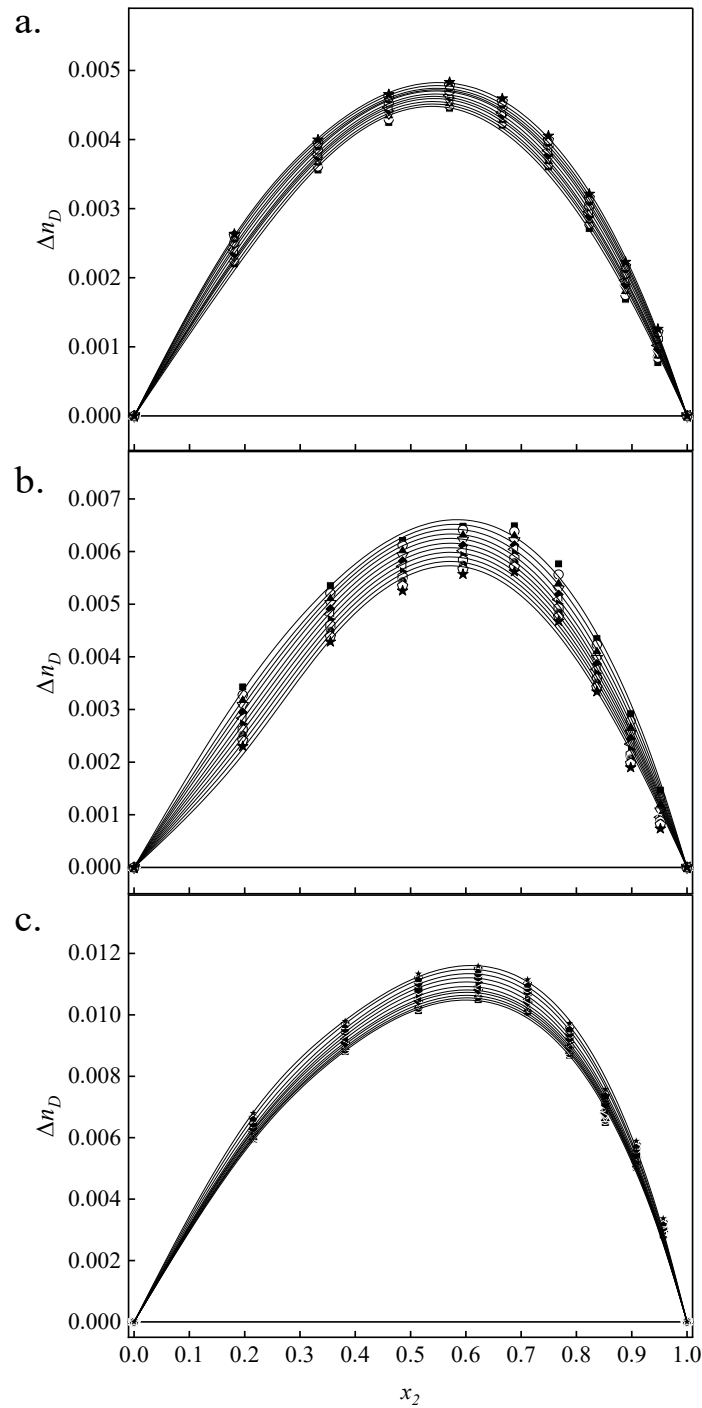


**Figure 16.** Refractive index deviations,  $\Delta n_D$ , for biodiesel mixtures as a function of the mole fraction  $x_2$ : (a) biodiesel (1) + ethyl levulinate (2) + MgO; (b) biodiesel (1) + ethyl acetoacetate (2) + MgO; (c) biodiesel (1) + ethyl pyruvate (2) + MgO:  $\blacksquare$ , 288.15 K;  $\circ$ , 293.15 K;  $\blacktriangle$ , 298.15 K;  $\nabla$ , 303.15 K;  $\blacklozenge$ , 308.15 K;  $\triangleleft$ , 313.15 K;  $\blacktriangleright$ , 318.15 K;  $\hexagon$ , 323.15 K;  $\bullet$ , 328.15 K;  $\pentagon$ , 333.15 K;  $\star$ , 338.15 K

#### 7.4. Stage 5. CFD Simulation validation

Combustor model showed in methodology section was simulated in Ansys Fluent 2021 R1 Academic to perform emission quantification. Temperature and CO<sub>2</sub> mass fraction contours were used to compare our simulation results with those reported by Dixit [32] and Balasubramanian [33]. Initially 2D geometry (Figure 2) was created by using Ansys Modeler. Then the geometry was meshed (Figure 17) resulting in a 12000 elements mesh with 0.99 orthogonal quality and 5.93E-3 skewness, these quality values indicate that mesh was adequate to perform the analysis.

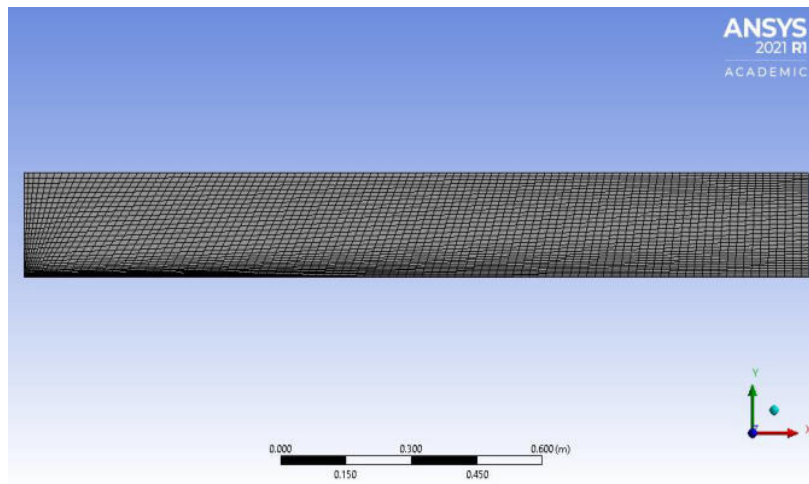
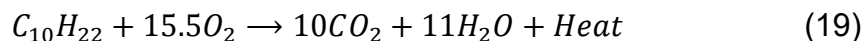


**Figure 17.** Combustor 2D geometry mesh.

Species Transport Model (STM) ,previously explained in section 6.2.5, was used for combustion analysis in Ansys software. To use this model the pure biodiesel and mixtures properties like density, viscosity, specific heat, and thermal conductivity was feed to the model to solve species transport and energy equations. Turbulence

in the combustor was modeled using k- $\epsilon$  model. Combustion reaction was performed using Eddy Dissipation (ED) model, which simulates rapid reactions in turbulent flow, being this the main characteristic of the combustion flames observed in internal combustion engines. If the reactions were slower and the flow were laminar the chemical kinetics will make an important influence so the Arrhenius model should be included in the reaction rate calculation [32].

In EDM combustion occurs whenever turbulence is present ( $k/\epsilon > 0$ ) and reaction rates are assumed to be controlled by the turbulence, this because turbulence enhances reaction rates by increasing the mixing of reactants and increasing the reaction surface area. This allows to assume that under turbulent conditions the reaction rates depends on how well reactant species are mixed and transported allowing to modeling the system depending on the species physical properties, avoiding Arrhenius kinetic calculations that implies the need of high computational resources [30]. For every fuel (Diesel, biodiesel or mixtures) EDM requires the chemical reaction and the fuel properties. For Diesel, ED model assumes a single reaction (Equation 19).



The boundary conditions were established for  $C_{10}H_{22}$  (Diesel) and air inlets with linear velocity of 50 m/s and 0.5 m/s respectively, for air flux 0.23  $O_2$  mass fraction was used. Once the boundary conditions were set the analysis was started, at the end of the calculations, temperature and species mass fractions profiles were obtained.

Temperature contour (Figure 18) shows a high temperature peak at 2110 K for Diesel combustion. On the other hand, Figure 19 shows CO<sub>2</sub> mass fraction and exhaust emissions varied between 0.16 and 0.18 molar fraction. Obtained Temperature and CO<sub>2</sub> mass fraction data shows similar trend than those reported by Dixit [32] and Balasubramanian [31] with the same conditions. Small differences in temperature values and regions in the profile could be to possible differences in properties like thermal conductivity of Diesel non-reported by the authors. Beside the slightly different values and profiles, simulation of a Diesel combustor was successfully built, allowing a preliminary validation of the data obtained in the simulation for the temperature and CO<sub>2</sub> mass fraction in Diesel combustion.

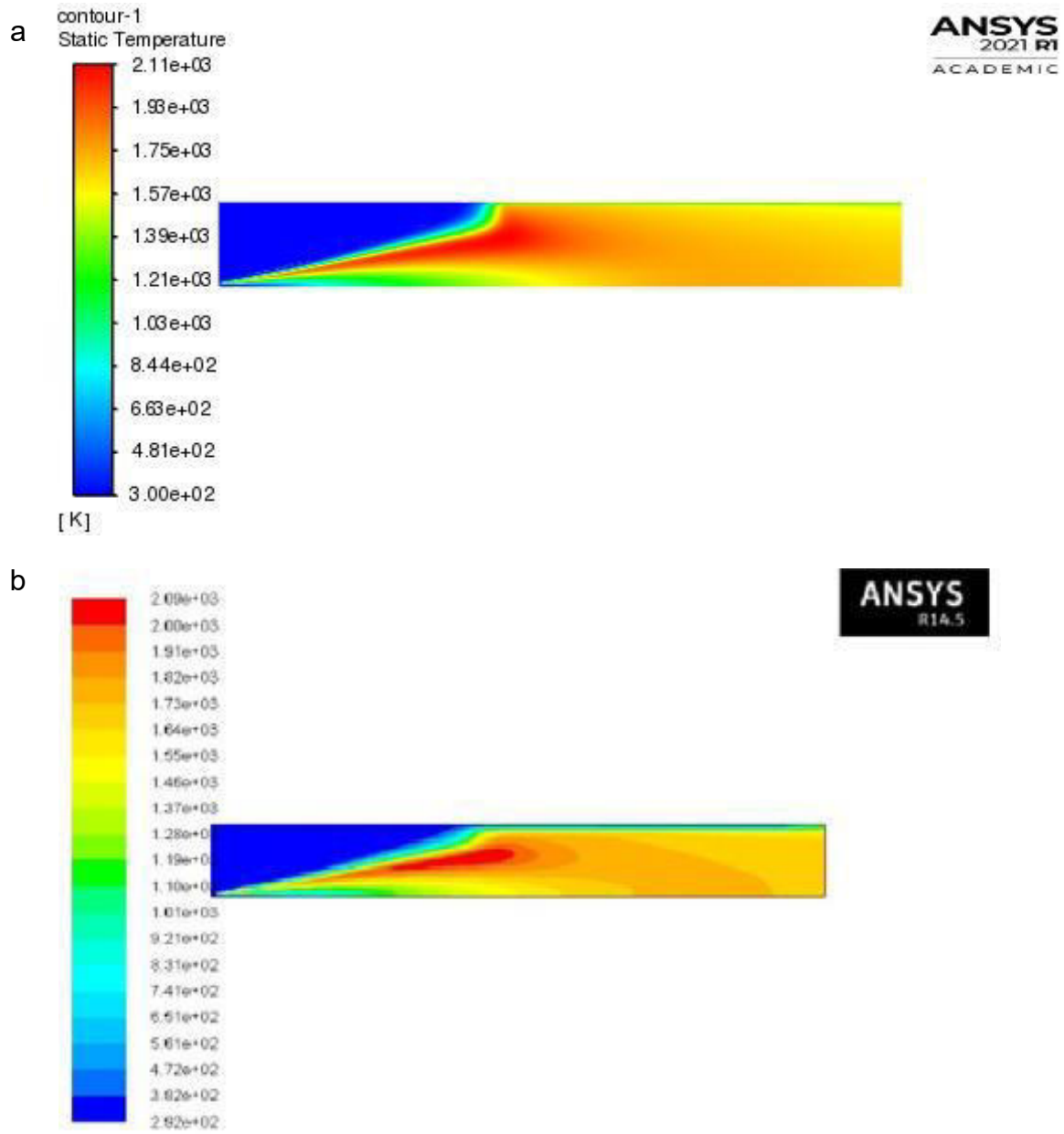


**Figure 18.** Temperature contour for Diesel combustion (a) this work (b) Dixit et al [32].

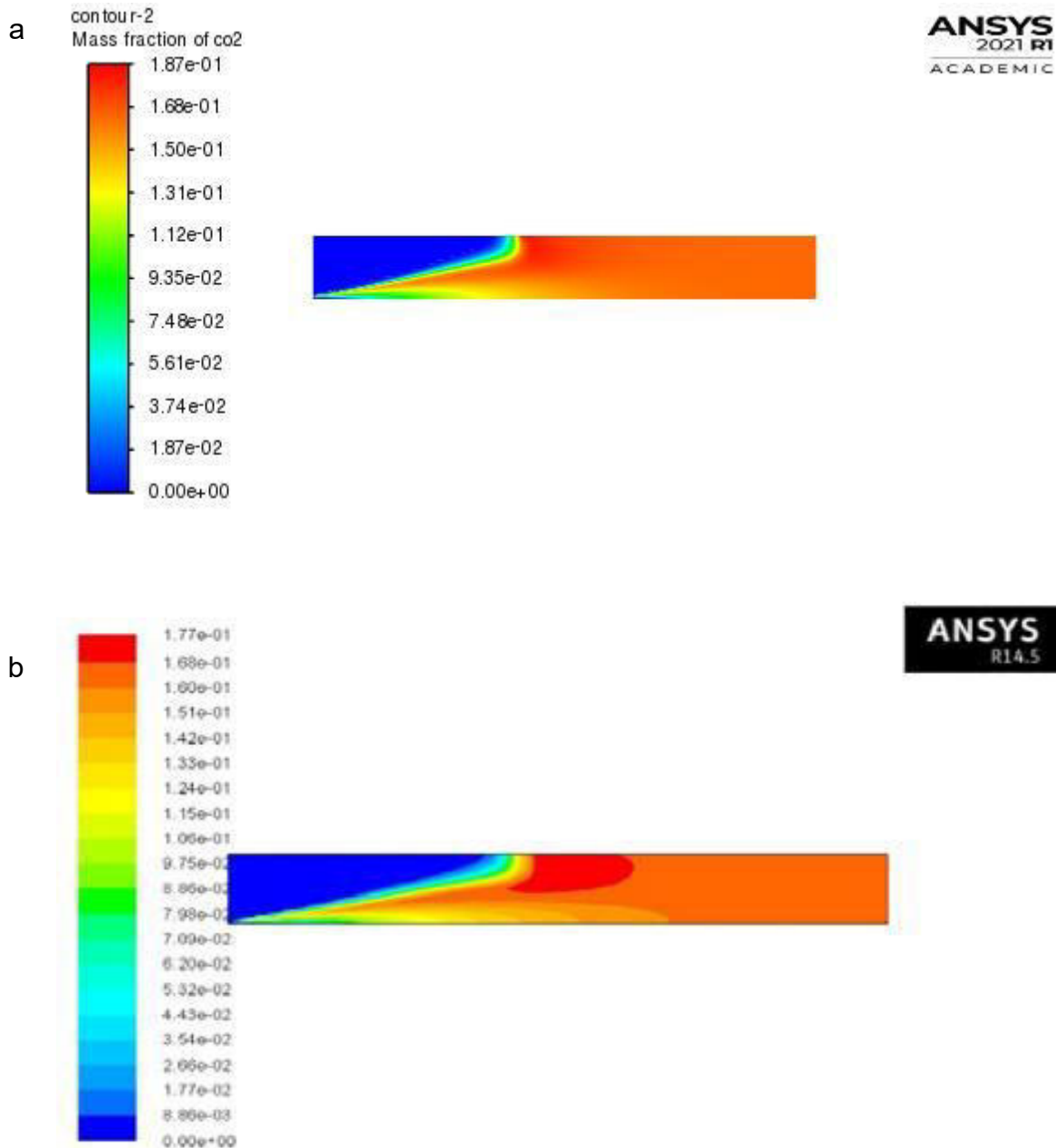


**Figure 19.** CO<sub>2</sub> mass fraction contour for Diesel combustion (a) this work (b) Dixit et al [32].

Initially, the temperature and CO<sub>2</sub> mass fraction profiles for pure biodiesel and three biodiesel binary mixtures were simulated using the same boundary conditions than for fossil Diesel simulation. The biodiesel mixtures were composed of 0.9

biodiesel mass fraction and 0.1 mass fraction of the three ethyl esters already aforementioned (ethyl levulinate, ethyl acetoacetate, and ethyl pyruvate). The single step reaction used for biodiesel; biodiesel + ethyl levulinate; biodiesel + ethyl acetate; and biodiesel + ethyl pyruvate is represented in the Equations 20, 21, 22, and 23, respectively. The values of combustion temperature and CO<sub>2</sub> mass fraction, obtained from the simulation, as well as the physical properties used in each simulation are shown in Table 11.

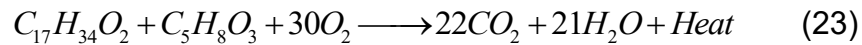
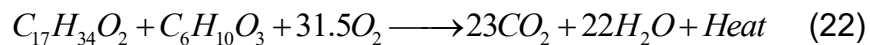
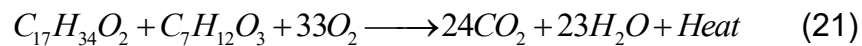
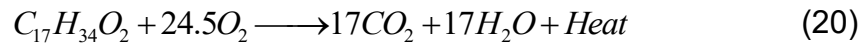


**Table 11.** Simulated values for combustion temperature (T Max) and CO<sub>2</sub> mass fraction for Biodiesel pure biodiesel and biodiesel binary mixtures.

Sample	T Max (K)	CO <sub>2</sub> mass fraction	Density (g/cm <sup>3</sup> )	Viscosity (mPa*s)	Cp (J/kg*K)
Biodiesel	1477.9	0.19324	0.8739	6.98	2050
Biodiesel 0.9 + Levulinate 0.1	1335.5	0.17484	0.8849	5.99	2041
Biodiesel 0.9 + Acetoacetate 0.1	1418.6	0.17642	0.8883	6.14	2031
Biodiesel 0.9 + Pyruvate 0.1	1425.9	0.18091	0.8937	6.55	1959

The simulated combustion temperature for the biodiesel produced in this study was 1477.9 K, some differences can be noted when is compared with the biodiesel combustion values reported by Dixit et al. [32] and Balasubramanian et al. [31] for their respective biodiesel samples which were 1350 K and 1520 K, respectively. These variations can be attributed to the different physical properties

like density and viscosity of this work biodiesel compared to the biodiesel simulated in the literature, this because the physical properties limits the reaction rates in the simulation. On the other hand, the addition of an ethyl ester allows to decrease the combustion temperature, because the addition of the ester affects the properties related with the temperature estimation (Equation 4) that is directly proportional to the mixture density and inverse to the mixture specific heat ( $C_p$ ). As it can be seen in Table 11, the lowest combustion temperature (1335.5 K) was obtained in the mixture biodiesel + ethyl levulinate, that presents the lowest density and highest  $C_p$  values among the three evaluated mixtures.

The addition of ethyl esters to biodiesel decreased the CO<sub>2</sub> mass fraction. The lowest CO<sub>2</sub> mass fraction (0.17484) was obtained with 0.9 biodiesel + 0.1 ethyl levulinate mixture. According to chemical reactions (Equations 20-23), one would expect that the total combustion of the mixture would produce more CO<sub>2</sub> than pure biodiesel combustion. This observation prompted us to consider the possibility that fuel mixture might not be undergoing complete combustion. To verify this, we examined the fuel mass fractions contour for the Biodiesel 0.9 + Levulinate 0.1 mixture (Figure 20), It was observed that there were some traces of unburned fuel at the combustor outlet, indicating incomplete combustion under the initial conditions established for the simulation.

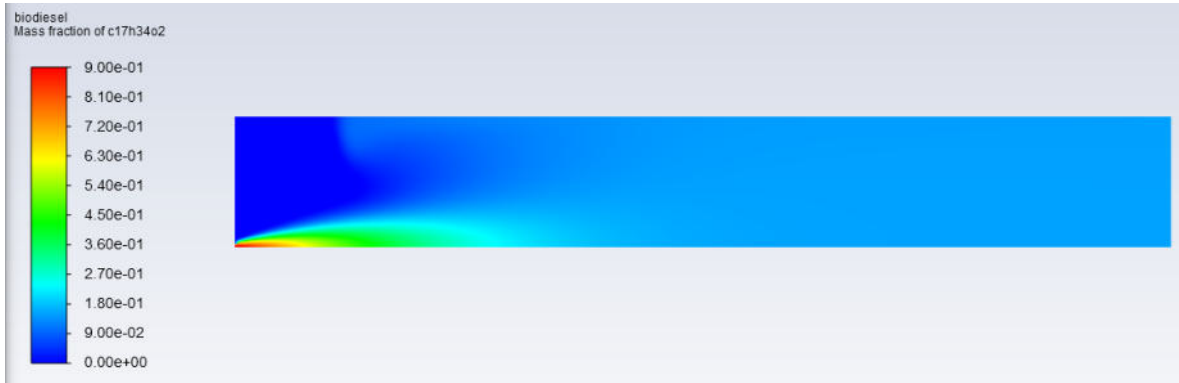


**Figure 20.** Biodiesel mass fraction profile for sample 0.9 biodiesel + 0.1 Levulinate

The incomplete combustion observed in Figure 20 can be attributed to the slightly higher density of the biodiesel mixture compared to pure biodiesel. This leads to more mass of the fuel entering the combustor, thereby affecting the air-fuel ratio (AFR). The AFR represents the amount of air required for the complete combustion of a specific mass of fuel. It is directly influenced by the composition of the fuel and is determined through the stoichiometry of the combustion process. However, accurately predicting the AFR for fuel mixtures is a complex task due to the intricate chemistry involved. Estimating the AFR for mixtures necessitates empirical modeling, which relies on either experimental or simulated data [90].

We used the simulation approach to determine the appropriate air ratio for biodiesel + ethyl levulinate mixture because it was the one with the lower temperature. This was achieved by maintaining a constant air linear velocity of 0.5 m/s and adjusting the mixture flow rate until no CO<sub>2</sub> mass fraction was observed at the combustor outlet. The fuel linear velocity that ensured complete combustion of the 0.9 biodiesel + 0.1 levulinate mixture was determined to be 21 m/s. The biodiesel mass fraction profile is presented in Figure 21. Subsequently, with the revised air-

fuel ratio, we recalculated the CO<sub>2</sub> mass fraction, which was determined to be 0.16664. This remains below the value observed for pure biodiesel, primarily due to its lower viscosity compared to the other mixtures. It is worth noting that CO<sub>2</sub> emissions are greatly influenced by the atomization of the fuel in the combustion chamber, which is directly tied to the viscosity of the fuel [91].



**Figure 21.** Biodiesel mass fraction profile for 0.9 biodiesel + 0.1 Levulinate mixture with adjusted air:fuel ratio

The MgO particles flux was included in the simulation for 0.9 biodiesel + 0.1 ethyl levulinate mixture, we have simulated the presence of MgO nanoparticles with  $16 \times 10^{-6}$  m particle diameter as obtained in previous researching [39]. We varied the MgO particles flux from 0.0005 kg/s to 0.001 kg/s to observe the variation of the temperature and emission of the mixture with the inclusion of MgO. Additionally we have enabled the NO<sub>x</sub> model to simulate the mixture NO<sub>x</sub> emissions. The simulated results for maximum combustion temperature, maximum CO<sub>2</sub> mass fraction and maximum NO<sub>x</sub> mass fraction are showed in Table 12.

**Table 12.** Simulated temperatures and emissions for Biodiesel + Ethyl levulinate + MgO mixture.

Sample	MgO (kg/s)	T Max (K)	CO <sub>2</sub> mass fraction	NOx Mass fraction
Biodiesel	0	1477.9	0.19324	4.20 x10 <sup>-8</sup>
Biodiesel 0.9 + Levulinate 0.1	0	1422.2	0.16663	2.01 x10 <sup>-8</sup>
Biodiesel 0.9 + Levulinate 0.1	0.0005	1421.3	0.16719	2.01 x10 <sup>-8</sup>
Biodiesel 0.9 + Levulinate 0.1	0.0010	1417.0	0.16728	1.89 x10 <sup>-8</sup>
Biodiesel 0.9 + Levulinate 0.1	0.0015	1412.6	0.16732	1.75 x10 <sup>-8</sup>
Biodiesel 0.9 + Levulinate 0.1	0.0020	1407.9	0.16734	1.65 x10 <sup>-8</sup>

It can be seen from Table 12 that the CO<sub>2</sub> mass fraction slightly increase 0.42% with the addition of 0.0025 kg/s MgO particles, in comparison with 0.9 biodiesel + 0.1 Levulinate mixture. This could be to a slight increase in the mixture viscosity caused because the MgO particles represents obstacles inside the mixture that increase its resistance to flow, as reported by Moreno Caballero et al [39]. As mentioned before, the simulated reaction rate is influenced by physical properties. Therefore, an increase in viscosity leads to more CO<sub>2</sub> formation.

The combustion temperature decreased with the increase in the mass rate of MgO particles. Temperature had 15 K reduction for 0.0020 kg/s MgO particles compared with the 0.9 biodiesel + 0.1 levulinate mixture. This because metal oxide particles can lead changes in the thermal conductivity and heat release transfer rates [27]. Metallic oxide particles could be a heat sink during combustion process, this to its high thermal conductivity, affecting the combustion temperature [92].

On the other hand, NOx mass fractions have also decrease with the presence of MgO particles. 17.9% less NOx emission with the addition of 0.0020 kg/s MgO particles, compared with the mixture 0.9 biodiesel + 0.1 Levulinate. This because

NO<sub>x</sub> formation is directly related with the combustion chamber temperature. Thermal NO<sub>x</sub> formation is mainly due to the molecular N<sub>2</sub> dissociation under an oxidizing environment and high temperatures, decreasing the combustion temperature avoids the N<sub>2</sub> dissociation and decreases the NO<sub>x</sub> emissions [93].

#### **7.4. Stage 6. Environmental impact assessment**

The assessment of the environmental impact of the process consisted in three scenarios comparison, all scenarios' boundaries being limited to the biodiesel production process including catalyst synthesis and grease extraction as shown in Figure 3 in the methodology (section 6.2.6).

The base scenario (scenario A) was the conventional biodiesel production process from sewage sludge, based on the methodology reported by Moreno-Caballero et al. [39] (Figure 3a). The other two scenarios consisted in one step process for biodiesel production using two different DES as catalysts: The scenario B with ChCl: PTSA and the scenario C with ChCl:OA respectively. Table 13 displays the main reaction parameters set for each scenario.

We have established 1 MJ biodiesel as functional unit (FU), and environmental inventory of mass and energy fluxes was built for all the scenarios (Table 14). Mass quantities were obtained through mass balances using experimental data and energy was calculated using energy equations showed in the methodology section.

**Table 13.** Reaction conditions for the three scenarios analyzed in the LCA.

Parameter	Scenario A	Scenario B	Scenario C
Biodiesel yield (%w/w)	90	97.01	65.37
Methanol ( $\text{mol}_{\text{methanol}}/\text{mol}_{\text{grease}}$ )	6	10	15
Reaction time (h)	9	4	6
Catalyst ( $w_{\text{catalyst}}/w_{\text{grease}}$ )			
H <sub>2</sub> SO <sub>4</sub>	0.07		
CaO	0.01		
ChCl: PTSA		0.09 <sup>a</sup>	
ChCl: OA			0.10 <sup>b</sup>

a. Equivalent to 0.1 mol DES/mol FFA

b. Equivalent to 0.2 mol DES/mol FFA

From environmental inventory (Table 14) it can be observed that base scenario (Scenario A) consumes 246.3 kJ/MJ<sub>biodiesel</sub>, displaying the highest electrical consumption of the three scenarios. Indeed, scenario A not only involves a certain number of grease extraction stages but has also the longest reaction time to produce biodiesel itself (9 hours). Scenario B showed the minor energy consumption, 73.1% less than base scenario, because of lesser purification stages and a shorter reaction time of 4 hours promoted by ChCl: PTSA DES. Scenario C showed also less energy consumption than base scenario but higher than scenario B, using 59.8% less energy than base scenario. Similarly to scenario B, improvements are brought up as compared to scenario A because of less purification stages but with a higher reaction time of 6h than 4h with ChCl:PTSA DES. These differences between scenarios B and C highlight the major impact of the DES on the faith of the reaction.

**Table 14.** Environmental inventory

	Scenario			Units
	A: H <sub>2</sub> SO <sub>4</sub>	B: PTSA DES	C: OA DES	
<b>Inlets</b>				
<i>Material</i>				
Sewage sludge	76	69	99	g
Sulfuric acid	5.4	3.6	4.4	g
Methanol	3.3	25.2	54.5	g
Water	29.1	26.1	37.7	g
Hexane	98	-	-	g
Eggshell	0.5	-	-	g
Choline chloride	-	0.67	2.4	g
Bound donor	-	1.8	1.5	g
<i>Energy</i>				
Electric power (Grease extraction)	126	21.4	29.6	kJ
Electric power (Catalyst synthesis)	39.4	2.7	3.3	kJ
Electric power (Esterification)	70.5	-	-	kJ
Electric power (Transesterification)	10.5	-	-	kJ
Electric power (One step)	-	42.3	66.1	kJ
<i>Total Energy</i>	246.3	66.3	99.0	kJ
<b>Outputs</b>				
<i>Products</i>				
Biodiesel	1	1	1	MJ
Glycerol	0.1	0.1	0.1	MJ

An attributional approach LCA was conducted using environmental inventory data (Table 14), the background data of inventory materials and energy production were taken from the Ecolnvent v2.2 database. The assessment model was made through the LCA software SimaPro 8.3® (PRe-Consultants, Amersfoort, the Netherlands). The life cycle assessment (LCA) was performed according to the ReCiPe method. The primary objective of the ReCiPe method is to transform a long list of life cycle inventory results into a limited number of indicator scores. These indicator scores express the relative severity of an environmental impact category.

Five environmental impact indicators were obtained for the three scenarios: climate change (CC), terrestrial acidification (TA), ozone depletion (OD), freshwater eutrophication (FE), and fossil depletion (FD). Figure 22 shows the five indicators values and the main contribution to their values for scenario A. Indicators in scenario A have the highest values between the three scenarios. The main contributors to the environmental impact of the scenario A were the electricity consumption (53.70% CC, 39.75% TA, 11.94%OD, 82.56% FE and, 20.30% FD), hexane (38.53% CC, 44.22% TA, 81.41%OD, 9.77% FE and, 68.73% FD), and to a lesser extent methanol (6.62% CC, 9.35% TA, 5.36% OD, 2.11% FE and, 9.78% FD). The critical stage of this scenario was the Soxhlet extraction due to its high consumption of hexane (98 gr/MJ biodiesel) and electricity (246.3 kJ/MJ biodiesel). The high impacts of electricity are strongly related to its fossil origin. Around 78% of Mexican electricity is produced through the combustion of fossil fuels being those mainly natural gas (42.6%), heavy fuel oil (21.6%) and coal (14%) [94]. On the other hand, Hexane's high environmental impacts are because it is produced by the naphtha distillation and according to EcoInvent database to produce 1 kg of hexane is needed 1.02 kg of naphtha and 3.2 MJ heating energy.

Indicators values for scenario B are given in Figure 23. The main contributors to the environmental impact of scenario B were methanol (41.61% CC, 41.45% TA, 62.44% OD, 48.74% FE and, 65.15% FD), followed by electricity (34.15% CC, 17.74% TA, 28.06% OD, 31.40% FE and, 13.01% FD) and to a lesser extent PTSA from DES (18.51% CC, 7.65% TA, 2.04% OD, 5.39% FE and, 20.07% FD). Methanol environmental impacts resides on the fact that it is obtained from natural gas

reforming process that requires high amount of energy. According to Ecolnvent to obtain 1 kg of Methanol 0.43 Nm<sup>3</sup> of gas natural and 7.7 MJ heating energy is needed. On the other hand, we can observe that impacts related to the DES (ChCl: PTSA) come mostly from the HBD that in this case is PTSA. This because one of the precursors of the PTSA is toluene (2.21 kg/ kg of PTSA [95]) that such as hexane is an organic solvent of fossil origin.

The indicators values for scenario C are shown in Figure 24. This scenario has lower values for four out of the five indicators as compared with scenario A (base scenario). The percentage reductions for the indicators were: 1.81% CC, 52.59% OD, 76.47% FE and, 18.77% FD. On the other hand, the TA indicator showed 15.21% increase as compared with base scenario. The main contributor to the environmental impact of scenario C is methanol (40.17% CC, 89.58% TA, 66.85 %OD, 49.38% FE and, 71.64% FD) as in scenario B, followed by oxalic acid from DES (29.06% CC, 50.97% TA, 12.60% OD, 13.75% FE and, 10.46% FD) and electricity (23.02% CC, 26.89% TA, 10.55% OD, 22.31% FE and, 10.52% FD). For this scenario, the increase in the methanol quantity has been reflected in a higher environmental impact that can be almost close or higher to the base scenario as we have seen for CC and TA indicators, respectively. Also, in this scenario oxalic acid represents another important factor to the environmental impact being close to the electricity contribution. This, since oxalic acid synthesis requires the use of high amounts of nitric acid (2.1 kg / kg oxalic acid) and heat (19.77 MJ/ kg oxalic acid).

Indicator values for scenario B are shown in Figure 23. This scenario displays the lowest values for all midpoint indicators evaluated. Compared with the base scenario, the percentage reductions for the indicators were: 56.3% CC, 52.17% TA, 76.42% OD, 88.82% FE and, 56.6% FD. A much lesser electricity consumption, a shorter reaction time and the suppression of two purification stages, i.e. Soxhlet extraction and evaporation, are the ingredients of a much more environmentally friendly process. Without the Soxhlet extraction due to the use of DES, scenario B directly omits the critical stage of the scenario A discarding all the environmental impacts produced by the hexane, showing the adequacy of DES as ecofriendly but efficient catalysts for biodiesel production.

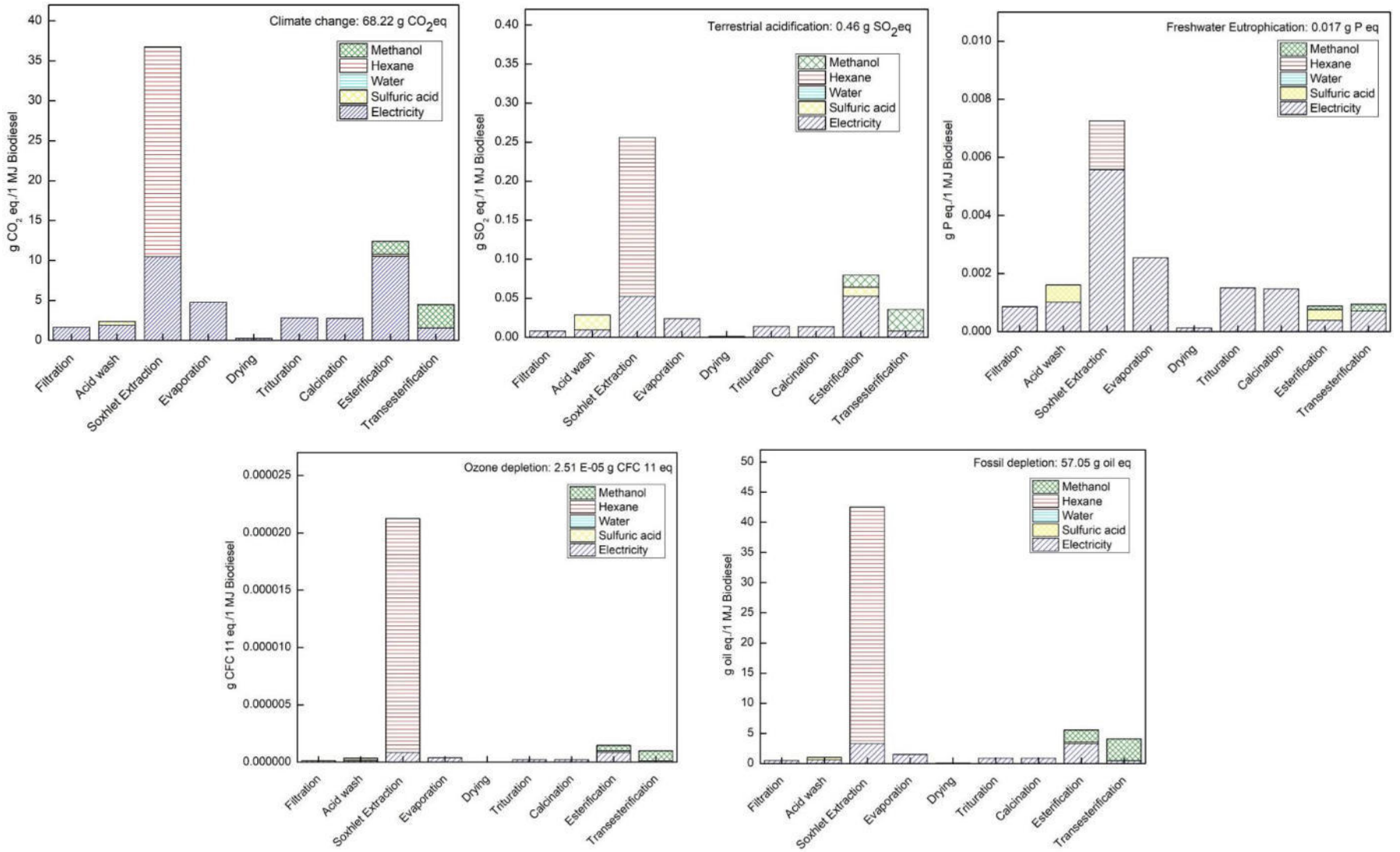
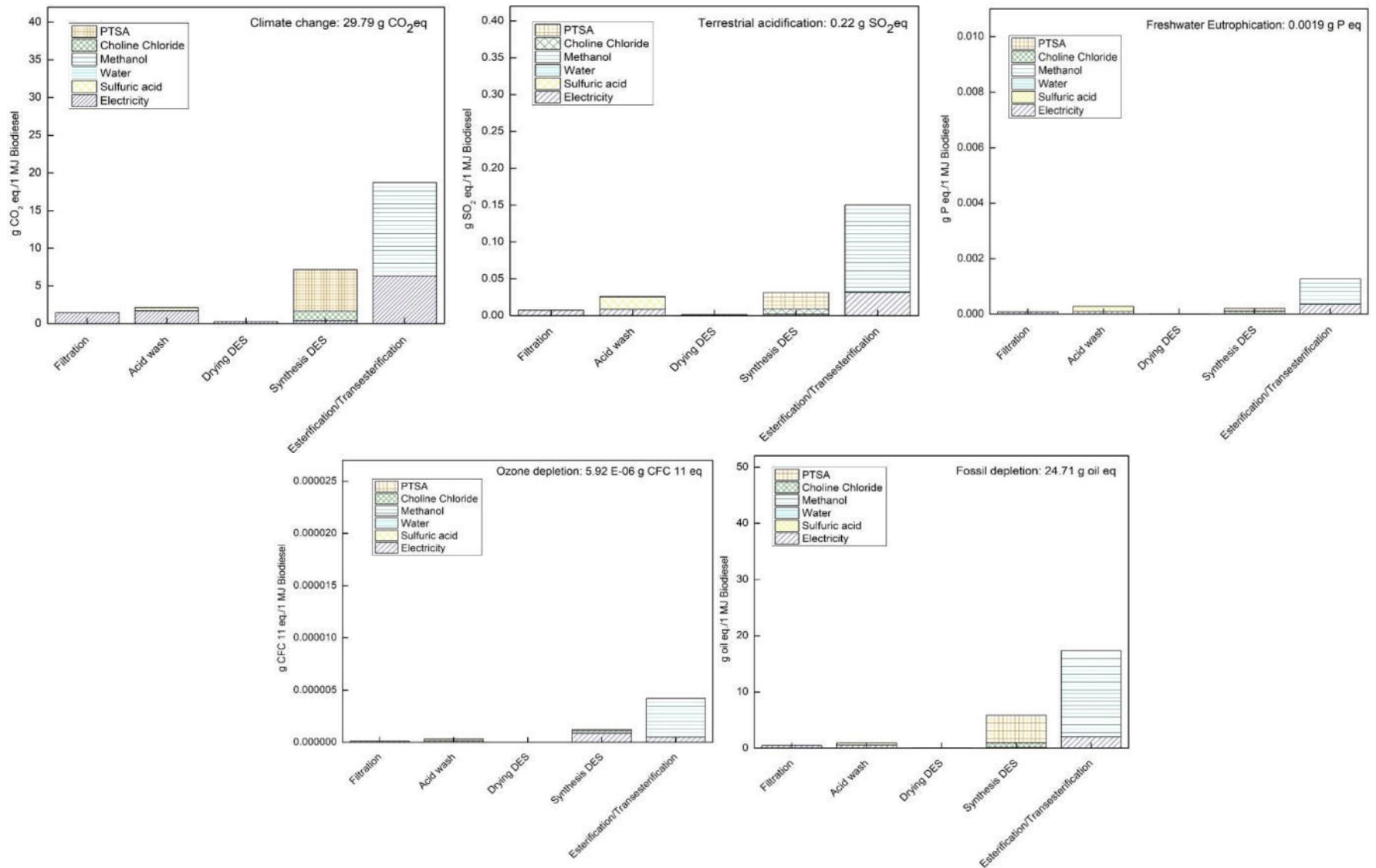


Figure 22. Five midpoint environmental impact indicators for scenario A (Base scenario)



**Figure 23.** Five midpoint environmental impact indicators for scenario B (DES ChCL:PTSA)

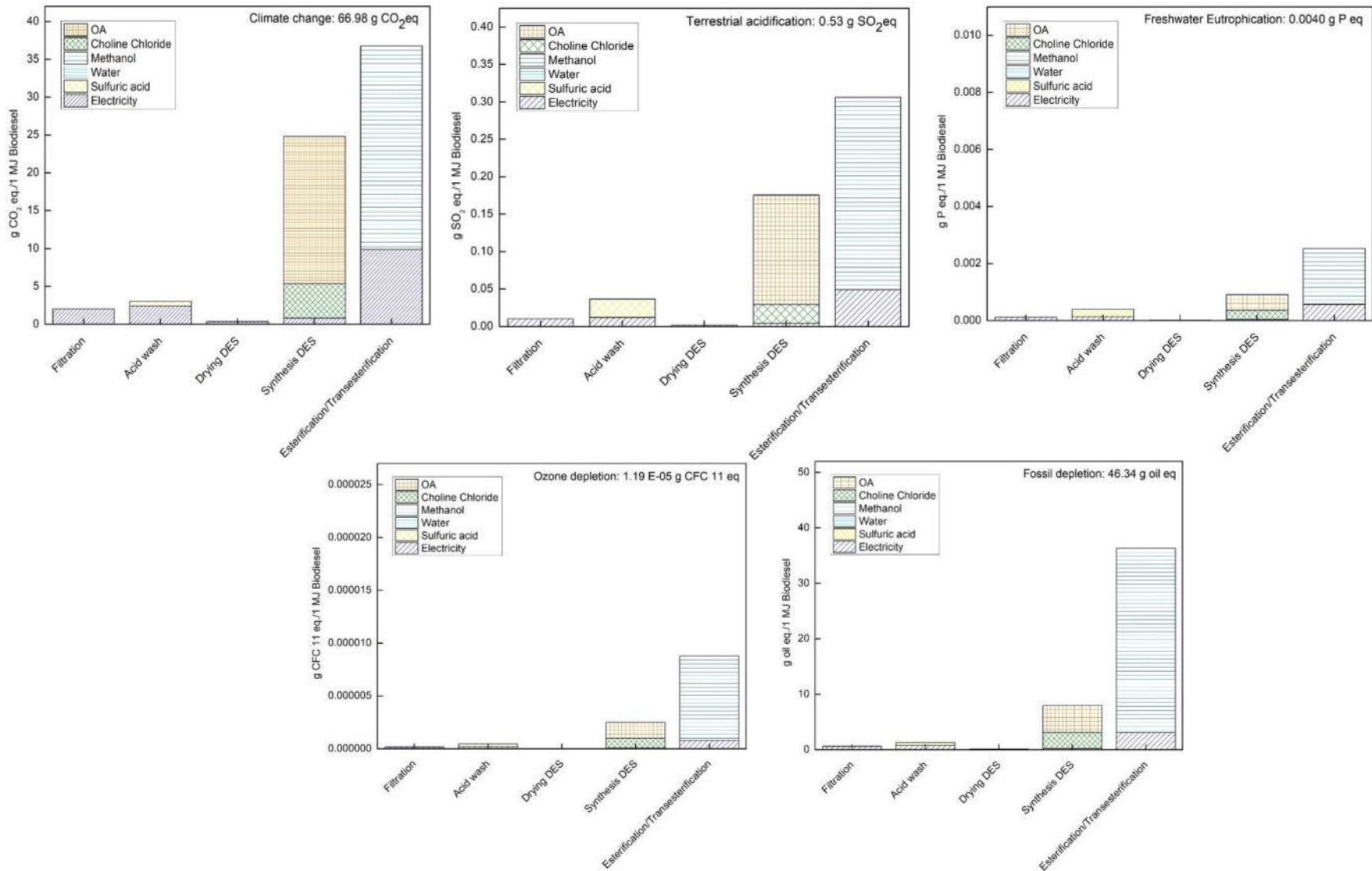


Figure 24. Five midpoint environmental impact indicators for scenario C (DES ChCL:OA)

## **8. INTENSIFICATION OF THE BIODIESEL PRODUCTION BY USING ULTRASOUND**

This thesis was carried out under a double degree agreement between Autonomous University of Nuevo León (UANL) and Grenoble-Alpes University (UGA). The preceding sections detail the research conducted at UANL in the first two years of the doctoral program. In this chapter, the experimental work carried out at the Rheology and Processes Laboratory (LRP) at UGA during the final year of the doctorate is presented. This work involved exploring ways to enhance biodiesel production using Deep Eutectic Solvents (DES) through the evaluation of additional DES together with low frequency ultrasound to overcome viscosity and heterogeneity of the reacting medium.

### **8.1. INTRODUCTION**

In the previous sections, we have demonstrated the adequate use of DES as novel catalysts for high biodiesel production, while highlighting their advantages like non-toxicity, easy preparation, short reaction times and reutilization possibility. The effectiveness of DES in biodiesel production, as detailed in Section 7.2, is a product of its dual functionality: enhancing mass transfer (Physical effect, governed by DES miscibility) and proton donation (Catalytic effect, governed by DES acidity). Even so, the strong heterogeneity of the reacting medium asks to further increase the effectiveness of DES by enhancing mass transfer. To overcome this, some studies

have combined DES biodiesel production with other green techniques like microwaves and ultrasound.

Microwave heating has been employed in biodiesel production using IL and DES as catalysts. As for example, Investigations like that of Balaraman et al. [96] have used microwave-assisted biodiesel production from karanja and chicken lard oils using a deep eutectic solvent consisting of benzyl-trimethyl-ammonium chloride (BTMAC) and oxalic acid (OA) at a 1:1 molar ratio and reached a 96.4% yield using 1:4 ( $\text{mol}_{\text{oil}}:\text{mol}_{\text{methanol}}$ ), 8 %v/v DES and 25 min reaction time. Their conclusion was that microwave enhanced the miscibility of the acyl donor with fatty acid under acidified conditions, thereby improving the mass transfer area by interaction of these components. Zhang et al. [97] conducted microwave-assisted production of biodiesel from horn seed oil using immobilized enzyme Novozym 435 in a DES composed of Choline chloride (ChCl) and glycerol (Gly). They reported a 95% yield with 8 % Novozym ratio, 1:4 ( $\text{mol}_{\text{oil}}:\text{mol}_{\text{methanol}}$ ), 400 W microwave power, 323 K and 120 min reaction time. Their findings indicated that microwaves promoted shorter reaction time as compared to conventional heating. However, It was crucial to control the temperature, because high temperatures could lead to the enzyme denaturation.

Similarly to microwave technology, ultrasound-assisted biodiesel synthesis offers several advantages over conventional mechanical stirring. These include higher yields with shorter reaction times and moderate to low energetic consumption. These improvements are attributed to capability of low frequency ultrasound to emulsify immiscible liquids; this phenomenon is driven by the collapse of cavitation bubbles, which disrupts the boundary between the different liquid phases, inducing

emulsification through the powerful ultrasonic jets directing one liquid into another one [98].

Two crucial parameters come into play when utilizing ultrasound in a reaction to improve a chemical system while paying attention to the energetic demand: amplitude (ultrasonic power) and continuous/pulse irradiation mode. Amplitude denotes the applied power to the system and is directly linked to the delivered energy to the submitted medium. Increasing the amplitude results in a greater energy input to the reaction medium, thus facilitating the reaction progress. The effect of amplitude is tied to the formation and implosion of cavitation bubbles. A greater amplitude accelerates bubble formation, facilitating mixing between the reacting species. However, excessively high amplitudes can lead to the generation of ineffective cloud bubbles. The formation of such clouds leads to the attenuation of ultrasonic waves. This is attributed to the absorption and scattering phenomena due to the presence of numerous bubbles under highly turbulent conditions. Consequently, the energy supplied to the system is dissipated, hindering emulsion in the reaction media [99].

Ultrasonic devices can operate in continuous or pulse mode. The pulse mode is represented as a ratio ON:OFF periods, where 'ON' denotes the time with ultrasound irradiation, and 'OFF' period represents the interval when ultrasound is not active. Pulse is an important parameter because it drives the energy consumption and related economic aspects of the process. Continuous ultrasound operation has shown higher energy consumption compared with pulsed operation and it can lead to erosion of the ultrasound equipment. Although several studies

[100]-[101] have explored biodiesel production using both continuous and pulsed ultrasound radiation, a clear consensus on which method yields superior biodiesel output remains elusive and seems to be highly related on the physicochemical properties of the components of the reaction (density, viscosity, etc.). Some researchers have achieved better results using pulse mode, while others have demonstrated advantages with continuous mode [100].

Masri et al. [99] and Ji et al. [102] have obtained best yields under continuous ultrasound irradiation, and both concluded that pulse led to less ultrasonic power supplied to the system and in that way less mixing effects. On the other hand, Martinez-Guerra et al. [103] have obtained 98% biodiesel yield under pulse sonication and 91% for continuous sonication. They concluded that pulsed irradiations could lead to better yields than continuous irradiation when reaction times are long, this being confirmed by Salamantina et al. [104] and Chand et al. [101]. As already aforementioned, the main physicochemical properties of the starting material to undergo biodiesel should be more finely scrutinized to eventually find out why in some cases continuous mode is more efficient than pulse one and vice-versa. In anyway, despite the varied opinions on the efficacy of pulse or continuous modes, a unanimous consensus emerged among researchers regarding the superior performance of low frequency ultrasound processing over magnetic stirring. This observation has prompted for deeper exploration of combining ultrasound with efficient catalysts like IL and DES.

Masri et al [99] enabled biodiesel production from oleic acid using a new dicationic ionic liquid [DABCODBS][CF<sub>3</sub>SO<sub>3</sub>]<sub>2</sub> under 20 kHz ultrasound irradiation

and achieved a 93.2% yield at optimized conditions [0.64 %mol catalyst, 14:3 (mol<sub>oil</sub>:mol<sub>methanol</sub>), 59°C temperature and 83 min reaction time]. They evaluated the esterification reaction in the absence of ultrasound or of the catalyst. In the absence of the ionic liquid catalyst, Masri et al. conducted the reaction under mechanical stirring and ultrasound and obtained 7% and 14%, respectively. This increase in yield with ultrasound alone in the absence of a catalyst strongly suggests an emulsification-enhancing effect due to cavitation bubbles generated by ultrasonic irradiation with the capacity of ultrasound to homogenize at most the heterogeneous medium. In the presence of the same catalyst, the yield further improved to 59% (with magnetic stirring) and 89% (with ultrasound). This enhancement was attributed to the acidic protonating effect of the ionic liquid, able to catalyse the reaction process.

Moreover, Balaraman et al. [105], investigated the ultrasound-assisted (20 kHz) biodiesel production from *Chlorella salina* using a Deep Eutectic Solvent (DES) consisting of Benzyl tributyl ammonium chloride (BTBAC) and Tartaric acid (TA). They reported a 90.8% biodiesel yield under the following conditions: 62.5% v/v DES/methanol ratio, 338 K temperature, and 25 min reaction time. They highlighted that low frequency ultrasound eliminated the need for required pre-extraction stages by damaging the algal cell walls, thus facilitating the extraction of lipids from the algal membrane. Additionally, the use of an acidic DES in the transesterification process reduced undesirable side reactions, enhancing the selectivity and quality of the biodiesel. This is attributed to the ability of low-viscosity DES to disperse efficiently

throughout the reacting medium, enhancing the reaction rate of the esterification process.

The protonation ability of the DES is closely tied to its acidity level. Greater acidity signifies a higher protonation capacity. The Hammett acidity method is an UV-analytical technique able to measure/quantify the acidity of neoteric solvents such as ionic liquids (IL) and DES whatever their hydrophobic/hydrophilic character. It monitors the protonation of a strong base, generally 4-nitroaniline compound, induced by an acidic substance present in the solution, which in this case is the DES (or the Ionic Liquid). This protonation process is measured by monitoring variations in the UV-vis absorbance of the strong base resulting from the addition of an acid [106].

Some researchers like Cui et al. [51] have used Hammett method to measure the acidity of four different DES at room temperature. They have performed Hammett method by using 4-nitroaniline and water as solvent to measure the acidity of four different DES. All of the DES were based on choline chloride (ChCl) and four different hydrogen donors: *p*-toluenesulphonic acid (PTSA), trichloroacetic acid (TCA), monochloroacetic acid (MCA), and, propionic acid (PA). They measured the maximum absorbance of 4-nitroaniline in water without DES at 380 nm, which decreased with the increasing added amount of the DES in the solution. They reported that the acidity sequence from the most acid DES was ChCl:PTSA > ChCl:TCA > ChCl:MCA > ChCl:PA. This mainly because higher acidity of the PTSA as hydrogen bond donor. Furthermore, we have observed that the sequence found by Cui et al. [51] follows the sequence of the pKa values of the pure acids: PTSA

(pKa: -2.84) > TCA (pKa: 0.66) > MCA (pKa: 2.86) > PA (pKa: 4.88). This indicates that the Hammett acidity scale aligns with the pKa values, highlighting the significant influence of the HBD on the acidity of the DES.

Based on the above, the research stay in France was structured around two main objectives: (i) Screen, synthesize, and select acidic DES for biodiesel esterification, along with establishing their acidity sequence via the Hammett acidity method, and (ii) Improve biodiesel production by integrating the use of DES as catalyst and the use of low frequency ultrasound irradiation with most favorable operating parameters.

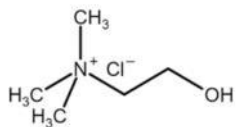
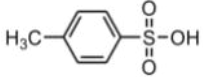
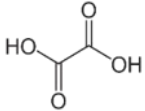
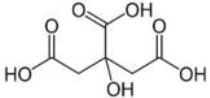
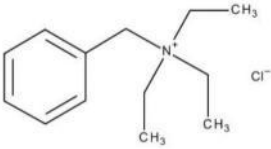
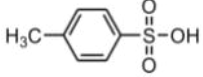
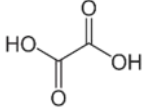
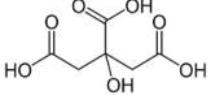
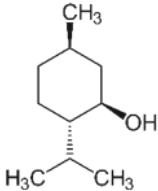
## **8.2. METHODOLOGY**

This section outlines the methodology designed to accomplish the two proposed objectives during the international research stay.

### **8.2.1 DES synthesis and characterization**

Seven different DES were synthesized by classical thermal method, as already exposed in the previous section 6.2.1. DESs were synthesized by mixing two components: (1) a halide salt as Hydrogen Bond Acceptor (HBA) and (2) a carboxylic or sulfonic acid as Hydrogen Bond Donor (HBD). The components for the seven DES are showed in Table 15.

**Table 15.** DES components and molar ratios.

Hydrogen bond acceptor (HBA)	Hydrogen bond donor (HBD)	Molar ratio (mol HBA:mol HBD)
<p>Choline chloride (ChCl)</p> 	<p><i>p</i>-toluene sulfonic acid (PTSA)</p> 	1:2
	<p>Oxalic acid (OA)</p> 	1:1
	<p>Citric acid (CA)</p> 	1:1
<p>Benzyltriethylammonium chloride (BTEAC)</p> 	<p><i>p</i>-toluene sulfonic acid (PTSA)</p> 	1:1
	<p>Oxalic acid (OA)</p> 	1:1
	<p>Citric acid (CA)</p> 	1:1
<p>Menthol</p> 	<p>Decanoic acid (DA)</p> 	1:1

To form the DES, both components were mixed at 80 °C with constant stirring of 300 rpm for one hour, until a liquid homogeneous mixture was obtained [19].

Subsequently, the DES was transferred to a glass flask and purged with nitrogen to prevent moisture absorption from the environment. The flask was then placed in a desiccator. The second choice of HBA is of particular insight. Indeed, several authors [107] [108] [109] highlighted that, in the dissolution process of cellulosic materials, this compound could help to enhance celluloses dissolution by further favorable intermolecular interactions notably London forces with celluloses. If so, with a same HBD, DES with BTEAC moiety may presumably enable London forces with our fats to improve biodiesel production [107].

Infrared (IR) analyses were conducted to confirm the formation of DES using a Thermo Scientific NICOLET iS10 spectrophotometer equipped with a diamond crystal. Both pure reagents and resulting DES were dehydrated in a vacuum desiccator with  $\text{CaCl}_2$  for 10 to 15 hours before IR analyses on ATR (Attenuated Total Reflectance) mode, with 64 scan sweeps.

Several different protocols to draw a Hammett acidity scale can be found in literature [106][110][111][112]. Therefore, a protocol had to be developed, tested, and validated for this research. This part of the project was developed in collaboration with two master students of Savoie Mont-Blanc University. Acidity of DES was measured by adapting methodologies in particular reported by [111][112]. 4-nitroaniline was used as the strong base indicator and anhydrous dimethylsulfoxide (DMSO) as solvent to allow the test of both hydrophilic and hydrophobic DES. The UV absorbance measurements were made in a UV-1900 SHIMADZU spectrophotometer. Initially, the indicator solutions were prepared by setting a 4-nitroaniline of  $5 \times 10^{-5}$  mol/L in DMSO. Subsequently solutions of DES in

DMSO were prepared; the DES concentration was  $2.5 \times 10^{-5}$  mol/L (50% of 4-nitroaniline concentration). Then, a constant quantity of each DES solution was added to indicator solutions (10  $\mu$ L of DES solution added, equivalent to  $2.5 \times 10^{-7}$  mol). These solutions were stirred for 20 minutes before being analyzed using UV-Visible spectroscopy.

### **8.2.2. Ultrasound-assisted biodiesel production**

Biodiesel production from residual fat involved two stages: (1) grease extraction, and (2) biodiesel synthesis. It is worth mentioning that the sludge from residual plants in the Grenoble area could not be utilized as raw material due to its very low grease content. As an alternative, waste from the grease trap of a local restaurant was employed.

In the extraction stage, waste from the grease trap was initially filtered to remove any undesired solids it may contain. The filtered material was then subjected to an acid bath process. However, the grease did not exhibit phase separation. This could be attributed to the fact that fats from grease traps do not contain as many suspended solid materials as sewage sludge, allowing for the recovery of grease through filtration alone. Therefore, the acid bath was omitted from this process. The percentage of free fatty acids (%FFA) in the obtained lipids was determined using the titration method (AOAC 942.15), with phenolphthalein as the indicator. This was done to establish the esterification conditions based on the FFA content of the residual grease.

Biodiesel was produced from the extracted grease through a one-step process. Methanol and residual grease were added in a constant molar ratio of 10 ( $\text{mol}_{\text{methanol}}/\text{mol}_{\text{FFA}}$ ) to a jacket reactor system at a constant temperature of 40 °C, the jacket temperature was maintained using a Lauda RK20 recirculating bath. The reactor was coupled to a Branson Sonifier 450 (20 kHz). The methanol ratio was chosen based on the optimal parameter identified in the prior Mexican investigation. Additionally, the temperature was selected to prevent methanol from undergoing evaporation.

To analyze the effects of pulse/continuous modes and intensity levels on the biodiesel production, we employed the DES ChCl:PTSA based on results obtained in section 7.2 , where ChCl:PTSA demonstrated the highest yield (97%) at a molar ratio of 0.1 ( $\text{mol}_{\text{DES}}/\text{mol}_{\text{FFA}}$ ), maximizing biodiesel production. Intensity was varied from 50% to 90%, and pulse ranged on 'ON' mode from 30% to 100% . All experiments were conducted with a set reaction time of one hour. After determining the optimal settings for intensity and pulse, we replicated the ultrasound-assisted reaction using the other DES. To assess changes in yield between the two methods, we conducted experiments under mechanical stirring conditions, so-called "silent" conditions, with same applied operating parameters. The only difference was that the mechanical stirring reaction was conducted for 3 hours as the reaction proceeded much more slowly than under ultrasound.

The biodiesel yield was determined by quantifying the reduction in %FFA content from the initial material to the final product using the acid-base titration method, as detailed in section 6.6.2.

## **8.2. RESULTS**

In this section, the experimental findings are presented, with each part corresponding to the specific objectives of the research stay.

### **8.2.1. DES synthesis and characterization**

Seven DESs have been prepared according to the methodology previously described in the last section. All DESs were obtained from solid phases HBD and HBA. At the end of the synthesis, all DESs were transparent showing a homogeneous phase. Whereas ChCl: PTSA, BTEAC:PTSA, ChCl: OA, BTEAC:OA and Menthol:DA were fluid at room temperature, ChCl: CA and BTEAC: CA showed an almost solid character at room temperature, but turned to liquid estate for temperatures over 40°C , this being due to the high freezing point of the citric acid (156°C) [52].

#### **8.2.1.1. FTIR analysis**

To confirm the DES formation, IR analyses were done on the HBDs and HBAs alone and subsequently formed DESs and respective spectra were superposed to assess the formation of the DES. Typical results for the DES ChCl:CA and Menthol:DA (ratio 1:1) are presented in Figures 25 and 26.

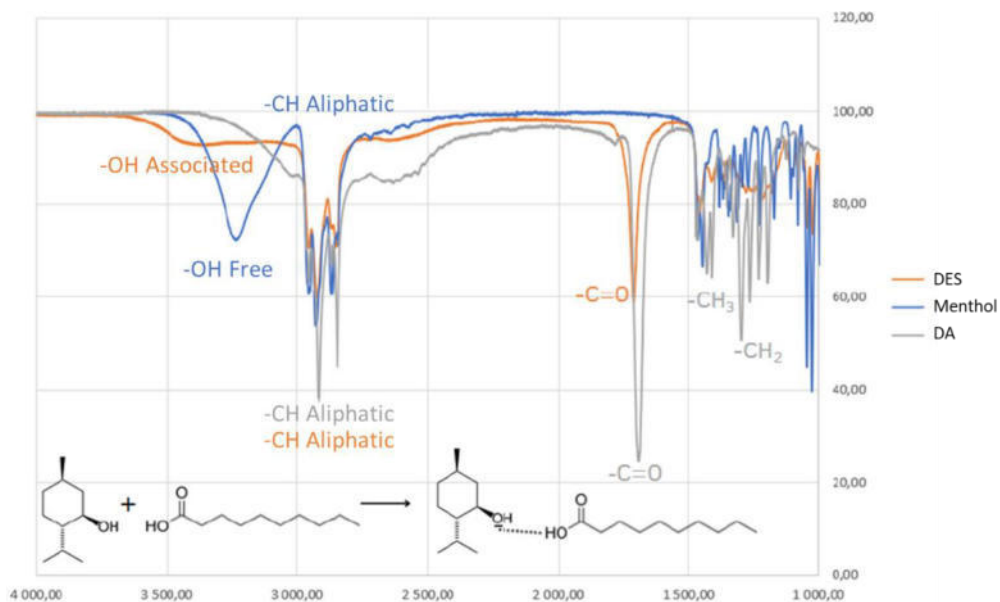


**Figure 25.** IR spectra superposition for Menthol:DA

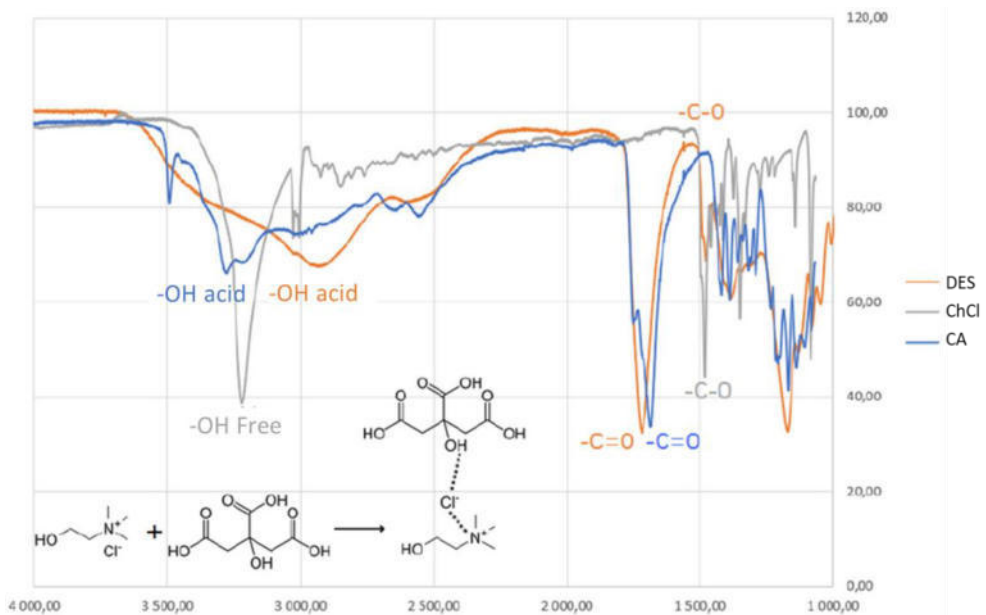


**Figure 26.** IR spectra superposition for ChCl:CA

The overlapping of the three IR spectra of a given DES highlights small changes in the aspect of the peaks in particular in the 2500-3500 cm<sup>-1</sup> region. It can be noted

that IR spectra of the DES are less well resolved than those of their corresponding powdered reagents. This could be due to the highly viscous nature of DES, which hinders the vibrations of the bonds due to strong intermolecular interactions. One solution to improve the resolution of these spectra could be to either to make an IR analysis with diluted DES or to make such an analysis at higher temperature to facilitate the movement and vibrations of molecular bonds.

In anyway, IR spectra show several characteristic peaks at  $3200\text{ cm}^{-1}$  (Hydroxyl group),  $2850\text{ cm}^{-1}$  (C-H stretching), peaks in the range between  $1500$  and  $1000\text{ cm}^{-1}$  representing C-O stretching and C-H bending, and peaks in the  $1750 - 1690\text{ cm}^{-1}$  range corresponding to the carboxylic groups (C = O) [113]. IR spectra of DES show attenuation of the  $3200\text{ cm}^{-1}$  peak (Figure 25 and Figure 26) and formation of broader peaks between  $3500$  and  $2500\text{ cm}^{-1}$  (Figure 25). These observations suggest the establishment of hydrogen bonding interactions. In the case of Menthol:DA, it arises between the OH groups of menthol and decanoic acid [114], while for ChCl:CA, it forms between the chlorine anion ( $\text{Cl}^-$ ) and the hydrogen from the citric acid [113]. This confirms the formation of the deep eutectic solvent (DES) through hydrogen bonding interactions between the HBA and HBD.

#### **8.2.1.2. Hammett acidity analysis**

The Hammett method consists on measuring the variation in the absorbance values of a strong basic indicator solution. As the added DES is more acidic, the non-protonated form of the basic indicator shows a decrease in absorbance,

characterizing the occurring acid-base reaction. To estimate the relative acidity of the DES the Hammett acidity function (Equation 24) was calculated as follows:

$$H_0 = pK(I) + \log\left(\frac{[I]}{[IH^+]}\right) \quad (24)$$

Where  $pK$  is a constant value that depends on the indicator. In this case of 4-nitroaniline, it is 0.99.  $[I]$  is the molarity of the non-protonated form of the indicator,  $[IH^+]$  is the molarity of the protonated form of the indicator. The  $[I]/[IH^+]$  ratio was obtained from the differences in absorbance measured after adding an equal molar amount of DES.

We measured the UV absorbance of eight samples, the first one is a solution of DMSO with concentration of 4-nitroaniline ( $5 \cdot 10^{-5}$  mol/L,  $pK_a = 0.99$ ) this solution is the Blanc solution and its maximum absorbance ( $A_{max}$ ) value was 1.110 at 393 nm. After this, we have measured the absorbance of seven indicator solutions bearing different concentrations mixed with a constant DES concentration (10  $\mu$ L of DES solution, equivalent to  $2.5 \cdot 10^{-7}$  mol). The UV spectra for the eight samples is showed in Figure 27.

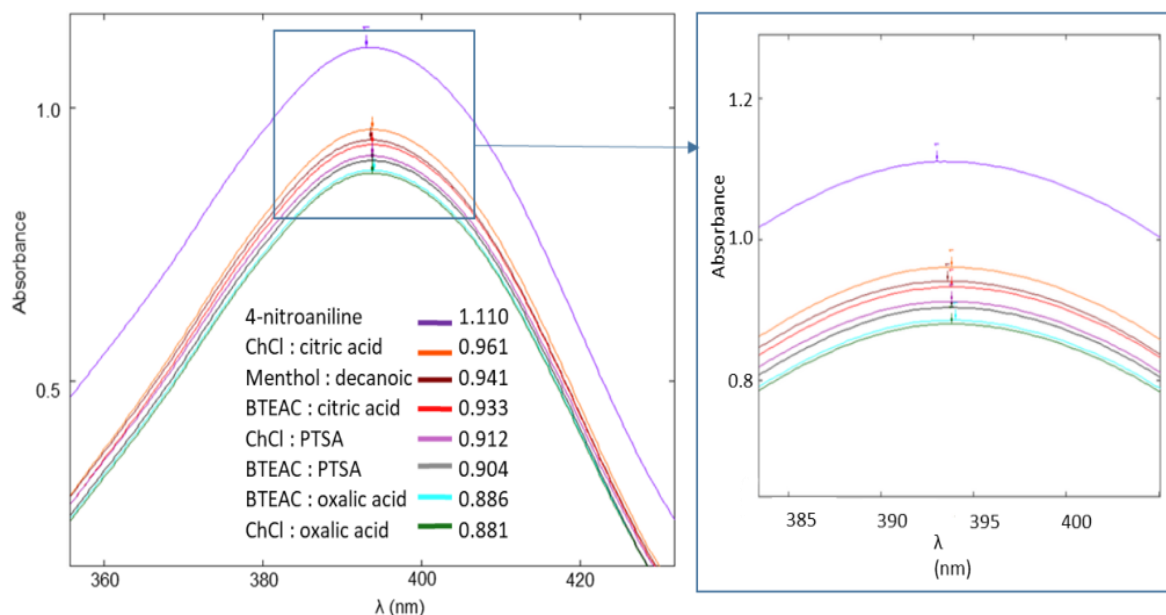


**Figure 27.** UV absorbance spectrums for Hammett method

It can be seen in Figure 27 that the DES addition promotes a decrease in the absorbance values of the indicator solution. The trend of absorbance reduction among the seven DES was: ChCl:CA > Menthol:DA > BTEAC:CA > ChCl:PTSA > BTEAC:PTSA > BTEAC:OA > ChCl:OA. Once the absorbance values were obtained, we calculated  $H_0$ , the values are showed in Table 16.

**Table 16.** Hammett acidity values for seven DES.

DES	$A_{max}$	$[I]%$	$[IH^+]%$	$H_0$
Blanc	1.110	100.0	0	-
ChCl:CA	0.961	86.6	13.4	1.80
Menthol:DA	0.941	84.8	15.2	1.74
BTEAC:CA	0.933	84.1	15.9	1.71
ChCl:PTSA	0.912	82.2	17.8	1.65
BTEAC:PTSA	0.904	81.4	18.6	1.63
BTEAC:OA	0.886	79.8	20.2	1.59
ChCl:OA	0.881	79.4	20.6	1.58

The acidity order of the formed DES, based on  $H_0$  values, was as follows: ChCl:OA > BTEAC:OA > BTEAC:PTSA > ChCl:PTSA > BTEAC:CA > Menthol:DA > ChCl:CA. This results indicates that ChCl:OA seems to exhibit relatively stronger Brønsted acidity as compared to the other six DES used in this study.

The found acidity values of the DES have been reported on a different manner on Figure 28 where the impact of the HBA (either ChCl or BTEAC moieties) is assessed. This figure highlights that the nature of the HBA does not exert any discernable influence on the found acidity values contrary to the nature of the HBD. A discernible trend emerged among the HBD pairs, indicating their influence on the overall DES acidity (Oxalic < PTSA < Citric). Notably, DES containing oxalic acid showed notably lower absorbance compared to those with citric acid and PTSA. However, we should also note that the acidity values of both OA and PTSA-based DES do exhibit similar values considering the error bars, rendering rather difficult to say with exactitude which of PTSA and OA-Based DES are really the more acidic moieties. When considering pKa values (PTSA: -2.8, OA: 1.2, CA: 4.1), this absorbance order seems inconsistent with their respective acidities. This discrepancy could arise from the fact that pKa values are indicative of acidity in water, not in DMSO. Additionally, the possible presence of water in the DES samples could have played a significant role in these results. Moisture levels were not controlled during measurements, potentially introducing variability. A more drastic methodology would be maybe needed to control the water level at all stages to prevent unwanted variations in found UV-Values as water, because to its amphoteric

character can play either the role of an acid or of a base, in particular here a role of acid by reacting with the 4-nitroaniline base UV-probe.

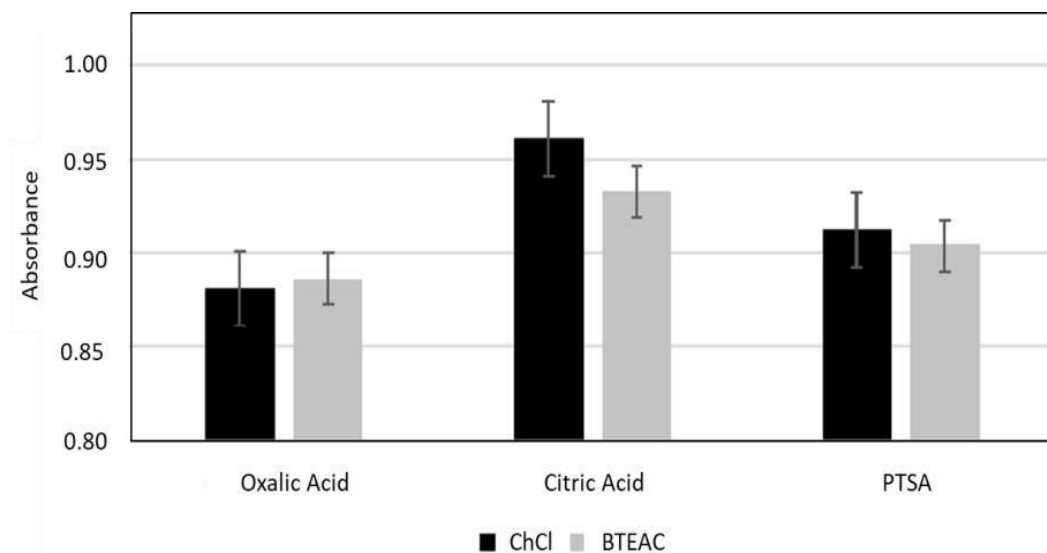


**Figure 28.** UV absorbance comparison between HBD and HBA pairs.

Based on this Hammett acidity results, we opted to proceed with five out of the initially proposed seven DES for the reaction tests. The chosen DES include ChCl:PTSA, BTEAC:PTSA, ChCl:OA, BTEAC:OA, and Menthol:DA. The DES containing CA were excluded due to their low acidity and high viscosity. Despite Menthol:DA displaying low acidity in the Hammett test, we included it in the study to explore whether its hydrophobic nature could influence its performance as a catalyst or could ease its recycling at the end of the biodiesel production.

### 8.2.2. Ultrasound-assisted biodiesel production

The free fatty acid percentage (%FFA) of the filtrated grease from the grease trap waste was measured by titration method (AOAC 942.15) and was found to be 95%. Once the initial %FFA value was determined, we have performed esterification/transesterification reaction with the best conditions found in Mexico using ChCl:PTSA at 0.1 ( $\text{mol}_{\text{DES}}/\text{mol}_{\text{FFA}}$ ), 10 ( $\text{mol}_{\text{methanol}}/\text{mol}_{\text{FFA}}$ ), 300 rpm magnetic stirring and 3 hours reaction time. Biodiesel yield was evaluated by measuring the decrease in the %FFA as previously showed in Equation 5. The yield for this first experiment was 98.90%, a similar value to those obtained in Mexico under the same conditions by using sewage sludge as raw material (97%). This experiment confirmed that those experimental conditions allowed to obtain high biodiesel yield from any kind of lipid material independently of its FFA content.

The next stage was then to implement ultrasound in the biodiesel production in the presence of these acidic DES. ChCl:PTSA was selected among the 5 DES as catalyst and the same conditions previously mentioned but under ultrasound conditions were applied. The reaction time under ultrasound has been intentionally decreased to 1h as compared to the 3h on mechanical stirring since it is expected that the mechanical effects brought by ultrasound up, would fight the strong heterogeneity of the system by mixing intimately components of the reaction and by increasing overall mass transfer. We have therefore set to 1 hour time irradiation time and 40°C temperature, this because exothermic release of heat from ultrasound process could promote the easy evaporation of methanol in temperatures near to its

boiling point (65°C). At first, we explored the impact of the ultrasound intensity from 40 and 90% on continuous irradiation mode as showed in Figure 29.

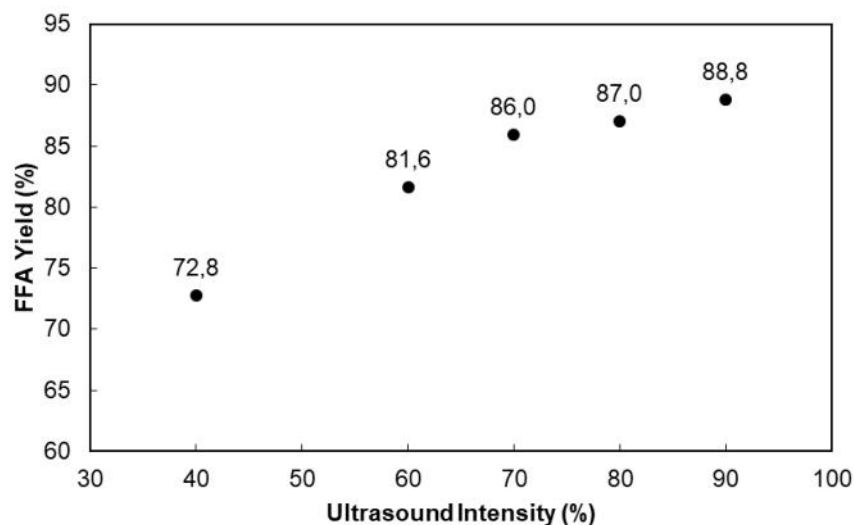


**Figure 29.** Effect of ultrasound intensity in biodiesel yield by using ChCl:PTSA as catalyst.

As it can be seen in Figure 29, biodiesel yield increased with the increase of the ultrasound intensity. This could be because ultrasound intensity represents the power that is applied to the reaction medium, higher energy promotes more efficient mixing in the reaction media and overcomes the mass transfer barrier between the immiscible methanol and grease phases [99]. For Intensity values higher than 70%, the biodiesel yield does not increase anymore significantly (less than 3% between 70 and 90% of intensity) showing that at one stage, giving more energy to the reaction medium does not improve much production yield. In a bid to minimize energy consumption, we have selected 70% intensity considering that from that point, none major yield improvements are expected as shown Figure 29.

After determining the better ultrasound intensity value, we conducted experiments under 70% ultrasound intensity, but by varying pulse values between 30 and 100% on “ON” mode. Figure 30 display results found on the variation of “ON” pulse intervals on biodiesel yield. Amazingly and controversially to some previous published works, the highest yield was obtained by using 30% pulse, whereas at higher pulse values, the yield decreased. This behavior could be because constant ultrasound irradiation (pulse 100%) promotes the formation of ineffective cloud bubbles, making a gaseous cushion that attenuates the ultrasound waves. On the other hand, pulsed irradiation promotes smaller bubbles size avoiding the cloud formation and its negatives effects over the ultrasound waves allowing a better energy distribution in the reaction media and enhancing the mixing effects [99]. It may also be highly desirable to explore further some key physicochemical properties of the biomaterial to be transformed, notably density, viscosity, etc. to eventually link those to the choice of either continuous or pulse irradiation mode.

After stablishing the best conditions of ultrasound intensity and pulse conditions, the next stage was to determine the adequate reaction time with other set operating parameters unchanged (methanol:oil molar ratio in 10:1, DES quantity at 0.1 mol<sub>DES</sub>/mol<sub>FFA</sub> and temperature at 40°C). We varied the reaction time between 30 and 90 min and the results are shown in Figure 31.

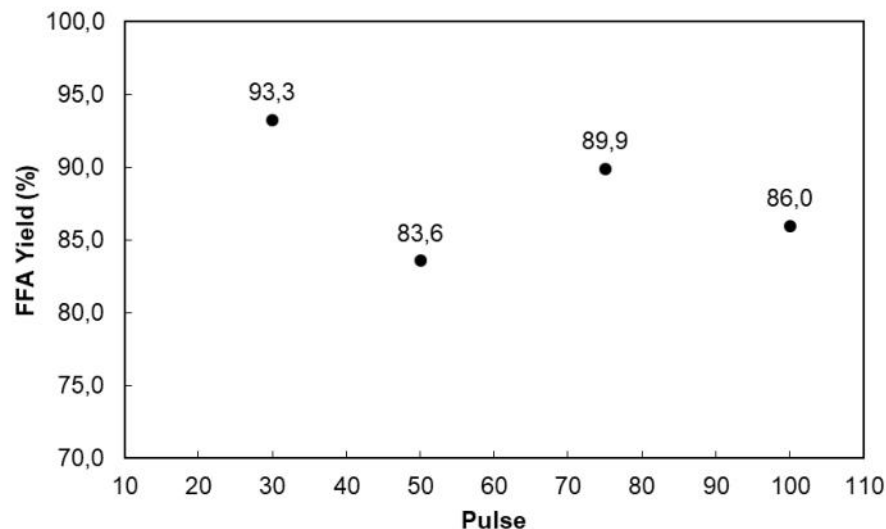


**Figure 30.** Effect of pulse in biodiesel yield by using ChCl:PTSA as catalyst

Figure 31 shows clearly that the yield does increase up to 60 minutes to then decrease with increased reaction time. Notably, high yields of 90.3% and 93.3% were achieved at reaction times of 30 and 60 min whereas at 90 minutes, the yield decreased. The increase of the yield from 30 to 60 minutes could be attributed to the enhancement of the mass transfer in the reaction media caused by ultrasound making that reaction reach equilibrium in short times. On the other hand, beyond 60 min the yield decreased. This could be attributed to a reduction in the amount of grease in the reaction medium. Since esterification is a reversible reaction, the decrease in grease and the increase in biodiesel content may lead to a shift in the equilibrium towards the reactants [115].

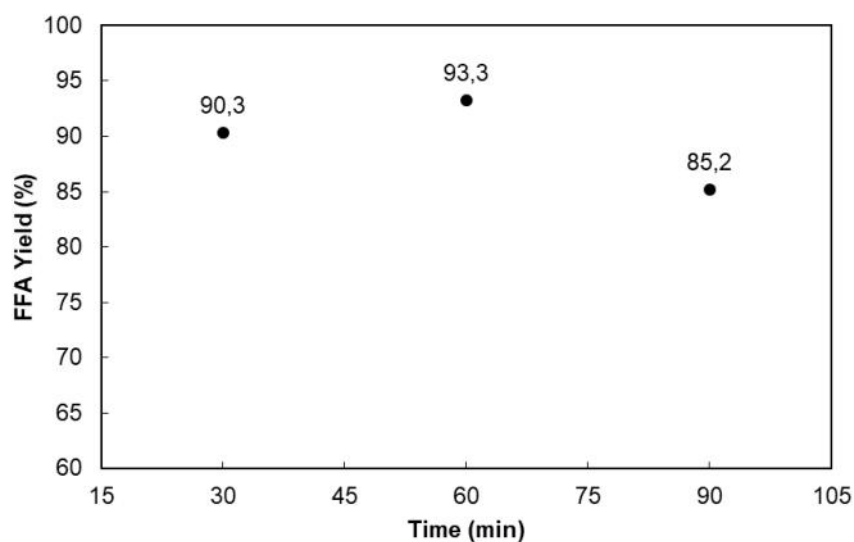


**Figure 31.** Effect of time in biodiesel yield by using ChCl:PTSA as catalyst

Experiments varying the reaction time revealed that equilibrium is reached at 60 minutes. This could help to explain better the yield difference obtained between pulsed and constant ultrasound irradiation. Typically, Masri et al. [99] and Martinez-Guerra et al. [103] indicated that continuous irradiation afforded better yields than pulsed one under short reaction times. This implies that 60 minutes might be excessive for the system under investigation in this research, and there may be potential to achieve higher yields in less than 30 minutes with continuous irradiation. Future studies should delve into this area to determine the most economically and environmentally viable option.

To further explore the key parameters in ultrasound-assisted biodiesel production with DES as catalysts, we investigated the influence of DES quantity to ensure using the optimal amount of catalyst to afford the highest possible biodiesel yield. We conducted ultrasound-assisted reactions under the established conditions of pulse (30%), ultrasound intensity (70%), reaction time (60 min), temperature (40°C), and methanol-to-grease molar ratio (10:1). The amount of DES was varied 0.05 to 0.3 mol<sub>DES</sub>/mol<sub>FFA</sub> and found results are presented in the Figure 32. Highest yield was 96.6% at 0.2 mol<sub>DES</sub>/mol<sub>FFA</sub>. please note here that this result matches closely yields obtained in Mexico (97%) using sewage sludge as raw material, highlighting consistency of the presented results here. The slight difference between the optimum DES quantity 0.1 (Mexico) and 0.2 (France) could be attributed to differences between the initial %FFA of the raw materials that was 81% and 95% respectively in Mexico and in France.

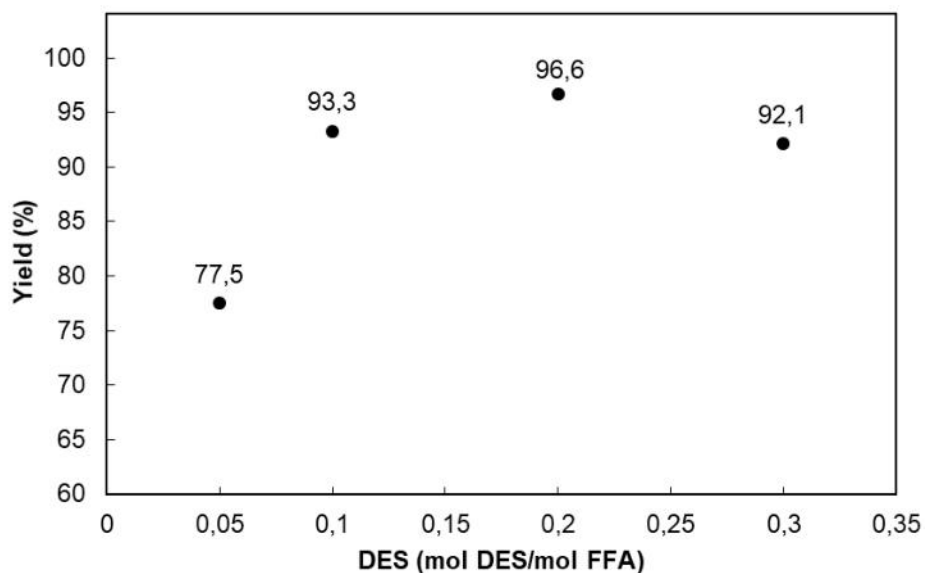


**Figure 32.** Effect of DES quantity in biodiesel yield by using ChCl:PTSA as catalyst

So-far presented results in this section have allowed us to determine key optimized parameters in the presence of ChCl:PTSA DES; whose are: intensity 70%, pulse 30, reaction time 60 min, temperature 40°C, methanol:grease molar ratio 10:1, and 0.2 mol<sub>DES</sub>/mol<sub>FFA</sub>.

The final parameter but not the least to be determined is the adequacy of the tested DES for the biodiesel production. We performed biodiesel reaction by using the selected DES from Hammett analysis: ChCl:OXA, BTEAC:PTSA, BTEAC:OXA, and Menthol:DA without omitting ChCl:PTSA which has been used previously to optimize other operating parameters. We have performed several reactions under both magnetic stirring and ultrasound irradiation with the conditions showed in Table 17 and results can be observed in Figure 33.

**Table 17.** Reaction conditions for ultrasound and magnetic stirring experiments.

Agitation	Intensity (%)	Pulse (%)	Temperature (°C)	Time (h)	Methanol (mol <sub>met</sub> /mol <sub>FFA</sub> )	DES (mol <sub>DES</sub> /mol <sub>FFA</sub> )
Magnetic stirring	-	-	60	3	10	0.1
Ultrasound	70	30	40	1	10	0.1
Ultrasound	70	30	40	1	10	0.2

We can observe from Figure 33 that higher yield was obtained by using PTSA as HBD. This could be because among all the HBD used, it is the one with the highest acidity value; what is also in agreement with the results obtained in Mexico. It can be observed that obtained yields between ChCl:PTSA and BTEAC:PTSA were quite similar allowing to demonstrate that for this DES the change in the HBA does not affect significantly to the biodiesel yield. This similar trend can be also observed for OA-based DES. Furthermore, ultrasound showed to greatly accelerate the

reaction rate as foreseen, allowing to obtain almost the same yield in one-third part of the time and 20°C less temperature when compared with magnetic stirring. This is attributed to the improvement in the mass transfer due to emulsifying effect of ultrasound of the reaction medium.

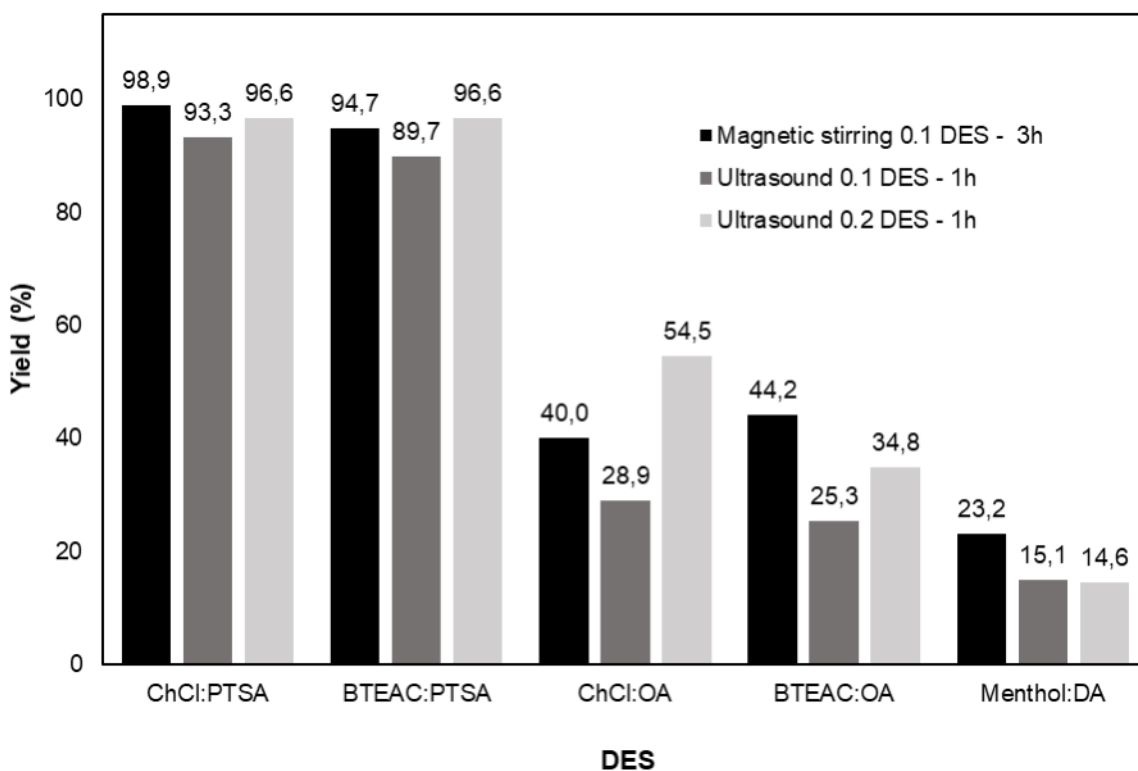


**Figure 33.** Biodiesel yield by using magnetic stirring and ultrasonic irradiation for five different DES.

Furthermore, it can be observed that ChCl:OA and BTEAC:OA exhibit similar yield values under magnetic stirring (40.0% and 44.2% respectively), consistent with the trend observed in experiments using PTSA as the HBD, where the yields achieve close values despite the change in HBA. This trend also persisted in the first scenario

using ultrasound and  $0.1 \text{ mol}_{\text{DES}}/\text{mol}_{\text{FFA}}$ , with values of 28.9% for ChCl:OA and 25.3% for BTEAC:OA. These values were lower than the yields obtained in reactions using magnetic stirring. This could be attributed to the reaction time. As seen in Figure 8 in section 7.2, esterification takes longer to reach equilibrium when using OA as HBD, due to the lower acidity of OA compared to PTSA. This suggests that one hour of reaction time may not be sufficient to obtain higher yields when using a DES with OA as HBD. This point is currently under investigation in our laboratory.

It was also observed that increasing the amount of DES from 0.1 to  $0.2 \text{ mol}_{\text{DES}}/\text{mol}_{\text{FFA}}$  led to a certain improvement in yield what can be expectable considering that more acidity within the reacting medium could lead to a more efficient acidic catalysis. In the case of ChCl:OA, this increase in DES quantity resulted in a yield of 54.5%, which is relatively close to the maximum yield found in previous experiments conducted in Mexico (59.7%). These experiments in Mexico determined that the optimal DES amount for ChCl:OA was  $0.2 \text{ mol}_{\text{DES}}/\text{mol}_{\text{FFA}}$ . It is worth noting that in the ultrasound-assisted process, the methanol:grease molar ratio was 10:1, whereas in the experiments in Mexico, it was 15:1. As previously mentioned, a high methanol:grease ratio of 15:1 was used in experiments conducted in Mexico to reduce the viscosity of the reaction medium and to facilitate better mass transfer. The experiment conducted with ultrasound, using the same amount of DES and less methanol, confirms that the limiting factor in the experiments showed in section 7 was indeed mass transfer in the medium due to its high viscosity and high heterogeneity of the reacting medium. This limitation can be overcome through the use of ultrasound.

Ultrasonic Experiments with BTEAC:OA also demonstrated an increase in yield with an increase in DES. However, the yields were not as high as those obtained with ChCl:PTSA. This could be because the DES with BTEAC:OA is more viscous than that made with ChCl, probably because of enhanced London forces between FFA and the DES when using BTEAC as compared to ChCl HBA. An excess of this DES can therefore affect the reaction yield. It is important to emphasize that experiments using OA as HBD were carried out under the most favorable conditions established with ChCl:PTSA. To conduct a comprehensive analysis using OA as the hydrogen bond donor (HBD), additional studies are imperative. These studies will find the optimum conditions but also enable us to ascertain if the trends observed in the experiments with PTSA persists under the refined parameters.

Finally, the lowest yield was obtained by using Menthol:DA as catalyst this could be explained because rather low acid value, the lowest of all tried DES when considered both Hammett methodology and pKa values of the corresponding free acids. It should be noted that also this one is the less viscous among the DES used for this study, being completely fluid at room temperature, so it allows us to say that even with a very low viscosity if the DES does not have strong acidity, the yield would not be high. The ultrasound experiments allowed to probe this point because increasing the mass transfer at maximum did not had any impact on the yield.

In this section, we observed that ultrasound and DES combination led to improvements in the reaction time and yield values. In the case of the DES with OA, it led to a decrease in the methanol:grease ratio, from 15:1 under magnetic stirring to 10:1 under ultrasound. This reduction is particularly significant for the environmental impact, as highlighted in the Life Cycle Assessment conducted in section 7.4. Methanol emerges as a substantial contributor to the environmental impact of the process. Studies varying the methanol molar ratio for DES with PTSA could have the same results, allowing decreasing the methanol:oil molar ratio to values lesser than 10:1. This part of the investigation opens the opportunities to conduct more studies about the biodiesel ultrasound-assisted production from residual greases and using DES as catalyst to study a complete optimization of the parameters of the process and by including energetic, environmental and economic factors.

## 9. CONCLUSIONS

- This project successfully produced biodiesel from wastewater sludge using deep eutectic solvents. This approach markedly reduced the process's environmental impact. Additionally, the inclusion of ethyl levulinate and magnesium oxide led to improved biodiesel properties, meeting European quality standards. These outcomes signify a substantial step towards sustainable, high-quality biodiesel production by using waste raw materials, green catalyst and combined effect additives.
- The highest biodiesel yield (97%) was achieved using 0.1 ChCl:PTSA : FFA molar ratio. The experimentation showed the importance of lower viscosity and higher acidity values in the esterification reaction. Recognizing these factors is essential, given the tunable nature of DES, which allows for the selection of components that enhance these properties.
- Biodiesel-Ethyl ester-MgO mixtures from 0.1 and 0.2 ethyl levulinate; 0.1 ethyl acetoacetate and 0.1 ethyl pyruvate mass fraction complied the limit values established by European biodiesel standard EN 14214. These mixtures introduce a promising category of biofuels, characterized by their minimal additive content.
- Excess molar volume and viscosity deviations reveal interactions among biodiesel mixture components, aiding in the comprehension of how properties like density

and viscosity change with additive inclusion and the impact of additive chain length, which produced the reduction of packing of ethyl ester molecules into the free volume of the biodiesel. This understanding is valuable for setting optimal operational parameters in internal combustion engines.

- The addition of 5 ppm<sub>m</sub> MgO increased the flash point and calorific value of the biodiesel. Conversely, the addition of ethyl esters to the biodiesel decreased the flash point, calorific value, and cetane index of the mixture at the same MgO concentration. This shows that the MgO concentration used can affect the properties of pure biodiesel. However, in biodiesel-ethyl ester mixtures, an increased MgO concentration is required to mitigate the effects on the flash point, calorific value, and cetane index, as observed previously.
- The addition of ethyl esters to biodiesel reduced simulated temperature and CO<sub>2</sub> mass fractions due to their viscosity-lowering effect. Viscosity emerged as a crucial parameter in biodiesel combustion modeling. These initial results were obtained under ideal and simplified conditions and will require further investigation through detailed chemistry to determine if viscosity remains a dominant factor.
- The inclusion of MgO particles in the combustion simulation have shown to decrease combustion temperature and NO<sub>x</sub> emissions. This effect can be attributed to the particles thermal dissipating effect. This insight allows for the

deliberate targeting of properties, such as thermal conductivity, when considering particulate additives for biodiesel.

- Environmental impact assessment shows that the use of hexane and the high electric consumption are the main contributors to environmental impact in the base scenario of biodiesel production from sewage sludge, this mainly due to the fossil origin of both factors. It emphasizes the necessity of prioritizing materials with sustainable origins, aligning with green chemistry principles.
- Biodiesel production using DES demonstrated a lower environmental impact compared to the base scenario. This can be attributed to reduced reaction time and purification stages, resulting in decreased electricity consumption and the elimination of hexane usage in the process. It is important to note that while the environmental benefits are promising, further research is needed to conduct an economic analysis, as none LCA has been performed with DES so far, except our current study. However, this represents a significant starting point for future investigations.
- In the scenario utilizing Oxalic acid DES, the notable increase in methanol consumption compared with the scenario involving PTSA DES, evidences that in high quantities methanol is also a critical aspect of the environmental impact, due to its fossil origin. For this reason, minimize the methanol use in the process must be necessary to decrease the biodiesel production impacts.

- The incorporation of ultrasound into biodiesel production using DES as a catalyst has shown significant advantages. This includes the reduction of key parameters like reaction time, temperature, and methanol molar ratio. These findings pave the way for future research to optimize the entire process. This includes evaluating the impact of ultrasound on the Life Cycle Assessment (LCA), ensuring its potential for substantial environmental impact reduction

## REFERENCES

- [1] International Energy Agency, "World Energy Balances 2019," *World Energy Balances Overview*, 2019.
- [2] J. Chow, R. J. Kopp, and P. R. Portney, "Energy Resources and Global Development," *Science (1979)*, 2003, doi: 10.1126/science.1091939.
- [3] W. S. Ebhota and T. C. Jen, "Fossil Fuels Environmental Challenges and the Role of Solar Photovoltaic Technology Advances in Fast Tracking Hybrid Renewable Energy System," *International Journal of Precision Engineering and Manufacturing - Green Technology*, 2020, doi: 10.1007/s40684-019-00101-9.
- [4] T. Beer, T. Grant, D. Williams, and H. Watson, "Fuel-cycle greenhouse gas emissions from alternative fuels in Australian heavy vehicles," *Atmos Environ*, 2002, doi: 10.1016/S1352-2310(01)00514-3.
- [5] M. N. Siddiquee and S. Rohani, "Lipid extraction and biodiesel production from municipal sewage sludges: A review," *Renewable and Sustainable Energy Reviews*, vol. 15, no. 2, pp. 1067–1072, 2011, doi: 10.1016/j.rser.2010.11.029.
- [6] L. T. Vargas-Ibáñez, G. A. Iglesias-Silva, J. J. Cano-Gómez, C. Escamilla-Alvarado, and M. A. Berrones-Eguiluz, "Densities and viscosities for binary liquid mixtures of biodiesel + 1-pentanol, 2-pentanol, or 2-methyl-1-butanol from (288.15 to 338.15) K at 0.1 MPa," *J Chem Eng Data*, vol. 63, no. 7, pp. 2438–2450, 2018, doi: 10.1021/acs.jced.7b00996.
- [7] S. V.D. Freitas, M. B. Oliveira, A. J. Queimada, M. J. Pratas, Á. S. Lima, and J. A. P. Coutinho, "Measurement and prediction of biodiesel surface tensions," *Energy and Fuels*, 2011, doi: 10.1021/ef201217q.
- [8] S. P. Singh and D. Singh, "Biodiesel production through the use of different sources and characterization of oils and their esters as the substitute of diesel: A review," *Renewable and Sustainable Energy Reviews*, vol. 14, no. 1, pp. 200–216, 2010, doi: 10.1016/j.rser.2009.07.017.
- [9] D. Mu, M. Addy, E. Anderson, P. Chen, and R. Ruan, "A life cycle assessment and economic analysis of the Scum-to-Biodiesel technology in wastewater treatment plants," *Bioresour Technol*, 2016, doi: 10.1016/j.biortech.2015.12.063.
- [10] M. C. Cammarota and D. M. G. Freire, "A review on hydrolytic enzymes in the treatment of wastewater with high oil and grease content," *Bioresour Technol*, vol. 97, no. 17, pp. 2195–2210, 2006, doi: 10.1016/j.biortech.2006.02.030.
- [11] V. G. Tacias Pascacio, A. Rosales Quintero, and B. Torrestiana Sánchez, "Evaluación y caracterización de grasas y aceites residuales de cocina para

la producción de biodiésel: Un caso de estudio,” *Revista Internacional de Contaminación Ambiental*, vol. 32, no. 3, 2016, doi: 10.20937/RICA.2016.32.03.05.

- [12] G. Pokoo-Aikins, A. Heath, R. A. Mentzer, M. Sam Mannan, W. J. Rogers, and M. M. El-Halwagi, “A multi-criteria approach to screening alternatives for converting sewage sludge to biodiesel,” *J Loss Prev Process Ind*, 2010, doi: 10.1016/j.jlp.2010.01.005.
- [13] M. K. Lam, K. T. Lee, and A. R. Mohamed, “Homogeneous , heterogeneous and enzymatic catalysis for transesterification of high free fatty acid oil ( waste cooking oil ) to biodiesel : A review,” *Biotechnol Adv*, vol. 28, no. 4, pp. 500–518, 2010, doi: 10.1016/j.biotechadv.2010.03.002.
- [14] G. Castellar, E. Angulo, and B. Cardozo, “Transesterificación de aceites vegetales empleando catalizadores heterogéneos,” *Prospect*, vol. 12, no. 2, pp. 90–104, 2014, doi: 10.1007/s11746-016-2798-5.
- [15] H. Zhao and G. A. Baker, “Ionic liquids and deep eutectic solvents for biodiesel synthesis: A review,” *Journal of Chemical Technology and Biotechnology*. 2013. doi: 10.1002/jctb.3935.
- [16] M. J. Earle, N. V. Plechkova, and K. R. Seddon, “Green synthesis of biodiesel using ionic liquids,” in *Pure and Applied Chemistry*, 2009. doi: 10.1351/PAC-CON-08-11-07.
- [17] Q. Wu, H. Chen, M. Han, D. Wang, and J. Wang, “Transesterification of cottonseed oil catalyzed by brønsted acidic ionic liquids,” *Ind Eng Chem Res*, vol. 46, no. 24, 2007, doi: 10.1021/ie070678o.
- [18] Y. Liu *et al.*, “Acidic deep eutectic solvents with long carbon chains as catalysts and reaction media for biodiesel production,” *Renew Energy*, vol. 162, pp. 1842–1853, Dec. 2020, doi: 10.1016/j.renene.2020.09.121.
- [19] P. Kalhor and K. Ghandi, “Deep eutectic solvents for pretreatment, extraction, and catalysis of biomass and food waste,” *Molecules*. 2019. doi: 10.3390/molecules24224012.
- [20] D. Z. Troter, Z. B. Todorović, D. R. Dokić-Stojanović, O. S. Stamenković, and V. B. Veljković, “Application of ionic liquids and deep eutectic solvents in biodiesel production: A review,” *Renewable and Sustainable Energy Reviews*. 2016. doi: 10.1016/j.rser.2016.04.011.
- [21] W. Huang, S. Tang, H. Zhao, and S. Tian, “Activation of commercial CaO for biodiesel production from rapeseed oil using a novel deep eutectic solvent,” *Ind Eng Chem Res*, 2013, doi: 10.1021/ie401292w.

- [22] L. Gu, W. Huang, S. Tang, S. Tian, and X. Zhang, "A novel deep eutectic solvent for biodiesel preparation using a homogeneous base catalyst," *Chemical Engineering Journal*, 2015, doi: 10.1016/j.cej.2014.08.026.
- [23] A. Gonzalo Callejo, "Producción de aditivos para la mejora de propiedades de biodiésel a partir de lignina y glicerina," Universidad de Zaragoza, 2014.
- [24] N. Ribeiro *et al.*, "The role of additives for diesel and diesel blended (ethanol or biodiesel) fuels: A review," *Energy and Fuels*, vol. 21, no. 4, pp. 2433–2445, 2007, doi: 10.1021/ef070060r.
- [25] H. Joshi, B. R. Moser, J. Toler, W. F. Smith, and T. Walker, "Ethyl levulinate: A potential bio-based diluent for biodiesel which improves cold flow properties," *Biomass Bioenergy*, 2011, doi: 10.1016/j.biombioe.2011.04.020.
- [26] A. Bohlouli and L. Mahdavian, "Catalysts used in biodiesel production: a review," *Biofuels*, vol. 0, no. 0, pp. 1–14, 2019, doi: 10.1080/17597269.2018.1558836.
- [27] V. Saxena, N. Kumar, and V. K. Saxena, "A comprehensive review on combustion and stability aspects of metal nanoparticles and its additive effect on diesel and biodiesel fuelled C.I. engine," *Renewable and Sustainable Energy Reviews*, vol. 70, no. December 2016, pp. 563–588, 2017, doi: 10.1016/j.rser.2016.11.067.
- [28] A. Keskin, M. Gürü, and D. Altıparmak, "Influence of metallic based fuel additives on performance and exhaust emissions of diesel engine," in *Energy Conversion and Management*, Elsevier Ltd, 2011, pp. 60–65. doi: 10.1016/j.enconman.2010.06.039.
- [29] J. Tu, G. H. Yeoh, and C. Liu, *Computational fluid dynamics: A practical approach*. 2018.
- [30] R. Govindan, "Computational Analysis of Thumba Biodiesel-Diesel Blends Combustion in CI Engine Using Ansys- Fluent," *International Journal of Computer & Mathematical Sciences*, 2014.
- [31] D. Balasubramanian, A. T. Hoang, I. Papla Venugopal, A. Shanmugam, J. Gao, and T. Wongwuttanasatian, "Numerical and experimental evaluation on the pooled effect of waste cooking oil biodiesel/diesel blends and exhaust gas recirculation in a twin-cylinder diesel engine," *Fuel*, 2021, doi: 10.1016/j.fuel.2020.119815.
- [32] S. Dixit, A. Kumar, S. Kumar, N. Waghmare, H. C. Thaku, and S. Khan, "CFD analysis of biodiesel blends and combustion using Ansys Fluent," in *Materials Today: Proceedings*, 2019. doi: 10.1016/j.matpr.2019.12.362.

- [33] R. Balasubramanian, A. Sircar, P. Sivakumar, and K. Anbarasu, "Production of biodiesel from dairy wastewater sludge: A laboratory and pilot scale study," *Egyptian Journal of Petroleum*, 2018, doi: 10.1016/j.ejpe.2018.02.002.
- [34] M. M. Gui, K. T. Lee, and S. Bhatia, "Feasibility of edible oil vs. non-edible oil vs. waste edible oil as biodiesel feedstock," *Energy*. 2008. doi: 10.1016/j.energy.2008.06.002.
- [35] A. P. Bora, D. P. Gupta, and K. S. Durbha, "Sewage sludge to bio-fuel: A review on the sustainable approach of transforming sewage waste to alternative fuel," *Fuel*. 2020. doi: 10.1016/j.fuel.2019.116262.
- [36] A. Mondala, K. Liang, H. Toghiani, R. Hernandez, and T. French, "Biodiesel production by in situ transesterification of municipal primary and secondary sludges," *Bioresour Technol*, vol. 100, no. 3, pp. 1203–1210, 2009, doi: 10.1016/j.biortech.2008.08.020.
- [37] M. N. Siddiquee, H. Kazemian, and S. Rohani, "Biodiesel Production from the Lipid of Wastewater Sludge Using an Acidic Heterogeneous Catalyst," *Chem Eng Technol*, vol. 34, no. 12, pp. 1983–1988, Dec. 2011, doi: <https://doi.org/10.1002/ceat.201100119>.
- [38] C. hao Bi *et al.*, "Process development for scum to biodiesel conversion," *Bioresour Technol*, vol. 185, pp. 185–193, 2015, doi: 10.1016/j.biortech.2015.01.081.
- [39] B. S. Moreno-Caballero, "Effect of metal oxides on the physicochemical properties of biodiesel produced from wastewater," Master Thesis, Autonomous University of Nuevo León, 2020.
- [40] T. Long, Y. Deng, S. Gan, and J. Chen, "Application of Choline Chloride·xZnCl<sub>2</sub> Ionic Liquids for Preparation of Biodiesel," *Chin J Chem Eng*, vol. 18, no. 2, pp. 322–327, Apr. 2010, doi: 10.1016/S1004-9541(08)60359-6.
- [41] W. N. R. W. Isahak, M. Ismail, M. Jahim, J. Salimon, and M. A. Yarmo, "Transesterification of Palm Oil by using Ionic Liquids as a New Potential Catalyst," *Trends Appl Sci Res*, vol. 6, pp. 1055–1062, 2011, Accessed: Feb. 27, 2023. [Online]. Available: <https://scialert.net/fulltext/?doi=tasr.2011.1055.1062&org=245#ref>
- [42] R. Manurung, D. A. Ramadhani, and S. Maisarah, "One step transesterification process of sludge palm oil (SPO) by using deep eutectic solvent (DES) in biodiesel production," in *AIP Conference Proceedings*, 2017. doi: 10.1063/1.4985531.
- [43] L. Cao, J. Wang, K. Liu, and S. Han, "Ethyl acetoacetate: A potential bio-based diluent for improving the cold flow properties of biodiesel from waste cooking

- oil,” *Appl Energy*, vol. 114, pp. 18–21, 2014, doi: 10.1016/j.apenergy.2013.09.050.
- [44] T. Lei *et al.*, “Performance and emission characteristics of a diesel engine running on optimized ethyl levulinate-biodiesel-diesel blends,” *Energy*, 2016, doi: 10.1016/j.energy.2015.11.059.
- [45] Z. Wang *et al.*, “Comparison of the Physical and Chemical Properties, Performance, and Emissions of Ethyl Levulinate-Biodiesel-Diesel and n-Butanol-Biodiesel-Diesel Blends,” *Energy and Fuels*, vol. 31, no. 5, pp. 5055–5062, 2017, doi: 10.1021/acs.energyfuels.6b02851.
- [46] A. Keskin, M. Gürü, and D. Altiparmak, “Influence of tall oil biodiesel with Mg and Mo based fuel additives on diesel engine performance and emission,” *Bioresour Technol*, vol. 99, no. 14, pp. 6434–6438, 2008, doi: 10.1016/j.biortech.2007.11.051.
- [47] A. Ranjan, S. S. Dawn, J. Jayaprabakar, N. Nirmala, K. Saikiran, and S. Sai Sriram, “Experimental investigation on effect of MgO nanoparticles on cold flow properties, performance, emission and combustion characteristics of waste cooking oil biodiesel,” *Fuel*, vol. 220, no. November 2017, pp. 780–791, 2018, doi: 10.1016/j.fuel.2018.02.057.
- [48] J. Dufour and D. Iribarren, “Life cycle assessment of biodiesel production from free fatty acid-rich wastes,” *Renew Energy*, 2012, doi: 10.1016/j.renene.2011.07.016.
- [49] M. E. Hums, R. A. Cairncross, and S. Spatari, “Life-Cycle Assessment of Biodiesel Produced from Grease Trap Waste,” *Environ Sci Technol*, vol. 50, no. 5, 2016, doi: 10.1021/acs.est.5b02667.
- [50] A. P. Abbott, D. Boothby, G. Capper, D. L. Davies, and R. K. Rasheed, “Deep Eutectic Solvents Formed between Choline Chloride and Carboxylic Acids: Versatile Alternatives to Ionic Liquids,” *J Am Chem Soc*, vol. 126, no. 29, pp. 9142–9147, Jul. 2004, doi: 10.1021/ja048266j.
- [51] Y. Cui, C. Li, J. Yin, S. Li, Y. Jia, and M. Bao, “Design, synthesis and properties of acidic deep eutectic solvents based on choline chloride,” *J Mol Liq*, 2017, doi: 10.1016/j.molliq.2017.04.052.
- [52] J. J. Cano-Gómez, G. A. Iglesias-Silva, P. Rivas, C. O. Díaz-Ovalle, and F. De Jesús Cerino-Córdova, “Densities and Viscosities for Binary Liquid Mixtures of Biodiesel + 1-Butanol, + Isobutyl Alcohol, or + 2-Butanol from 293.15 to 333.15 K at 0.1 MPa,” *J Chem Eng Data*, vol. 62, no. 10, pp. 3391–3400, 2017, doi: 10.1021/acs.jced.7b00440.
- [53] M. U. Kaisan, F. O. Anafi, J. Nuszowski, D. M. Kulla, and S. Umaru, “Calorific value, flash point and cetane number of biodiesel from cotton, jatropha and

- neem binary and multi-blends with diesel,” *Biofuels*, 2020, doi: 10.1080/17597269.2017.1358944.
- [54] Y. Ding, G. Zhang, H. Wu, B. Hai, L. Wang, and Y. Qian, “Nanoscale magnesium hydroxide and magnesium oxide powders: Control over size, shape, and structure via hydrothermal synthesis,” *Chemistry of Materials*, vol. 13, no. 2, pp. 435–440, 2001, doi: 10.1021/cm000607e.
- [55] J. G. Speight, “Chapter 10 - Combustion of hydrocarbons,” in *Handbook of Industrial Hydrocarbon Processes (Second Edition)*, Second Edition., J. G. Speight, Ed., Boston: Gulf Professional Publishing, 2020, pp. 421–463. doi: <https://doi.org/10.1016/B978-0-12-809923-0.00010-2>.
- [56] ANSYS, “ANSYS FLUENT User Guide v12,” *Acta Psychiatr Scand*, vol. 123, no. 6, 2011.
- [57] E. R. Vasquez and T. Eldredge, “18 - Process modeling for hydrocarbon fuel conversion,” in *Advances in Clean Hydrocarbon Fuel Processing*, M. R. Khan, Ed., in Woodhead Publishing Series in Energy. , Woodhead Publishing, 2011, pp. 509–545. doi: <https://doi.org/10.1533/9780857093783.5.509>.
- [58] E. Ramírez Lara *et al.*, “A comprehensive hazardous waste management program in a Chemistry School at a Mexican university,” *J Clean Prod*, 2017, doi: 10.1016/j.jclepro.2016.11.158.
- [59] M. B. Taysun, E. Sert, and F. S. Atalay, “Physical properties of benzyl trimethyl ammonium chloride based deep eutectic solvents and employment as catalyst,” *J Mol Liq*, vol. 223, pp. 845–852, Nov. 2016, doi: 10.1016/j.molliq.2016.07.148.
- [60] B. Y. Zhao, P. Xu, F. X. Yang, H. Wu, M. H. Zong, and W. Y. Lou, “Biocompatible Deep Eutectic Solvents Based on Choline Chloride: Characterization and Application to the Extraction of Rutin from *Sophora japonica*,” *ACS Sustain Chem Eng*, 2015, doi: 10.1021/acssuschemeng.5b00619.
- [61] M. H. Shafie, R. Yusof, and C. Y. Gan, “Synthesis of citric acid monohydrate-choline chloride based deep eutectic solvents (DES) and characterization of their physicochemical properties,” *J Mol Liq*, vol. 288, 2019, doi: 10.1016/j.molliq.2019.111081.
- [62] M. Jablonsky, A. Butor Skulcova, L. Kamenska, M. Vrška, and J. Sima, “Deep Eutectic Solvents: Fractionation of Wheat Straw,” *Bioresources*, vol. 10, pp. 8039–8047, Oct. 2015, doi: 10.15376/biores.10.4.8039-8047.
- [63] Z. Zhu, H. Lü, M. Zhang, and H. Yang, “Deep eutectic solvents as non-traditionally multifunctional media for the desulfurization process of fuel oil,” *Physical Chemistry Chemical Physics*, 2021, doi: 10.1039/d0cp05153e.

- [64] N. Rodriguez Rodriguez, L. MacHiels, and K. Binnemans, "P-Toluenesulfonic Acid-Based Deep-Eutectic Solvents for Solubilizing Metal Oxides," *ACS Sustain Chem Eng*, 2019, doi: 10.1021/acssuschemeng.8b05072.
- [65] C. Florindo, F. S. Oliveira, L. P. N. Rebelo, A. M. Fernandes, and I. M. Marrucho, "Insights into the synthesis and properties of deep eutectic solvents based on cholinium chloride and carboxylic acids," *ACS Sustain Chem Eng*, 2014, doi: 10.1021/sc500439w.
- [66] S. K. Saha, S. Dey, and R. Chakraborty, "Effect of choline chloride-oxalic acid based deep eutectic solvent on the ultrasonic assisted extraction of polyphenols from *Aegle marmelos*," *J Mol Liq*, 2019, doi: 10.1016/j.molliq.2019.110956.
- [67] Y. Zhou, H. Qin, H. Cheng, L. Chen, B. Zhang, and Z. Qi, "Reactive extraction for synthesizing long chain ester butyl hexanoate intensified by deep eutectic solvent," *Chin J Chem Eng*, vol. 36, 2021, doi: 10.1016/j.cjche.2020.10.005.
- [68] J. T. Davies, "A quantitative kinetic theory of emulsion type. I. Physical chemistry of the emulsifying agent. In: Gas/Liquid and Liquid/Liquid Interfaces," *2nd International Congress Surface Activity*, vol. 42, pp. 6–438, 1957, [Online]. Available: <https://citeseerx.ist.psu.edu/viewdoc/download?doi=10.1.1.473.424&rep=rep1&type=pdf>
- [69] S. M. Miraboutalebi, P. Kazemi, and P. Bahrami, "Fatty Acid Methyl Ester (FAME) composition used for estimation of biodiesel cetane number employing random forest and artificial neural networks: A new approach," *Fuel*, vol. 166, 2016, doi: 10.1016/j.fuel.2015.10.118.
- [70] L. T. Vargas-Ibáñez, J. J. Cano-Gómez, G. A. Iglesias-Silva, I. A. Santos-López, O. E. Benavides-Moran, and P. Zwolinski, "Physical properties of biodiesel blended with hexanol isomers at different temperatures: surface tension, density, viscosity, and refractive index," *J Chem Eng Data*, vol. 65, pp. 3706–3727, 2020, doi: 10.1021/acs.jced.0c00328.
- [71] H. Ariba, Y. Wang, C. Devouge-Boyer, R. P. Stateva, and S. Leveneur, "Physicochemical Properties for the Reaction Systems: Levulinic Acid, Its Esters, and  $\gamma$ -Valerolactone," *J Chem Eng Data*, vol. 65, pp. 3008–3020, 2020, doi: 10.1021/acs.jced.9b00965.
- [72] H. Guerrero, C. Lafuente, F. Royo, L. Lomba, and B. Giner, "P P T behavior of several chemicals from biomass," *Energy and Fuels*, vol. 27, pp. 3009–3013, 2011, doi: 10.1021/ef200653s.

- [73] L. Lomba, B. Giner, I. Bandrés, C. Lafuente, and M. R. Pino, "Physicochemical properties of green solvents derived from biomass," *Green Chemistry*, vol. 13, pp. 2062–2070, 2011, doi: 10.1039/c0gc00853b.
- [74] G. J. Cox and M. L. Dodds, "Some Alkyl Esters of Levulinic Acid," *J Am Chem Soc*, 1933, doi: 10.1021/ja01335a059.
- [75] N. A. S. Ramli and F. Abdullah, "Study of Density, Surface Tension, and Refractive Index of Binary Mixtures Containing Alkyl Levulinate and n-Alcohol from 298.15 to 323.15 K," *J Chem Eng Data*, vol. 66, pp. 1856–1876, 2021, doi: 10.1021/acs.jced.0c00694.
- [76] Y. W. Sheu and C. H. Tu, "Densities, viscosities, refractive indices, and surface tensions for 12 flavor esters from T = 288.15 K to T = 358.15 K," *J Chem Eng Data*, vol. 50, pp. 1706–1710, 2005, doi: 10.1021/je050170x.
- [77] Y. W. Sheu and C. H. Tu, "Densities and viscosities of binary mixtures of ethyl acetoacetate, ethyl isovalerate, methyl benzoate, benzyl acetate, ethyl salicylate, and benzyl propionate with ethanol at T = (288.15, 298.15, 308.15, and 318.15) K," *J Chem Eng Data*, vol. 51, pp. 545–553, 2006, doi: 10.1021/je050402s.
- [78] B. Kabane, R. Chokkareddy, and G. G. Redhi, "Molecular interaction studies of binary systems comprising [C 2 mim] [BF 4 ] with ethyl acetoacetate or benzaldehyde," *Heliyon*, vol. 5, p. e01548, 2019, doi: 10.1016/j.heliyon.2019.e01548.
- [79] J. N. Nayak, M. I. Aralaguppi, and T. M. Aminabhavi, "Density, Viscosity, Refractive Index, and Speed of Sound in the Binary Mixtures of 1,4-Dioxane + Ethyl Acetoacetate, + Diethyl Oxalate, + Diethyl Phthalate, or + Dioctyl Phthalate at 298.15, 303.15, and 308.15 K," *J Chem Eng Data*, vol. 48, pp. 1489–1494, 2003, doi: 10.1021/je0301489.
- [80] V. Sajith, C. B. Sobhan, and G. P. Peterson, "Experimental investigations on the effects of cerium oxide nanoparticle fuel additives on biodiesel," *Advances in Mechanical Engineering*, 2010, doi: 10.1155/2010/581407.
- [81] M. Gürü, A. Koca, Ö. Can, C. Çınar, and F. Şahin, "Biodiesel production from waste chicken fat based sources and evaluation with Mg based additive in a diesel engine," *Renew Energy*, vol. 35, no. 3, pp. 637–643, 2010, doi: 10.1016/j.renene.2009.08.011.
- [82] Ü. Ağbulut, S. Sarıdemir, U. Rajak, F. Polat, A. Afzal, and T. N. Verma, "Effects of high-dosage copper oxide nanoparticles addition in diesel fuel on engine characteristics," *Energy*, 2021, doi: 10.1016/j.energy.2021.120611.
- [83] H. Djojoputro and S. Ismadji, "Density and viscosity of binary mixtures of ethyl-2-methylbutyrate and ethyl hexanoate with methanol, ethanol, and 1-propanol

- at (293.15, 303.15, and 313.15) K,” *J Chem Eng Data*, vol. 50, pp. 1343–1347, 2005, doi: 10.1021/je0500633.
- [84] I. Barabás and I. A. Todoruț, “Predicting the temperature dependent viscosity of biodiesel-diesel- bioethanol blends,” *Energy and Fuels*, 2011, doi: 10.1021/ef2007936.
- [85] R. Ahluwalia, R. K. Wanchoo, S. K. Sharma, and J. L. Vashisht, “Density, viscosity, and surface tension of binary liquid systems: Ethanoic acid, propanoic acid, and butanoic acid with nitrobenzene,” *J Solution Chem*, vol. 25, pp. 905–917, 1996, doi: 10.1007/BF00972581.
- [86] A. Aucejo, M. Cruz Burguet, and R. Muñoz, “Densities , Viscosities , and Refractive Indices of Some Binary Liquid Systems of Ethanol + Isomers of Hexanol at 298 . 15 K,” *J Chem Eng Data*, vol. 41, pp. 1131–1134, 1996, doi: 10.1021/je9601265.
- [87] G. P. Dubey, M. Sharma, and N. Dubey, “Study of densities, viscosities, and speeds of sound of binary liquid mixtures of butan-1-ol with n-alkanes (C6, C8, and C10) at T = (298.15, 303.15, and 308.15) K,” *Journal of Chemical Thermodynamics*, 2008, doi: 10.1016/j.jct.2007.05.016.
- [88] D. Bala Karuna Kumar, T. Srinivasa Krishna, B. Oruganti, C. V. Pramod, and G. Srinivasa Rao, “Investigation of molecular interactions by volumetric, transport, spectral and DFT studies in some liquid binaries of N-methyl-2-pyrrolidone with N-alkyl anilines in the temperature range 303.15–318.15 K,” *J Mol Liq*, vol. 337, p. 116449, 2021, doi: 10.1016/j.molliq.2021.116449.
- [89] H. Wang, N. Zhang, and X. Wang, “Densities and Viscosities for the Binary Mixtures of n-Nonane with 1-Heptanol, 1-Octanol, 1-Nonanol, and 1-Decanol,” *J Chem Eng Data*, vol. 67, no. 1, pp. 74–87, Jan. 2022, doi: 10.1021/acs.jced.1c00746.
- [90] M. Jagadish, Donepudi, Kumar, Puli Ravi and K. Madhu, “Performance and emission characteristics of diesel engine run on biofuels based on experimental and semi analytical methods,” *International Journal of Energy and Environment*, vol. 2, no. 5, 2011.
- [91] U. Rajak, P. Nashine, P. K. Chaurasiya, and T. N. Verma, “A numerical investigation of the species transport approach for modeling of gaseous combustion,” *Journal of Thermal Engineering*, vol. 7, 2021, doi: 10.18186/THERMAL.1051312.
- [92] A. T. Hoang, “Combustion behavior, performance and emission characteristics of diesel engine fuelled with biodiesel containing cerium oxide nanoparticles: A review,” *Fuel Processing Technology*, vol. 218. 2021. doi: 10.1016/j.fuproc.2021.106840.

- [93] G. A. Ban-Weiss, J. Y. Chen, B. A. Buchholz, and R. W. Dibble, "A numerical investigation into the anomalous slight NO<sub>x</sub> increase when burning biodiesel; A new (old) theory," *Fuel Processing Technology*, vol. 88, no. 7, 2007, doi: 10.1016/j.fuproc.2007.01.007.
- [94] E. Santoyo-Castelazo, H. Gujba, and A. Azapagic, "Life cycle assessment of electricity generation in Mexico," *Energy*, vol. 36, no. 3, 2011, doi: 10.1016/j.energy.2011.01.018.
- [95] J. Wang, W. H. Wang, and W. Zhu, "CN101845004B: Method for preparing p-toluenesulfonic acid by toluene sulfonation," 2010 Accessed: Feb. 06, 2023. [Online]. Available: <https://patents.google.com/patent/CN101845004B/en?q=para+toluene+sulfonic+acid+with+sulphuric+acid>
- [96] H. B. Balaraman and S. K. Rathnasamy, "Kinetics and microwave-assisted extractive transesterification studies of high octane methyl esters (HOME) from karanja and chicken lard oil using protic deep eutectic solvent," *Fuel*, vol. 268, 2020, doi: 10.1016/j.fuel.2020.117299.
- [97] Y. Zhang *et al.*, "Green deep eutectic solvent assisted enzymatic preparation of biodiesel from yellow horn seed oil with microwave irradiation," *J Mol Catal B Enzym*, vol. 123, 2016, doi: 10.1016/j.molcatb.2015.10.013.
- [98] W. Guo, H. Li, G. Ji, and G. Zhang, "Ultrasound-assisted production of biodiesel from soybean oil using Brønsted acidic ionic liquid as catalyst," *Bioresour Technol*, vol. 125, 2012, doi: 10.1016/j.biortech.2012.08.132.
- [99] A. N. Masri, M. I. Abdul Mutalib, W. Z. N. Yahya, N. F. Aminuddin, and J. M. Leveque, "Rapid esterification of fatty acid using dicationic acidic ionic liquid catalyst via ultrasonic-assisted method," *Ultrason Sonochem*, vol. 60, 2020, doi: 10.1016/j.ultsonch.2019.104732.
- [100] E. Martinez-Guerra and V. G. Gude, "Determining optimum pulse mode for ultrasound enhanced biodiesel production," *Journal of Industrial and Engineering Chemistry*, vol. 35, 2016, doi: 10.1016/j.jiec.2016.01.004.
- [101] P. Chand, V. R. Chintareddy, J. G. Verkade, and D. Grewell, "Enhancing biodiesel production from soybean oil using ultrasonics," *Energy and Fuels*, vol. 24, no. 3, 2010, doi: 10.1021/ef9011752.
- [102] J. Ji, J. Wang, Y. Li, Y. Yu, and Z. Xu, "Preparation of biodiesel with the help of ultrasonic and hydrodynamic cavitation," *Ultrasonics*, vol. 44, no. SUPPL., 2006, doi: 10.1016/j.ultras.2006.05.020.
- [103] E. Martinez-Guerra and V. G. Gude, "Continuous and pulse sonication effects on transesterification of used vegetable oil," *Energy Convers Manag*, vol. 96, 2015, doi: 10.1016/j.enconman.2015.02.073.

- [104] B. Salamatinia, H. Mootabadi, I. Hashemizadeh, and A. Z. Abdullah, "Intensification of biodiesel production from vegetable oils using ultrasonic-assisted process: Optimization and kinetic," *Chemical Engineering and Processing: Process Intensification*, vol. 73, 2013, doi: 10.1016/j.cep.2013.07.010.
- [105] H. Balaraman, M. Sekar, S. Detchanamoorthy, and S. Rathnasamy, "Synergetic effect of sustainable protic deep eutectic solvent and sonochemical extractor for extractive transesterification of biodiesel from *Chlorella salina*," *Fuel*, vol. 333, 2023, doi: 10.1016/j.fuel.2022.126410.
- [106] T. Robert, L. Magna, H. Olivier-Bourbigou, and B. Gilbert, "A Comparison of the Acidity Levels in Room-Temperature Ionic Liquids," *J Electrochem Soc*, vol. 156, no. 9, 2009, doi: 10.1149/1.3169857.
- [107] Z. Zhang *et al.*, "Physicochemical transformation and enzymatic hydrolysis promotion of reed straw after pretreatment with a new deep eutectic solvent," *Carbohydr Polym*, vol. 290, 2022, doi: 10.1016/j.carbpol.2022.119472.
- [108] Y. Liu, X. Zheng, S. Tao, L. Hu, X. Zhang, and X. Lin, "Process optimization for deep eutectic solvent pretreatment and enzymatic hydrolysis of sugar cane bagasse for cellulosic ethanol fermentation," *Renew Energy*, vol. 177, 2021, doi: 10.1016/j.renene.2021.05.131.
- [109] Y. Liu *et al.*, "Enhanced Enzymatic Hydrolysis and Lignin Extraction of Wheat Straw by Triethylbenzyl Ammonium Chloride/Lactic Acid-Based Deep Eutectic Solvent Pretreatment," *ACS Omega*, vol. 4, no. 22, 2019, doi: 10.1021/acsomega.9b02709.
- [110] Y. Zhao *et al.*, "Catalytic amounts of Brønsted acidic ionic liquids promoted esterification: Study of acidity-activity relationship," *Catal Commun*, vol. 10, no. 5, 2009, doi: 10.1016/j.catcom.2008.11.030.
- [111] X. Liu *et al.*, "SO<sub>3</sub>H-functionalized ionic liquids for selective alkylation of p-cresol with tert-butanol," *Ind Eng Chem Res*, vol. 47, no. 15, 2008, doi: 10.1021/ie070647t.
- [112] A. N. Masri, M. I. Abdul Mutalib, N. F. Aminuddin, and J. M. Lévêque, "Novel SO<sub>3</sub>H-functionalized dicationic ionic liquids – A comparative study for esterification reaction by ultrasound cavitation and mechanical stirring for biodiesel production," *Sep Purif Technol*, vol. 196, 2018, doi: 10.1016/j.seppur.2017.08.061.
- [113] D. I. M. Al-Risheq, M. S. Nasser, H. Qiblawey, M. M. Ba-Abbad, A. Benamor, and I. A. Hussein, "Destabilization of stable bentonite colloidal suspension using choline chloride based deep eutectic solvent: Optimization study,"

*Journal of Water Process Engineering*, vol. 40, 2021, doi: 10.1016/j.jwpe.2020.101885.

- [114] H. H. Ali, M. M. Ghareeb, M. Al-Remawi, and F. T. Al-Akayleh, "New insight into single phase formation of capric acid/menthol eutectic mixtures by Fourier-transform infrared spectroscopy and differential scanning calorimetry," *Tropical Journal of Pharmaceutical Research*, vol. 19, no. 2, 2020, doi: 10.4314/tjpr.v19i2.19.
- [115] R. Saha and V. V. Goud, "Ultrasound assisted transesterification of high free fatty acids karanja oil using heterogeneous base catalysts," *Biomass Convers Biorefin*, vol. 5, no. 2, 2015, doi: 10.1007/s13399-014-0133-7.

## APPENDIX A

### Experimental densities, viscosities, and refractive index for biodiesel + ethyl ester + MgO (5 ppm<sub>m</sub>) mixtures

**Table A1.** Experimental Densities,  $\rho$ (g·cm<sup>-3</sup>), Viscosities,  $\eta$ (mPa·s), and Refractive Index  $n_D$ , for Biodiesel (1) + Ethyl Levulinate (2) + MgO (3),  $w_3 = 5$  ppm<sub>m</sub> in mass fraction, at  $p = 0.1$  MPa<sup>a</sup>

$w_2$	$x_2$	$\rho$	$\eta$	$n_D$									
		$T = 288.15$ K			$T = 293.15$ K			$T = 298.15$ K			$T = 303.15$ K		
0.000	0.000	0.8812	9.46	1.4521	0.8776	8.06	1.4501	0.8739	6.98	1.4481	0.8703	6.06	1.4462
0.100	0.181	0.8924	8.08	1.4489	0.8886	6.91	1.4469	0.8849	5.99	1.4449	0.8811	5.21	1.4430
0.200	0.332	0.9039	6.93	1.4459	0.9000	5.94	1.4439	0.8961	5.15	1.4419	0.8923	4.49	1.4399
0.300	0.460	0.9159	5.96	1.4430	0.9119	5.13	1.4409	0.9079	4.45	1.4389	0.9039	3.89	1.4369
0.400	0.570	0.9282	5.14	1.4402	0.9241	4.45	1.4381	0.9200	3.86	1.4360	0.9159	3.38	1.4340
0.500	0.666	0.9413	4.46	1.4374	0.9371	3.88	1.4353	0.9329	3.37	1.4332	0.9286	2.96	1.4311
0.600	0.749	0.9551	3.89	1.4346	0.9508	3.41	1.4325	0.9464	2.97	1.4304	0.9420	2.62	1.4283
0.700	0.823	0.9697	3.40	1.4318	0.9652	3.01	1.4297	0.9607	2.63	1.4276	0.9562	2.34	1.4255
0.800	0.888	0.9847	2.99	1.4291	0.9801	2.67	1.4270	0.9754	2.34	1.4248	0.9708	2.10	1.4228
0.900	0.947	1.0006	2.65	1.4267	0.9959	2.39	1.4246	0.9912	2.10	1.4224	0.9864	1.89	1.4203
1.000	1.000	1.0174	2.36	1.4246	1.0125	2.15	1.4224	1.0077	1.90	1.4202	1.0028	1.71	1.4180
		$T = 308.15$ K			$T = 313.15$ K			$T = 318.15$ K			$T = 323.15$ K		
0.000	0.000	0.8666	5.33	1.4442	0.8630	4.72	1.4422	0.8599	4.21	1.4402	0.8557	3.77	1.4382
0.100	0.181	0.8773	4.60	1.4410	0.8736	4.09	1.4390	0.8703	3.66	1.4371	0.8660	3.29	1.4351
0.200	0.332	0.8884	3.97	1.4379	0.8845	3.54	1.4359	0.8811	3.17	1.4339	0.8767	2.86	1.4319
0.300	0.460	0.8999	3.44	1.4349	0.8959	3.08	1.4329	0.8923	2.77	1.4309	0.8879	2.50	1.4289
0.400	0.570	0.9118	3.00	1.4320	0.9077	2.70	1.4300	0.9040	2.43	1.4280	0.8995	2.20	1.4259
0.500	0.666	0.9244	2.64	1.4291	0.9202	2.39	1.4271	0.9164	2.16	1.4251	0.9118	1.96	1.4231
0.600	0.749	0.9377	2.35	1.4263	0.9333	2.14	1.4243	0.9292	1.94	1.4223	0.9246	1.77	1.4202
0.700	0.823	0.9517	2.11	1.4234	0.9472	1.93	1.4214	0.9429	1.76	1.4194	0.9383	1.61	1.4174
0.800	0.888	0.9662	1.90	1.4207	0.9616	1.75	1.4187	0.9571	1.60	1.4167	0.9524	1.47	1.4147
0.900	0.947	0.9817	1.72	1.4183	0.9769	1.59	1.4162	0.9722	1.46	1.4142	0.9674	1.35	1.4122
1.000	1.000	0.9979	1.56	1.4159	0.9930	1.45	1.4139	0.9881	1.34	1.4118	0.9832	1.23	1.4097

<sup>a</sup>Standard uncertainties  $u$  are  $u(w_2) = 0.002$ ,  $u(x_2) = 0.002$ ,  $u_r(\rho) = 5 \times 10^{-4}$ ,  $u_r(\eta) = 0.03$ ,  $u_r(n_D) = 2 \times 10^{-4}$ ,  $u(T) = 0.01$  K for density,  $u(T) = 0.03$  K for viscosity,  $u(T) = 0.05$  K for refractive index and  $u(p) = 10$  kPa.

**Table A1. Continued**

$w_2$	$x_2$	$\rho$	$\eta$	$n_D$	$\rho$	$\eta$	$n_D$	$\rho$	$\eta$	$n_D$
		$T = 328.15 \text{ K}$			$T = 333.15 \text{ K}$			$T = 338.15 \text{ K}$		
0.000	0.000	0.8521	3.40	1.4362	0.8484	3.08	1.4342	0.8448	2.81	1.4322
0.100	0.181	0.8623	2.98	1.4331	0.8585	2.71	1.4312	0.8547	2.48	1.4292
0.200	0.332	0.8729	2.60	1.4299	0.8690	2.37	1.4280	0.8651	2.17	1.4260
0.300	0.460	0.8839	2.28	1.4269	0.8799	2.09	1.4249	0.8759	1.92	1.4229
0.400	0.570	0.8954	2.01	1.4239	0.8913	1.85	1.4219	0.8872	1.70	1.4199
0.500	0.666	0.9076	1.80	1.4210	0.9033	1.66	1.4190	0.8991	1.53	1.4170
0.600	0.749	0.9202	1.63	1.4182	0.9159	1.51	1.4162	0.9115	1.40	1.4141
0.700	0.823	0.9338	1.49	1.4153	0.9293	1.38	1.4133	0.9248	1.28	1.4113
0.800	0.888	0.9478	1.36	1.4126	0.9431	1.27	1.4106	0.9385	1.18	1.4086
0.900	0.947	0.9626	1.25	1.4101	0.9579	1.16	1.4081	0.9531	1.08	1.4060
1.000	1.000	0.9783	1.14	1.4076	0.9734	1.06	1.4055	0.9685	0.99	1.4034

<sup>a</sup>Standard uncertainties  $u$  are  $u(w_2) = 0.002$ ,  $u(x_2) = 0.002$ ,  $u_r(\rho) = 5 \times 10^{-4}$ ,  $u_r(\eta) = 0.03$ ,  $u_r(n_D) = 2 \times 10^{-4}$ ,  $u(T) = 0.01 \text{ K}$  for density,  $u(T) = 0.03 \text{ K}$  for viscosity,  $u(T) = 0.05 \text{ K}$  for refractive index and  $u(p) = 10 \text{ kPa}$ .

**Table A2.** Experimental Densities,  $\rho$ (g·cm<sup>-3</sup>), Viscosities,  $\eta$ (mPa·s), and Refractive Index  $n_D$ , for Biodiesel (1) + Ethyl acetoacetate (2) + MgO (3),  $w_3 = 5$  ppm<sub>m</sub>, at  $p = 0.1$  MPa<sup>a</sup>

$w_2$	$x_2$	$\rho$	$\eta$	$n_D$									
		$T = 288.15$ K			$T = 293.15$ K			$T = 298.15$ K			$T = 303.15$ K		
0.000	0.000	0.8812	9.46	1.4521	0.8776	8.06	1.4501	0.8739	6.98	1.4481	0.8703	6.06	1.4462
0.100	0.197	0.8959	8.24	1.4494	0.8921	7.06	1.4472	0.8883	6.14	1.4451	0.8845	5.35	1.4430
0.200	0.355	0.9096	7.03	1.4464	0.9057	6.05	1.4442	0.9017	5.27	1.4420	0.8978	4.61	1.4399
0.300	0.486	0.9230	5.96	1.4432	0.9190	5.14	1.4410	0.9149	4.49	1.4388	0.9108	3.94	1.4366
0.400	0.595	0.9367	5.02	1.4401	0.9325	4.34	1.4379	0.9283	3.80	1.4357	0.9241	3.34	1.4334
0.500	0.688	0.9507	4.19	1.4372	0.9464	3.64	1.4350	0.9420	3.19	1.4327	0.9376	2.82	1.4305
0.600	0.768	0.9654	3.49	1.4340	0.9609	3.05	1.4316	0.9564	2.70	1.4293	0.9519	2.40	1.4270
0.700	0.837	0.9807	2.92	1.4304	0.9761	2.58	1.4281	0.9714	2.30	1.4258	0.9667	2.06	1.4235
0.800	0.898	0.9973	2.49	1.4271	0.9925	2.22	1.4248	0.9876	1.99	1.4224	0.9828	1.79	1.4201
0.900	0.952	1.0148	2.15	1.4240	1.0098	1.93	1.4216	1.0048	1.74	1.4193	0.9997	1.58	1.4169
1.000	1.000	1.0328	1.87	1.4210	1.0277	1.69	1.4188	1.0224	1.53	1.4166	1.0172	1.39	1.4143
		$T = 308.15$ K			$T = 313.15$ K			$T = 318.15$ K			$T = 323.15$ K		
0.000	0.000	0.8666	5.33	1.4442	0.8630	4.72	1.4422	0.8599	4.21	1.4402	0.8557	3.77	1.4382
0.100	0.197	0.8807	4.73	1.4408	0.8768	4.20	1.4387	0.8736	3.75	1.4365	0.8693	3.37	1.4344
0.200	0.355	0.8939	4.08	1.4377	0.8899	3.63	1.4355	0.8865	3.25	1.4334	0.8820	2.93	1.4312
0.300	0.486	0.9067	3.49	1.4344	0.9026	3.11	1.4322	0.8990	2.79	1.4300	0.8945	2.52	1.4279
0.400	0.595	0.9198	2.97	1.4312	0.9156	2.65	1.4290	0.9118	2.39	1.4268	0.9072	2.16	1.4246
0.500	0.688	0.9333	2.51	1.4283	0.9289	2.26	1.4261	0.9249	2.05	1.4238	0.9202	1.86	1.4216
0.600	0.768	0.9474	2.15	1.4248	0.9428	1.95	1.4225	0.9386	1.78	1.4203	0.9338	1.63	1.4181
0.700	0.837	0.9620	1.86	1.4212	0.9573	1.69	1.4190	0.9528	1.55	1.4167	0.9479	1.43	1.4144
0.800	0.898	0.9779	1.62	1.4178	0.9730	1.48	1.4156	0.9683	1.36	1.4133	0.9633	1.26	1.4110
0.900	0.952	0.9947	1.43	1.4146	0.9896	1.31	1.4124	0.9846	1.21	1.4102	0.9795	1.12	1.4080
1.000	1.000	1.0120	1.27	1.4121	1.0067	1.17	1.4099	1.0015	1.08	1.4077	0.9963	1.00	1.4055

<sup>a</sup>Standard uncertainties  $u$  are  $u(w_2) = 0.002$ ,  $u(x_2) = 0.002$ ,  $u_r(\rho) = 5 \times 10^{-4}$ ,  $u_r(\eta) = 0.03$ ,  $u_r(n_D) = 2 \times 10^{-4}$ ,  $u(T) = 0.01$  K for density,  $u(T) = 0.03$  K for viscosity,  $u(T) = 0.05$  K for refractive index and  $u(p) = 10$  kPa.

**Table A2.** Continued

$w_2$	$x_2$	$\rho$	$\eta$	$n_D$	$\rho$	$\eta$	$n_D$	$\rho$	$\eta$	$n_D$
		$T = 328.15 \text{ K}$			$T = 333.15 \text{ K}$			$T = 338.15 \text{ K}$		
0.000	0.000	0.8521	3.40	1.4362	0.8484	3.08	1.4342	0.8448	2.81	1.4322
0.100	0.197	0.8655	3.05	1.4323	0.8617	2.76	1.4301	0.8579	2.50	1.4279
0.200	0.355	0.8781	2.64	1.4290	0.8742	2.40	1.4268	0.8702	2.18	1.4246
0.300	0.486	0.8904	2.28	1.4257	0.8863	2.08	1.4234	0.8822	1.90	1.4212
0.400	0.595	0.9030	1.97	1.4224	0.8987	1.80	1.4201	0.8945	1.65	1.4179
0.500	0.688	0.9158	1.71	1.4194	0.9114	1.57	1.4171	0.9071	1.44	1.4149
0.600	0.768	0.9292	1.49	1.4158	0.9247	1.38	1.4135	0.9202	1.28	1.4112
0.700	0.837	0.9432	1.32	1.4122	0.9385	1.22	1.4099	0.9338	1.13	1.4076
0.800	0.898	0.9584	1.17	1.4087	0.9535	1.09	1.4064	0.9486	1.01	1.4041
0.900	0.952	0.9744	1.04	1.4057	0.9693	0.97	1.4035	0.9643	0.91	1.4012
1.000	1.000	0.9910	0.93	1.4033	0.9857	0.87	1.4011	0.9804	0.82	1.3988

<sup>a</sup>Standard uncertainties  $u$  are  $u(w_2) = 0.002$ ,  $u(x_2) = 0.002$ ,  $u_r(\rho) = 5 \times 10^{-4}$ ,  $u_r(\eta) = 0.03$ ,  $u_r(n_D) = 2 \times 10^{-4}$ ,  $u(T) = 0.01 \text{ K}$  for density,  $u(T) = 0.03 \text{ K}$  for viscosity,  $u(T) = 0.05 \text{ K}$  for refractive index and  $u(p) = 10 \text{ kPa}$ .

**Table A3.** Experimental Densities,  $\rho$ (g·cm<sup>-3</sup>), Viscosities,  $\eta$ (mPa·s), and Refractive Index  $n_D$ , for Biodiesel (1) + Ethyl Pyruvate (2) + MgO (3),  $w_3 = 5$  ppm<sub>m</sub>, at  $p = 0.1$  MPa<sup>a</sup>

$w_2$	$x_2$	$\rho$	$\eta$	$n_D$									
		$T = 288.15$ K			$T = 293.15$ K			$T = 298.15$ K			$T = 303.15$ K		
0.000	0.000	0.8812	9.46	1.4521	0.8776	8.06	1.4501	0.8739	6.98	1.4481	0.8703	6.06	1.4462
0.100	0.215	0.9016	8.65	1.4485	0.8977	7.48	1.4465	0.8937	6.55	1.4444	0.8898	5.75	1.4424
0.200	0.382	0.9168	7.22	1.4440	0.9127	6.25	1.4419	0.9085	5.47	1.4399	0.9044	4.79	1.4378
0.300	0.514	0.9308	5.79	1.4395	0.9265	4.99	1.4374	0.9221	4.37	1.4352	0.9177	3.83	1.4331
0.400	0.622	0.9451	4.70	1.4351	0.9406	4.06	1.4329	0.9360	3.56	1.4307	0.9315	3.13	1.4286
0.500	0.712	0.9604	3.74	1.4307	0.9556	3.24	1.4284	0.9508	2.85	1.4262	0.9460	2.51	1.4240
0.600	0.788	0.9760	2.97	1.4259	0.9710	2.59	1.4237	0.9660	2.28	1.4214	0.9610	2.02	1.4192
0.700	0.852	0.9929	2.38	1.4209	0.9877	2.09	1.4186	0.9824	1.85	1.4163	0.9772	1.65	1.4141
0.800	0.908	1.0111	1.91	1.4170	1.0056	1.69	1.4146	1.0001	1.51	1.4123	0.9946	1.36	1.4100
0.900	0.957	1.0314	1.57	1.4126	1.0256	1.41	1.4104	1.0198	1.27	1.4080	1.0139	1.15	1.4055
1.000	1.000	1.0530	1.29	1.4079	1.0469	1.17	1.4055	1.0409	1.07	1.4030	1.0348	0.98	1.4006
		$T = 308.15$ K			$T = 313.15$ K			$T = 318.15$ K			$T = 323.15$ K		
0.000	0.000	0.8666	5.33	1.4442	0.8630	4.72	1.4422	0.8599	4.21	1.4402	0.8557	3.77	1.4382
0.100	0.215	0.8858	5.10	1.4404	0.8819	4.50	1.4384	0.8785	4.00	1.4363	0.8740	3.57	1.4343
0.200	0.382	0.9002	4.24	1.4357	0.8961	3.78	1.4337	0.8925	3.37	1.4317	0.8878	3.01	1.4296
0.300	0.514	0.9134	3.39	1.4310	0.9090	3.01	1.4289	0.9052	2.68	1.4268	0.9003	2.41	1.4247
0.400	0.622	0.9269	2.79	1.4264	0.9224	2.50	1.4242	0.9182	2.25	1.4221	0.9133	2.04	1.4200
0.500	0.712	0.9412	2.23	1.4219	0.9364	2.00	1.4197	0.9320	1.80	1.4175	0.9269	1.63	1.4153
0.600	0.788	0.9560	1.81	1.4169	0.9510	1.64	1.4146	0.9463	1.49	1.4124	0.9410	1.37	1.4102
0.700	0.852	0.9719	1.50	1.4118	0.9667	1.37	1.4095	0.9616	1.25	1.4073	0.9562	1.15	1.4050
0.800	0.908	0.9890	1.24	1.4076	0.9835	1.14	1.4053	0.9781	1.05	1.4030	0.9724	0.97	1.4007
0.900	0.957	1.0081	1.05	1.4031	1.0023	0.97	1.4008	0.9965	0.90	1.3984	0.9906	0.84	1.3960
1.000	1.000	1.0287	0.90	1.3982	1.0226	0.83	1.3958	1.0165	0.77	1.3934	1.0104	0.72	1.3909

<sup>a</sup>Standard uncertainties  $u$  are  $u(w_2) = 0.002$ ,  $u(x_2) = 0.002$ ,  $u_r(\rho) = 5 \times 10^{-4}$ ,  $u_r(\eta) = 0.03$ ,  $u_r(n_D) = 2 \times 10^{-4}$ ,  $u(T) = 0.01$  K for density,  $u(T) = 0.03$  K for viscosity,  $u(T) = 0.05$  K for refractive index and  $u(p) = 10$  kPa.

**Table A3.** Continued

$w_2$	$x_2$	$\rho$	$\eta$	$n_D$	$\rho$	$\eta$	$n_D$	$\rho$	$\eta$	$n_D$
		$T = 328.15 \text{ K}$			$T = 333.15 \text{ K}$			$T = 338.15 \text{ K}$		
0.000	0.000	0.8521	3.40	1.4362	0.8484	3.08	1.4342	0.8448	2.81	1.4322
0.100	0.197	0.8655	3.05	1.4323	0.8617	2.76	1.4301	0.8579	2.50	1.4279
0.200	0.355	0.8781	2.64	1.4290	0.8742	2.40	1.4268	0.8702	2.18	1.4246
0.300	0.486	0.8904	2.28	1.4257	0.8863	2.08	1.4234	0.8822	1.90	1.4212
0.400	0.595	0.9030	1.97	1.4224	0.8987	1.80	1.4201	0.8945	1.65	1.4179
0.500	0.688	0.9158	1.71	1.4194	0.9114	1.57	1.4171	0.9071	1.44	1.4149
0.600	0.768	0.9292	1.49	1.4158	0.9247	1.38	1.4135	0.9202	1.28	1.4112
0.700	0.837	0.9432	1.32	1.4122	0.9385	1.22	1.4099	0.9338	1.13	1.4076
0.800	0.898	0.9584	1.17	1.4087	0.9535	1.09	1.4064	0.9486	1.01	1.4041
0.900	0.952	0.9744	1.04	1.4057	0.9693	0.97	1.4035	0.9643	0.91	1.4012
1.000	1.000	0.9910	0.93	1.4033	0.9857	0.87	1.4011	0.9804	0.82	1.3988

<sup>a</sup>Standard uncertainties  $u$  are  $u(w_2) = 0.002$ ,  $u(x_2) = 0.002$ ,  $u_r(\rho) = 5 \times 10^{-4}$ ,  $u_r(\eta) = 0.03$ ,  $u_r(n_D) = 2 \times 10^{-4}$ ,  $u(T) = 0.01 \text{ K}$  for density,  $u(T) = 0.03 \text{ K}$  for viscosity,  $u(T) = 0.05 \text{ K}$  for refractive index and  $u(p) = 10 \text{ kPa}$ .